THERMAL DISORDER IN IONIC CRYSTALS

A Thesis presented

by

BRIAN JOHN HAYDEN JACKSON

in partial fulfilment of the requirements

for the Degree of Doctor of Philosophy,

University of London.

Department of Chemical Engineering
  and Chemical Technology,
Imperial College of Science and Technology,
LONDON, S.W.7.

September, 1968

To my parents and Jane

ABSTRACT

The conductance and space-charge polarization capacity of single crystals of thallous chloride have been measured as a function of frequency between 350°K. and temperatures approaching the melting point. Correlation with available diffusion data indicates that Schottky disorder is present with the chlorine ion vacancy as the predominant charge carrier. Analysis of the capacitance results using a modified space-charge theory gives new values of the enthalpies of formation and motion of the vacancies present. Thus $\Delta H_s = 1.36$ eV. ; $\Delta H_{m(cv)} = 0.40$ eV. ; $\Delta H_{m(av)} = 0.09$ eV. The defect concentration at the melting point is ~ 0.08 atomic %.

Similar measurements on thallous bromide show that Schottky defects probably exist in this material with the bromine ion vacancy the more mobile species. The characteristic defect parameters for the bromide closely resemble those for the chloride.

The conductivity of single crystals of pure and magnesium doped lithium iodide has been measured from room temperature up to 40°K. below the melting point. Intrinsic and extrinsic regions are identified although magnesium appears to be far less soluble in lithium iodide than in the other lithium halides. Assuming the presence of Schottky defects with mobile lithium ion vacancies we obtain $\Delta H_s = 1.06$ eV. and $\Delta H_{m(cv)} = 0.43$ eV. The estimated defect concentration at the melting point of 0.18 atomic % is consistent with other systems. Preliminary data for the space-charge polarization in lithium

iodide indicate conformity with the predictions of the novel theory developed for the thallous halides, but accurate results are difficult to obtain.

In general terms, the complex dielectric susceptibility yields useful values of the defect parameters provided the electrodes are blocking and surface conditions are not otherwise disturbed. For materials which may not be doped with altervalent ions this method may be the only one which is readily available.

ACKNOWLEDGEMENTS

CONTENTS

<div align="center">Title   Page No.</div>

CHAPTER I

INTRODUCTION TO THERMAL DISORDER

1.1. POINT DEFECTS IN CRYSTALS

In common with all real crystalline materials, single ionic crystals are structurally defective in the sense that strict lattice periodicity is broken by line and point imperfections present singly or in interacting arrays[1]. The line imperfections, which may be broadly classified into edge and screw dislocations, are not in thermodynamic equilibrium with the host, but are stabilised by balanced strains. Point defects, on the other hand, though frequently present in excessive concentration, can be in thermodynamic equilibrium with the host and with aliovalent impurities in solid solution. Such equilibria arise from the existence of positive entropies of mixing of the point defects with the lattice sites. The two most important types of point defect originally introduced to account for electrolytic transport, termed the Schottky[2] pair and the Frenkel[3] pair, are most conveniently described by reference to univalent-univalent ionic systems such as sodium chloride and silver bromide, which crystallize with the rock-salt structure.

In a Schottky pair one cation and one anion are displaced from their normal lattice sites to the crystal surface leaving the crystal neutral overall. Formation of Schottky defects thus does not conserve lattice sites. On the other hand, in a Frenkel pair one ion moves into an

interstitial site of the conjugate sub-lattice leaving behind a vacant site on the host sub-lattice. Lattice sites are therefore conserved in a Frenkel defect.

1.1.1. The Statistical Distribution of Defects

If, as in the case of Schottky disorder, a definite amount of energy is required to remove one ion from its normal lattice site to the crystal surface there will, at any given temperature, be an equilibrium concentration of Schottky defects which may be calculated by normal statistical methods[4].

Let ΔG_s be the Gibbs free energy required to form a Schottky pair. This may be written as

$$\Delta G_s = \Delta G_{f(av)} + \Delta G_{f(cv)} \qquad (1.1)$$

where $\Delta G_{f(av)}$ and $\Delta G_{f(cv)}$ represent the Gibbs free energy of formation of the anion and cation vacancy respectively. If we now consider one type of vacancy alone and introduce $n_{(av)}$ anion vacancies into the crystal the free energy of the crystal will be increased by an amount $n_{(av)} \Delta G_{f(av)}$ but at the same time decreased by the configurational entropy, $kT \ln.W$, arising out of the mixing of $n_{(av)}$ vacancies and N normal lattice sites. The change in free energy ΔG associated with the anion vacancies is then given by

$$\Delta G = n_{(av)} \Delta G_{f(av)} - kT \ln \left[\frac{N!}{(N - n_{(av)})! \; n_{(av)}!} \right] \tag{1.2}$$

The equilibrium value of $n_{(av)}$ is then found by minimizing ΔG with respect to composition at constant T and P, which gives (for $n_{(av)} \ll N$)

$$\frac{n_{(av)}}{N} = x_{(av)} = \exp \left(\frac{-\Delta G_{f(av)}}{kT} \right) \tag{1.3}$$

where $x_{(av)}$ is the atom fraction of anion vacancies. Similarly for the cation vacancies

$$\frac{n_{(cv)}}{N} = x_{(cv)} = \exp \left(\frac{-\Delta G_{f(cv)}}{kT} \right) \tag{1.4}$$

Multiplying Eq. (1.3) by Eq. (1.4) we obtain

$$\frac{n_{(av)}}{N} \cdot \frac{n_{(cv)}}{N} = \exp \left[\frac{-(\Delta G_{f(av)} + \Delta G_{f(cv)})}{kT} \right]$$

or $\quad x_{(av)} \cdot x_{(cv)} = \exp \left(\frac{-\Delta G_s}{kT} \right) \tag{1.5}$

$$= x_o^2 = K^{-1} \tag{1.6}$$

where x_o is the atom fraction of either anion or cation vacancies in the pure material. This equation emphasizes the 'solubility product' nature of the relationship between $x_{(av)}$ and $x_{(cv)}$ in that the product of the fraction

of vacant anion sites with the fraction of vacant cation sites is always

equal to exp $-\dfrac{\Delta G_s}{kT}$ even in more complex situations where $x_{(av)} \neq x_{(cv)}$.

$\Delta G_{f(av)}$ and $\Delta G_{f(cv)}$, which, according to Eq. (1.5), are equal for the

pure crystal may, of course, be written as

$$\Delta G_{f(av)} = \Delta H_{f(av)} - T\Delta S_{f(av)} \tag{1.7}$$

$$\Delta G_{f(cv)} = \Delta H_{f(cv)} - T\Delta S_{f(cv)} \tag{1.8}$$

where $\Delta H_{f(av)}$, $\Delta H_{f(cv)}$, $\Delta S_{f(av)}$, and $\Delta S_{f(cv)}$ represent the corresponding

enthalpies and entropies of formation of the anion and cation vacancy.

Following the pioneering work of Wagner, Schottky and Jost[5], great

efforts have been made to determine these characteristic enthalpies and

entropies of formation as well as the corresponding mobility parameters in

various substances using a range of techniques, but much of the earlier

work has been vitiated by spurious experimental effects including surface

diffusion and significant, but unrecognised, impurities in the nominally

pure crystals.

Thus even today, after forty years of research, the defect parameters

are known with precision for only five systems, all possessing the

rock-salt structure ($NaCl$[6], KCl[7], $AgCl$[8], $AgBr$[9], LiF[10]). Even here the

entropy of formation is uncertain to factors of 2, and the enthalpies of

formation are continually being challenged.

It is therefore of value to study other crystal systems, such as the thallous halides, which exhibit the cesium chloride structure, in order to determine the type of disorder present and the characteristic defect parameters. Such determinations together with knowledge of the crystal structure will clarify the underlying principles involved in the transport of matter through ionic materials.

1.2. EXPERIMENTAL TECHNIQUES FOR DETERMINING POINT DEFECT PARAMETERS

A direct estimation of the concentration of point defects present in a crystal may be made by measuring the linear thermal expansion of the material using simultaneous macroscopic $\left(\dfrac{\Delta l}{l_o}\right)$ and X-ray $\left(\dfrac{\Delta a}{a_o}\right)$ methods on the sample. Then for isotropic media, θ, the atom fraction of vacant sites is given by[11]

$$\theta = 3\left(\frac{\Delta l}{l_o} - \frac{\Delta a}{a_o}\right)$$

This approach has proved valuable for metals[12], but does not yield reproducible results for ionic crystals[13] owing to the difficulty in eliminating thermal strains and high temperature creep, although it is useful in predicting the type of defect present since it can detect the increased concentration of substitutional ionic sites produced by the formation of Schottky pairs, an effect which is absent from Frenkel systems.

Measurements of specific heat[14] can also produce useful data when the

expected defect concentration is high and the specific heat of the crystal,
in the absence of defect formation, can be accurately extrapolated to the
melting point.

In general terms, the direct measurement of equilibrium properties
has proved disappointing for ionic crystals. However, in contrast to
metallic systems, ionic crystals are suitable media for studying the
macroscopic, correlated motion of charged lattice defects by electrical
techniques which, in the event, provide a rich spectrum of detailed
information far outweighing that from any other approach. Such phenomena
as diffusion, ionic conductivity, and dielectric relaxation, all belong to
a class of thermally activated processes characterized by a temperature
dependence proportional to $\exp\left(\frac{-\Delta U}{kT}\right)$ where ΔU represents the energy
barrier between adjacent potential minima in phase space. Self-diffusion
data are of fundamental importance in this respect but electrical
investigations involving the measurement of ionic conduction, dielectric
loss and space-charge polarization lend themselves to a more detailed
interpretation.

This work, therefore, is concerned with the study of ionic
conductivity and polarization in monocrystalline material under the
influence of such externally variable parameters as temperature, A.C.
frequency and voltage.

In order to correlate this macroscopic motion of lattice defects
with the atomic model of jumping vacancies and interstitials, we shall

consider some aspects of the theoretical approach in the next section.

1.3. CALCULATIONS OF DIFFUSION RATES AND ACTIVATION ENERGIES

These calculations may be divided into:

(i)   the calculation of defect formation energies at lattice sites, and

(ii) the calculation of the frequency of defect jumps.

1.3.1. Defect Formation Energies

The computation of such energies involve considerations of the coulombic interactions, electronic and displacement polarization, together with elastic terms, both before and after formation of the defect.   Such calculations have always been based on the Born ionic model with some form of Born-Mayer repulsive potential, but the treatment of the polarization appears to be rather more intuitive.

The Mott-Littleton approach[15] treats the crystal beyond nearest neighbour ions as a quasi-continuum dielectric in order to calculate the total electric polarization, subsequently dividing it in proportion to the electronic and displacement polarizabilities of the ions. Mullen[16], however, has pointed out the importance of next-nearest neighbour interactions in the fluorite structure and Brauer[17] has shown that defects are a source of elastic strain, consequently adding an elastic term to the displacement field.   Hardy and Lidiard[18] have attempted to determine the true relaxed configuration of the lattice by Fourier transformation of the

equilibrium equations of lattice statics ensuring no resultant force on
any of the complete set of normal co-ordinates introduced. This provides
the true asymptotic displacement and polarization fields - the displacement
being further split into strain and polarization components. In the limit,
however, this approach may be reduced to Mott-Littleton mechanistics
illustrating the fundamental validity of this latter model. Calculations
often agree quite well with experimental values but are more useful in
predicting relative trends since theoreticians often claim too much for
their own particular model in that separate calculations may agree with
different empirical values. In this respect Rao and Rao[19] have calculated
a value of 1.05 eV. for ΔH_s in cesium chloride in agreement with Morlin's[20]
experimental determination of 1.06 eV. whereas Harvey and Hoodless[21] claim
a value of 1.34 eV. which is more in line with Boswarva's[22] calculation of
1.34 eV. where elastic terms and deformation dipoles have been included.

1.3.2. Jump Frequencies

All jumping mechanisms are thermally activated in the sense that they
operate through normal thermal fluctuations which supply the local
concentrations of energy and momentum necessary for the ions to pass through
the intermediate high energy configuration or saddle-point, already
mentioned, between one lattice site and another. It is useful to think of
a vibrating crystal as a continuum of such saddle-points when it remains to
calculate the probability $\omega.dT$ that in any interval of time dT the ion is

at the rigid lattice saddle-point with a velocity directed towards the
final position. Wert's theory[23] was based on this approach, invoking
the basic assumption that all important saddle-points are situated on the
plane midway between initial and final lattice sites. This yields an
expression of the type

$$\omega = \nu \exp\left(-\frac{\Delta G_m}{kT}\right) \tag{1.9}$$

(the jump probably
   per unit time)

where ν is the frequency of vibration of an ion in the mean potential field
about its equilibrium position in the jump direction. In addition to
this, since the ion is constrained in a force field due to the remaining
ions in a vibrating, and not static, lattice the potential barrier has the
nature of a free energy ΔG_m - the free energy of activated mobility.

Vineyard[24] generalized Wert's theory, removing the basic assumption
concerning saddle-points, by considering a reaction path and saddle-point
in N-dimensional space for the whole crystal. Once again the frequency
of crossing the saddle-point could be calculated by equilibrium statistical
mechanics in the harmonic approximation.

Rice[25] provided an alternative approach to this activation problem
with his 'dynamical theory' . He considered a complex consisting of a
vacancy and the jumping ion surrounded by a large number of other ions
(three shells): the rest of the crystal acting as a heat-bath. An

ion-vacancy exchange then occurred when one of a set of critical configurations of atomic co-ordinates is attained - the frequency of such interchange being again evaluated in the harmonic approximation. It is now considered that predictions of the dynamical theory are contained within the Vineyard formalism when the same approximations are made and most modern theories are based on one or other approach.

Franklin[26] has attempted to evaluate the importance of the anharmonic effect since in the harmonic approximation interactions between lattice vibrations are not possible and much of the dissipation of energy by the diffusing species is not accounted for.

A somewhat novel approach to vacancy diffusion has recently been discussed by Omini[27] where ions near a vacancy are described by a Gaussian distribution in vibrational amplitudes and are assumed to jump into adjacent lattice sites when a certain critical amplitude is reached. Using a Debye model it is possible to obtain a simple expression for the rate of diffusion allowing a direct comparison with experimental data, which is not the case with the theories of Rice and Vineyard. Such correlation studies have in general been restricted to metallic lattices where agreement is sometimes good, but often unpredictable[28].

Nevertheless, the basic Eq. (1.9) together with our knowledge of the equilibrium concentration of defects enables us to evaluate the conductivity, which is determined solely by the product of the defect concentration and mobility.

1.4. IONIC CONDUCTIVITY

Shewmon[28] (p. 52) obtains an equation for $D_{(cv)}$ the diffusion coefficient of a cation (or anion) vacancy in a uni-univalent lattice:

$$D_{(cv)} = a_0^2 \cdot x_{(cv)} \cdot \omega \qquad (1.10)$$

where a_0 is the lattice spacing parameter and ω is again the probability per unit time that any ion will jump into a particular vacant site. $D_{(cv)}$ is related to $\sigma_{(cv)}$, the conductivity of a cation vacancy, by the Nernst-Einstein equation[4] below

$$\frac{\sigma_{(cv)}}{D_{(cv)}} = \frac{Ne^2}{kT} \qquad (1.11)$$

which equates the diffusion of entities down a concentration gradient with their drift in an electric field. Eqs. (1.4), (1.9), (1.10) and (1.11) then combine to give

$$\sigma_{(cv)} = \frac{Na_0^2 e^2 \nu}{kT} \exp\left(-\frac{\Delta G_{f(cv)}}{kT}\right) \cdot \exp\left(-\frac{\Delta G_{m(cv)}}{kT}\right) \qquad (1.12)$$

$$\text{or } \sigma_{(cv)} \cdot T = \frac{Na_0^2 e^2 \nu}{kT} \exp\left(+\frac{\Delta S_{f(cv)} + \Delta S_{m(cv)}}{k}\right) \cdot$$
$$\exp\left(-\frac{\Delta H_{f(cv)} - \Delta H_{m(cv)}}{kT}\right) \qquad (1.13)$$

18
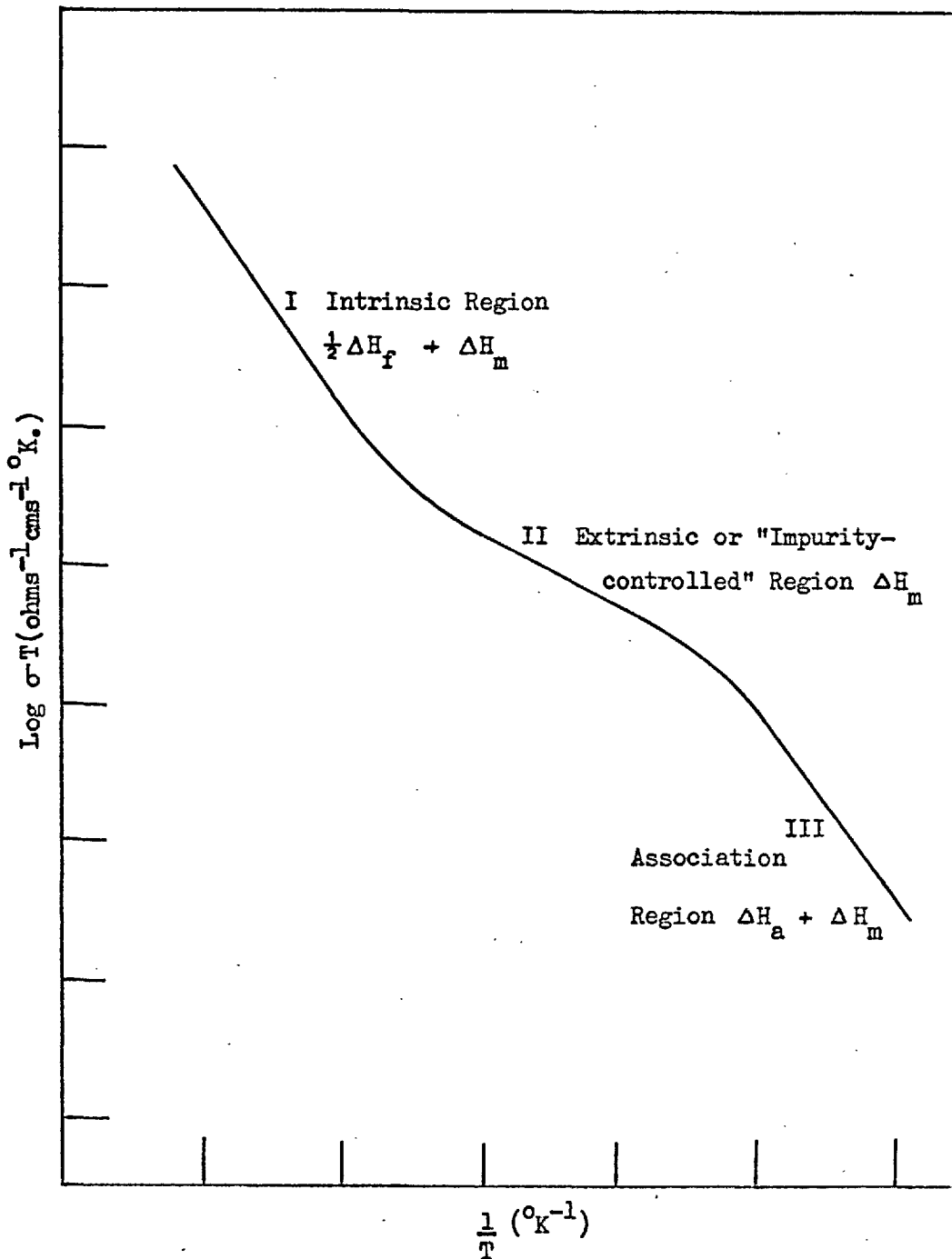
The Classical Conductivity Curve

Fig. (1.1)

$$= \sigma_o \exp - \left(\frac{\Delta H_{f(cv)} + \Delta H_{m(cv)}}{kT} \right) \qquad (1.14)$$

where σ_o is constant if the entropies and enthalpies are assumed independent of temperature.

The temperature dependence of the ionic conductivity σ in crystalline material is therefore most meaningfully represented graphically as $\log \sigma T$ against reciprocal temperature which, in general, provides a curve similar in shape to the classical plot[4] displayed in Fig.(1.1). These three regions can be treated quite separately in terms of a simple model originally due to Teltow[29]. The conductivity σ may, of course, be made up of contributions from a number of mobile charge carrying species (anion vacancies, cation vacancies, interstitials, etc.), where σ_i and t_i represent the conductivity and transport number of the ith species, such that,

$$\sigma = \sum_i \sigma_i t_i \qquad (1.15)$$

and $$\sum_i t_i = 1.$$

In order to simplify this discussion we shall consider only Schottky disorder, with mobile cation vacancies, although the treatment is quite general both in its application to mobile anion vacancies and Frenkel disorder.

1.4.1. Region I

This is known as the intrinsic region. Thermally created defects predominate and the conductivity, according to equation (1.14) may be given as

$$\sigma = \frac{\sigma_o}{T} \exp - \left(\frac{\frac{1}{2}\Delta H_s + \Delta H_{m(cv)}}{kT} \right) = \frac{\sigma_o}{T} \exp - \frac{\Delta H_1}{kT} \qquad (1.16)$$

where $\Delta H_{f(cv)}$ has been replaced by one half of ΔH_s, the enthalpy of formation of a Schottky defect. In fact we only know that $\Delta G_{f(av)} = \Delta G_{f(cv)}$, but theoretical calculations[22] indicate that $\Delta H_{f(av)} \approx \Delta H_{f(cv)}$ as well. However, cation and anion vacancies are always found in pairs and it is only possible to measure, in effect, the value of $\frac{1}{2}\Delta H_s$. As in all other investigations of this type, therefore, we shall assume that $\Delta H_{f(cv)} = \frac{1}{2}\Delta H_s$.

Experimentally, it is often found that region I is not straight, as Eq.(1.16) would predict, particularly at high temperatures, the principal cause being the presence of additional charge carriers such as mobile anion vacancies or interstitials. The curvature is then a natural consequence of the non-equivalent enthalpies of motion of the conducting species. In such cases we must write $\sum \sigma_i t_i$ for the conductivity and calculate σ_i and t_i from self-diffusion data using the Nernst-Einstein equation and the all important concept of jump correlation, discussed later. Fuller and Reilly[30], and other workers, have attempted the reverse of this process in

the sense that they have separated the intrinsic conductivity due to Schottky defects into anion and cation vacancy contributions by a least squares analysis of the curve in this region. This approach, however, quite apart from its mathematical shortcomings, involves the accurate knowledge of a number of critical parameters including $\Delta H_{m(av)}$ and $\Delta H_{m(cv)}$, and often provides irreproducible values of the transport numbers in variance with those obtained by classical electrolytic methods.

The high concentration of defects in this region also provides a basis for defect interaction and such concepts as vacancy pairs[31], "lattice-loosening"[32], and Debye-Huckel ionic atmospheres[8] have been invoked, sometimes unnecessarily, to explain deviations from the classical theory.

1.4.2. Region II

We know that, in general,

$$x_{(av)} \cdot x_{(cv)} = x_o^2 = K^{-1} \qquad (1.17)$$

and, for the pure crystal, that

$$x_{(av)} = x_{(cv)} = x_o$$

However, the presence of aliovalent impurities when substitutionally

incorporated in the host lattice will give rise to an increased concentration of one or other type of vacancy through the necessary condition of over-all charge neutrality. Thus

$$x_{(cv)} = x_{(av)} + x_c \qquad (1.18)$$

where x_c is the atom fraction of divalent cationic impurities present in the crystal. When $x_c \gg x_0$ (at lower temperatures), $x_{(cv)}$ is determined by x_c alone and the conductivity in this extrinsic or impurity-controlled region becomes, according to Eq.(1.10),

$$\sigma = \frac{x_c \cdot N a_0^2 e^2 \nu}{kT} \exp - \frac{\Delta G_{m(cv)}}{kT} \qquad (1.19)$$

$$= \frac{x_c \cdot \sigma_0'}{T} \exp - \frac{\Delta H_{m(cv)}}{kT} \qquad (1.20)$$

$$= \frac{x_c \cdot \sigma_0'}{T} \exp - \frac{\Delta H_2}{kT}$$

where σ_0' is another constant. For constant temperature, therefore, a plot of σ against x_c should be linear for impurity-controlled conduction if cation vacancies are the only mobile charge carriers. For example the incorporation of divalent manganese[6] into sodium chloride, which exhibits Schottky disorder with mobile cation vacancies, raises the conductivity by virtue of the increased concentration of mobile vacant sites whereas the

addition of oxide[33] lowers the conductivity by increasing $x_{(av)}$, subsequently reducing $x_{(cv)}$ through Eq.(1.17). Furthermore, in a substance like strontium chloride[34], intrinsically disordered by anionic Frenkel pairs, the addition of monovalent sodium enhances the conductivity whereas trivalent yttrium reduces it, indicating mobile chlorine vacancies .

Aliovalent anion impurity doping - mainly oxide - has been far less successful partly because of the difficulty in analytically determining the oxide. Since, however, a divalent metallic cation has a virtual positive charge when substitutionally dissolved in a uni-univalent lattice, it may be effectively complexed as a pair by either a vacant cation site[35] or an oxide ion, both of which have a virtual negative charge at their respective lattice sites. This means that the oxide ion could extend region I to a lower temperature by nullifying the effect of the divalent cation through Eq.(1.17), an effect, the study of which is becoming increasingly popular on account of the experimental difficulties involved in removing all traces of oxide from the crystal. Indeed the unremarked presence of oxide ions has probably been the largest single influence in causing irreproducibility in earlier work.[7]

1.4.3. Region III

The impurity-vacancy complex pairs previously mentioned determine the conductivity in this region with

$$\sigma = \frac{\sigma_0{}''}{T} \exp - \left(\frac{\Delta H_{a(iv)} + \Delta H_{m(cv)}}{kT} \right) \qquad (1.21)$$

$$= \frac{\sigma_0{}''}{T} \exp - \frac{\Delta H_3}{kT}$$

where $\Delta H_{a(iv)}$ is the binding energy of the impurity-vacancy complex and $\Delta H_{m(cv)}$ is, as usual, the enthalpy of motion of the dissociated cation vacancy. The data in this "association region" with respect to impurity concentration and related conductivity may be analysed using the well-known Teltow association[29] theory and Debye-Huckel interaction theory. Correlation over small concentration ranges inherent in the Teltow approach is often very good, but background impurities are difficult to treat. As predicted theoretically the binding energy of the impurity-vacancy complex increases with the ionic radius of the impurity ion.[39]

1.4.4. Below Region III

The conductivity below region III is characterized by precipitation and aggregation of the impurities[6,40], but the results are often irreproducible. This is often due to the long periods of time required to reach equilibrium at these low temperatures but Chang[41] has used the kinetics of precipitation as a novel means for determining the defect formation enthalpy of sodium chloride.

1.5. POLARIZATION EFFECTS

In the presence of an electric field, ionic crystals generally display some time-dependent, transient phenomena in the conductivity such that:

$$\sigma_t(\infty) = \sigma_t(o) - \sigma_{transient}$$

This effect is best observed under D.C. conditions when time–current curves[38] may be produced to indicate the extent of polarization in the dielectric. However, different phenomena manifest themselves depending on the temperature and it has been found useful to discuss the high temperature polarization, where defects are dissociated, quite separately from the low temperature polarization where impurity interactions may predominate[42,43]. At temperatures below these the static dielectric constant is determined by the electronic and lattice polarization of the crystal.

A.C. and D.C. values of the conductivity are known to agree quite closely in the low temperature region[6] but at the high temperatures which concern us, the A.C. value is always the greater. Here the frequency dependent accumulation of space–charge is known to occur reducing σ, and the passage of D.C. current may effect electrolysis, chemically altering the nature of the material. The high frequency A.C. conductivity is

therefore the meaningful value.

1.5.1.   High Temperature Polarization

Polarization effects arising from the motion of charge carriers under
the influence of an externally applied electric field in materials with
blocking electrodes have been investigated in the past both theoretically
and experimentally[44].   Chang and Jaffé[45] extended this concept to the
treatment of semi-conductors and electrolytes by analogy with Jaffé's
earlier work on electrolytic solutions, but more recently Macdonald[46] and
Friauf[47] have independently developed more meaningful theories, discussed
in Chapter 2, because it was felt that previous treatments were
insufficiently applicable to some physical situations which might be
important in practice, particularly in connection with the association of
charge carriers and their relative mobilities.

Macdonald obtained an extremely complicated general solution for the
A.C. admittance of an ionic crystal treated as a slab of conducting
dielectric, but found that it could be reduced in certain limiting cases
and subsequently related to the capacitive and resistive components of
current flowing through the crystal.   Friauf deduced the equivalent
parallel circuit arrangement of these two components, both of which can be
frequency dependent, but more recently Raleigh[48] has pointed out that this
arrangement can be equally well represented by a frequency independent
capacitance and resistance in series which therefore become the physically

meaningful parameters. This approach may well be simpler theoretically and experimentally in defining perturbations of the frequency dependence, but will not, of course indicate the nature of such perturbations any more than the parallel representation.

Jacobs[49,50,51] and co-workers, working on potassium chloride, have made the only systematic attempt to correlate experimental data with theoretical predictions, but have encountered many difficulties in determining the extent of polarization in terms of the experimentally measured capacity. Thus, values of the capacity may vary over two orders of magnitude for identical experiments, exhibit strong temperature hysteresis and will depend markedly on the material and physical nature of the electrode. Without doubt, the electrode is the most important single factor in determining the capacity and the concept of complete blocking[51] has been modified to include the possibility of partial blocking, but the 'ad hoc' nature of this approach is inevitable since the type of electrode processes involved is little understood. It is therefore wiser to work, whenever possible, with electrodes that are known to be completely blocking.

1.6. DISORDER IN CRYSTAL SYSTEMS

The experimental work on ionic crystals (for a review see Ref. 52) has been concentrated almost entirely on face-centred cubic structures in the alkali halides and silver halides. Sodium chloride and potassium

chloride are both known to exhibit Schottky disorder, with the cation

vacancy appreciably more mobile, whereas in silver chloride and silver

bromide the charge is carried almost exclusively on the cation sub-lattice

with interstitial silver ions some 2-10 times more mobile than vacant

cation sites. Limited studies on the fluorite structure[34] indicate

that the principal disorder is anion Frenkel.

Both the cesium halides[21] and the thallous halides, which possess the

simple cubic, cesium chloride, structure are thought to exhibit Schottky

disorder, but the experimental data are often conflicting and analysis

made more complex by the fact that both anion and cation contribute

significantly to the conductivity.

1.6.1. Thallous Chloride and Thallous Bromide

Earlier studies on the ionic conductivity of thallous chloride in the

temperature range 425°K. - 600°K. are in good agreement (see Table 1.1),

although all results, except those of Friauf who used single crystals,

were obtained on pressed pellets. Today single crystals are used, wherever

possible, as they provide greater reproducibility in the absolute value of

the conductivity, values obtained with polycrystalline material being too

low. For the measurement of space-charge effects single crystals are

essential otherwise the results are liable to be vitiated by charge-carrier

blocking at internal boundaries and short-circuiting of the charge along

preferred conduction paths at the grain boundaries.

Author	Temperature °K.	ΔH_1 eV.	σ (575°K.) ohm^{-1}cm.$^{-1}$
Friauf[53]	640° - 690°	0.85	
Friauf	430° - 640°	0.75	3.8×10^{-4}
Lehfeldt[54]	320° - 680°	0.82	2.5×10^{-4}
Phipps and Partridge[55]	400° - 660°	0.75	2.2×10^{-4}
Hauffe and Griessbach-Vierk[56]	420° - 520°	0.72	1.5×10^{-4}

$$\sigma = \frac{\sigma_0}{T} \exp \frac{-\Delta H_1}{kT} \quad \text{for thallous chloride.}$$

Table (1.1)

Hauffe added $PbCl_2$ to some of his crystals in concentrations varying between 0.1 and 3 mole %. This effectively reduced the conductivity in the intrinsic region indicating mobile thallium ion interstitials or chlorine ion vacancies, but the lead chloride appeared to be of only limited solubility as no further reduction in the conductivity was observed for impurity concentrations greater than 0.2 mole %.

Friauf[57] has measured the self-diffusion coefficients in thallous chloride and found that both ions are appreciably mobile with the chlorine ion always possessing the greater mobility. This is in accordance with the cesium halides, where the mobility of the anion is slightly greater, but in direct contrast to the alkali halides having the rock-salt structure

where the cation is the predominant charge carrier in conduction.   In general, where Schottky disorders exists in a crystal, both ions are appreciably mobile which is not the case with Frenkel disorder.   In the light of the self-diffusion data, therefore, Hauffe's results indicate Schottky disorder in thallous chloride with mobile chlorine ion vacancies. This will be confirmed in this work by accurate correlation of Friauf's self-diffusion data with our own conductivity results using the jump correlation arguments described in Chapter 2.

A recent comparison by Christy and Dobbs,[58] assuming Schottky disorder, of Friauf's diffusion results with their own thermoelectric power data has given preliminary estimates of the energies of formation and motion of the anion and cation vacancy, together with the equilibrium defect concentration as a function of temperature.   The present work provides a wholly independent estimate of the defect concentration using polarization measurements, which moreover does not depend on any assumptions, inherent in Christy's analysis, concerning the solubility or eventual complex formation of divalent cations, and consequently leads to a new set of parameters.

Like the chloride, thallous bromide is known to be an almost exclusively ionic conductor[55], but knowledge of the conductivity is more limited — Table (1.2).

Author	Temperature °K.	ΔH_1 eV.	$\sigma (500°K)$ ohm^{-1}cm.$^{-1}$
Phipps and Partridge[55]	$400°$ – $660°$	0.76	9.0×10^{-6}
Hermann[60]	$425°$ – $575°$	0.83	6×10^{-6}

$$\sigma = \frac{\sigma_0}{T} \exp - \frac{\Delta H_1}{kT} \text{ for thallous bromide.}$$

Table (1.2)

Hermann has also measured the transport number of the bromine ion as 0.9 ± 0.1 at $570°$K down to 0.7 near the melting point. This increasing cationic contribution to the conductivity should reveal itself as a slight but distinct, curvature in the $\log \sigma T$ against $\frac{1}{T}$ plot at higher temperatures, but unfortunately Hermann's conductivity results scatter by as much as 100% in some cases.

1.6.2. Lithium Iodide

Haven[61] has investigated the ionic conductivity in the pure and magnesium-doped lithium halides. Assuming Schottky disorder, he analysed his results in the extrinsic region using Teltow's simple theory and obtained good correlation between the conductivity and impurity concentration for the fluoride, chloride, and bromide. However, his results for the iodide were scant and inconclusive although he managed to obtain the preliminary values given in Table (1.3) in spite of his $\log \sigma T$ against $\frac{1}{T}$

plot for the pure material being continuously curved at temperatures above 500°K.

Author	ΔH_1 eV.	ΔH_2 eV.	$x_{(cv)}$ atomic % at m.p.
Haven[57]	1.06	0.42	1.15

$$\sigma = \frac{\sigma_o}{T} \exp - \frac{\Delta H_1}{kT}, \qquad \sigma = x_c \cdot \frac{\sigma_o'}{T} \exp - \frac{\Delta H_2}{kT} \quad \text{for lithium iodide.}$$

Table (1.3)

There have been no investigations of polarization effects or space-charge build-up in any of these three materials.

CHAPTER 2

THEORETICAL CONSIDERATIONS

We shall here develop formal theories for correlated diffusion and space-charge effects in a uni-univalent Schottky system and refer only to Frenkel systems where appropriate, although the theoretical approach is quite general and equally applicable to Frenkel disorder.

2.1. CORRELATION EFFECTS FOR DIFFUSION

2.1.1. The Nernst-Einstein Equation

As pointed out in section 1.4.1. the diffusion coefficient $D_{(cv)}$ of a cation vacancy (or anion vacancy) is related to its mobility $\mu_{(cv)}$ in an electric field by the Einstein equation[4].

$$\frac{\mu_{(cv)}}{D_{(cv)}} = \frac{e}{kT} \tag{2.1}$$

The conductivity $\sigma_{(cv)}$ of a cation vacancy is given by $n_{(cv)}e\mu_{(cv)}$, and therefore,

$$\frac{\sigma_{(cv)}}{D_{(cv)}} = \frac{n_{(cv)}e^2}{kT} \tag{2.2}$$

This relation is rigorously correct, but it does not allow for comparison with experimental values as we are unable to obtain $D_{(cv)}$

directly. The quantities that are usually measured are the total conductivity $\sigma = \sum \sigma_i = \sigma_{(cv)} + \sigma_{(av)}$ (for Schottky disorder) and the diffusion coefficients for the two ions, D_c^* and D_a^*, which may be obtained separately using tracer techniques. It therefore remains for us to obtain a relationship between D_c^*, the diffusion coefficient of the cation, and $D_{(cv)}$. Such a relationship is derived rigorously in section 2.1.2., but we give the result below in order that we may modify Eq.(2.2).

$$\frac{D_{(cv)}}{D_c^*} = \frac{n_{(cv)}}{N} = x_{(cv)} \tag{2.3}$$

In practice, therefore, the microscopic Einstein relation, Eq.(2.2), is replaced by the macroscopic Nernst-Einstein equation below,

$$\frac{\sigma_{(cv)}}{D_c^*} = \frac{Ne^2}{kT} \tag{2.4}$$

where N is once again the concentration of cation (or anion) sites. We may extend this treatment to include mobile anion vacancies such that in general, for Schottky disorder,

$$\sigma_{(cv)} + \sigma_{(av)} = \frac{Ne^2}{kT} \left(D_c^* + D_a^* \right) \tag{2.5}$$

$$= \sigma$$
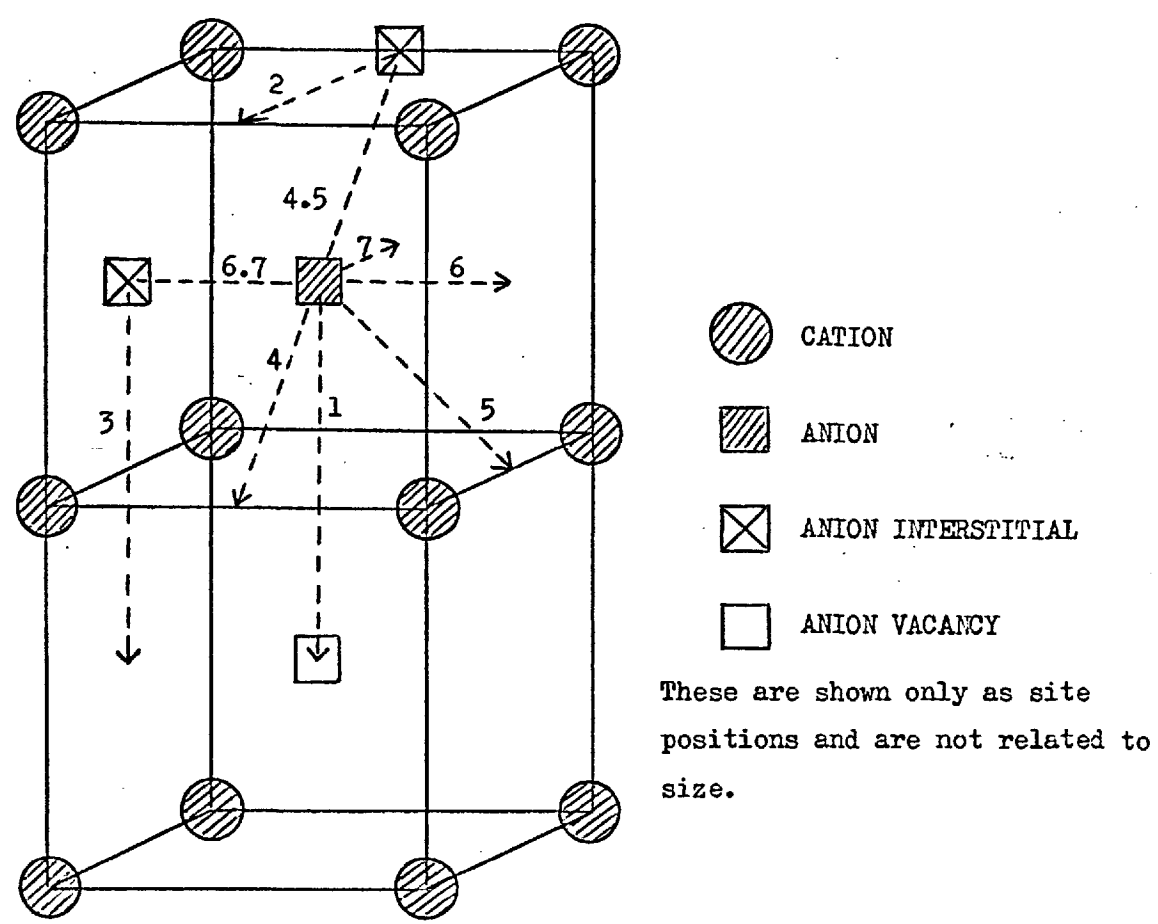
Some possible jumping mechanisms in the thallous chloride lattice.

     1. Vacancy

     2. Direct interstitial

     3. Direct interstitial

     4. Collinear interstitialcy

     5. Non-collinear interstitialcy

     6. Collinear interstitialcy

     7. Non-collinear interstitialcy

Fig. (2.1)

or
$$\frac{\sigma}{(D_c^* + D_a^*)} = \frac{Ne^2}{kT} \qquad (2.6)$$

A similar equation is obtained for Frenkel disorder.

Four effects, present to different extents in different systems, may cause deviation from Eq.(2.6) which, as a result, is usually only approximately satisfied when experimental values are inserted.

(i) Vacancy jumps are completely random in time and amongst the available directions as determined by the crystal structure, whereas there is correlation between the directions of successive jumps of the tracer ion which can in fact only jump when it is adjacent to a vacancy. This will be discussed in section 2.1.2.

(ii) There may be charge carriers other than vacancies, such as electrons.

(iii) Under the restrictive condition that a jumping interstitial ion never undergoes exchange with the ions of the host lattice, the concept of the defect and its ionic charge do not become spatially separated. However, for a class of interstitial jumping mechanisms in which defect/host exchange is allowed, the displacement of the defect differs from that of any of the ions involved (see Fig. (2.1) for the interstitialcy mechanism). This effect is not present for vacancy jumping, but it will be mentioned again later.

(iv) There may be a neutral complex, such as a cation/anion vacancy pair or a vacancy/aliovalent ion dipole, that contributes to the diffusion,

but not to the conductivity.

Eq.(2.6) must therefore include an experimentally determined over-all correlation factor f^o which may contain the influence of all four of the effects described above such that

$$\frac{\sigma}{\left(D_c^{\ast} + D_a^{\ast}\right)} = \frac{f^o N e^2}{kT} \qquad (2.7)$$

The factor f^o may then be written as

$$f^o = \frac{f_j \cdot f_d}{f_c} \qquad (2.8)$$

where f_j, the jump correlation factor, arises out of (i), the non-random jumping motion of the tracer ion, and f_d, the displacement factor, accounts for the non-equivalent jump displacements of tracer and defect described in (iii). f_c is the charge transference number of the vacancies.

If we assume the absence of any neutral complexes, the essence of the problem is then the theoretical calculation of f_j and f_d for various diffusion mechanisms such that Eq.(2.7) may be satisfied.

2.1.2 The Random-Flight Problem and Jump Correlation

If we consider the motion of an ion on a crystalline sub-lattice containing vacancies as the only defects, it is quite a simple problem to obtain an equation for the motion of such an ion through a sequence of

discrete jumps. The motion of any one vacancy throughout the sub-lattice is entirely random since after every jump its neighbours are identical, which means that each jump of the vacancy is entirely independent of any preceding jump. When, on the other hand, we follow the motion of the tracer ion, it may be seen that each successive jump of the tracer is not wholly independent of what has gone before, since after any jump all of its neighbours are not identical − one is a vacancy − and the most probable next jump of the tracer is back to the vacant site. We demonstrate the important consequence that the mean square displacement of the tracer after n jumps will be less than that for a vacancy which took the same number of jumps.

The theory of random-flight[28] gives the mean square displacement of any particle after n jumps, $\overline{R_n^2}$, in a general form:

$$\overline{R_n^2} = nr^2 \left(1 + \frac{2}{n} \overline{\sum_{j=1}^{n-1} \sum_{i=1}^{n-j} \cos \theta_{i,i+j}} \right) \qquad (2.9)$$

where r is the displacement distance of the jump and $\theta_{i,i+j}$ is the angle between the jump directions of the ith and (i+j)th jumps.

If each jump is independent of all preceding jumps (as in the case of vacancy jumping) the average value of the term in Eq.(2.9) involving the double sum will be zero giving

$$\overline{R_n^2} \text{ (vacancy)} = \overline{R_v^2} = nr^2 \qquad (2.10)$$

As a preliminary to discussing the theory of correlation effects, it is necessary to establish the relationship between this microscopic treatment of diffusion, involving a sequence of discrete jumps, and the macroscopic approach, where the distribution of particles is governed by classical diffusion equations and the mean square displacement is given by[28]

$$\overline{R^2} = 6Dt \tag{2.11}$$

Since the mean square displacement of a particle after a very large number of discrete jumps must correspond to the prediction of the macroscopic approach, the diffusion coefficient for cation (or anion) vacancies is found by combining Eq.(2.10) and Eq.(2.11)

$$D_{(cv)} = \frac{1}{6}\frac{nr^2}{t} \tag{2.12}$$

or $$D_{(cv)} = \frac{1}{6}\Gamma_{(cv)}r^2 \tag{2.13}$$

with $\Gamma_{(cv)}$ the average number of jumps per second for each vacancy.

In order for a tracer ion to make a jump, a vacancy must be next to it, and the probability of this is $Z.\frac{n_{(cv)}}{N}$ where Z is the number of nearest neighbour sites of the tracer ion. The probability that the vacancy will jump towards the tracer, however, is only $\frac{1}{Z}$ and hence the over-all jump

frequency for the tracer cation Γ_c is

$$\Gamma_c = \frac{1}{Z} \cdot Z \cdot \frac{n_{(cv)}}{N} \Gamma_{(cv)}$$

$$= \frac{n_{(cv)}}{N} \Gamma_{(cv)} \tag{2.14}$$

By analogy with the treatment of vacancies the mean square displacement of the tracer cation $\overline{R_c^2}$ is found to be

$$\overline{R_n^2} \text{ (tracer cation)} = nr^2 = \overline{R_c^2}$$

or $\quad \overline{R_c^2} = \Gamma_c r^2 t \tag{2.15}$

$$= 6D_c^{\ast} t \tag{2.16}$$

in the case that the double sum term in Eq.(2.9) may again be put to zero. Combining Eqs.(2.13)-(2.16) we find that

$$\frac{D_{(cv)}}{D_c^{\ast}} = \frac{n_{(cv)}}{N} = x_{(cv)} \tag{2.17}$$

This relationship between the microscopic and macroscopic diffusion coefficients for the vacancy and tracer respectively is extremely important

in connecting Eq.(2.2), the microscopic Einstein relation, to Eq.(2.4), the macroscopic Nernst-Einstein equation. The latter equation was extended to give Eq.(2.6) below,

$$\frac{\sigma}{(D_c^{\ast} + D_a^{\ast})} = \frac{Ne^2}{kT}$$

but the four invalidating effects already mentioned in connection with this equation may now be specified.

(i) The directions of successive jumps of the tracer ion must be at random so that the double sum term in Eq.(2.9) is zero. This is not the case for a tracer ion moving by a vacancy mechanism so that the jump correlation factor which may be defined as

$$f_j = \lim_{n \to \infty} \frac{\overline{R_n^2} \ (\text{tracer})}{\overline{R_n^2} \ (\text{defect})} \tag{2.18}$$

is not equal to 1.

(ii) The displacement of the vacancy and tracer ion must be the same so that the jump distance r is identical for both species.

(iii) All the current must be carried by free vacancies so that f_c may be put equal to 1.

2.1.3. The Calculation of the Jump Correlation and Displacement Factors

According to Eq.(2.18) the jump correlation factor for vacancy

diffusion, $f_{j(v)}$, is given by

$$f_{j(v)} = \lim_{n \to \infty} \frac{\overline{R_n^2} \text{ (tracer)}}{\overline{R_n^2} \text{ (vacancy)}}$$

$$= \lim_{n \to \infty} \left(1 + \frac{2}{n} \overline{\sum_{j=1}^{n-1} \sum_{i=1}^{n-j} \cos \theta_{i,i+j}} \right) \qquad (2.19)$$

where θ now refers to the angle between tracer jump directions. The bar in this equation means to average the double sums for a large number of diffusing particles. The same quantity can be obtained by averaging the values of $\cos \theta$ for a large number of particles and summing these. That is we can substitute

$$\overline{\sum_{j=1}^{n-1} \sum_{i=1}^{n-j} \cos \theta_{i,i+j}} \equiv \sum_{j=1}^{n-1} \sum_{i=1}^{n-j} \overline{\cos \theta_{i,i+j}}$$

As a final aid in reformulating this expression, we note that in any cubic or close-packed lattice all solute jumps are equivalent except for their orientation, which is to say that all tracer-vacancy pairs that have just completed an exchange are indistinguishable, aside from their orientation. The value of $\overline{\cos \theta}_{i,i+j}$ is therefore the same for each value of i.

Designating this new average as $\overline{\cos \theta}_j$ we can write Eq.(2.19) as

$$f_{j(v)} = \lim_{n \to \infty} \left(1 + \frac{2}{n} \sum_{j=1}^{n-1} (n-j) \, \overline{\cos \theta}_j \right) \tag{2.20}$$

In the limit as $n \to \infty$, $\frac{(n-j)}{n} \to 1$ for the initial terms of the series and Eq.(2.20) may be written

$$f_{j(v)} = 1 + 2\overline{\cos \theta}_1 + 2\overline{\cos \theta}_2 + - - - - \tag{2.21}$$

The problem is now reduced to calculating the mean value of the cosine of the angle between the ith (arbitrarily selected) and the (i+1)th jump vectors ($\overline{\cos \theta}_1$), the mean value of $\cos \theta$ for the ith and (i+2)th jump vectors ($\overline{\cos \theta}_2$), etc.

Compaan and Haven[62] have shown that $(\overline{\cos \theta}_j) = (\overline{\cos \theta}_1)^j$ for a vacancy mechanism and therefore Eq.(2.21) becomes

$$f_{j(v)} = 1 + 2(\overline{\cos \theta}_1) + 2(\overline{\cos \theta}_1)^2 + - - - - \tag{2.22}$$

In order to compute $(\cos \theta_1)$ it is necessary to calculate the probability of the tracer making its next jump to each of its Z nearest neighbours, having exchanged with the vacancy on its previous, or ith, jump. Compaan and Haven did this for a number of lattices by considering only one vacancy to be present. This is equivalent to assuming that the

density of vacancies is so low that no other vacancy will exchange with the tracer before the vacancy has randomized its position with respect to the initial solute-vacancy exchange. Some of their results are given in Table (2.1).

Lattice	z	$f_{j(v)}$
Two dimensional:		
Square	4	0.467
Hexagonal	6	0.560
Three dimensional:		
Diamond	4	$\frac{1}{2}$
Simple cubic	6	0.655
Body-centred cubic	8	0.721
Face-centred cubic	12	0.781

Values of the jump correlation factor for vacancy diffusion in various lattices[62].

Table (2.1)

For direct interstitial diffusion (see Fig. (2.1), 2 and 3) the environment of the tracer is identical after each discrete jump and its motion is consequently random. The jump correlation factor for a tracer ion moving by a direct interstitial mechanism is therefore equal to 1. In

general, there will be jump correlation for diffusion by the interstitialcy mechanism and f_j will vary between 0 and 1.

On the other hand, the displacement factor, f_d, for vacancy diffusion will equal 1 as both vacancy and tracer have identical jump displacements. Similarly f_d will be 1 for direct interstitial diffusion, but for the interstitialcy mechanism the displacement factor will vary again between 0 and 1. For example the collinear anion interstitialcy jumps in Fig.(2.1) are characterized by a displacement factor of $\frac{1}{2}$ as the defect moves twice the distance of the interstitial tracer ion.

There are two possible interstitial positions for an ion in the thallous chloride structure as shown in Fig. (2.1). The one situated at the edge centre of its own sub-lattice is favoured by repulsive energy whereas the other at the face-centre is favoured by Coulombic energy. However, when we consider the geometry of the lattice, there appears to be little space for the interstitial ion, particularly the anion, at either position on account of the large sizes of the two ions ($Tl^+ =$ 1.51Å, $Cl^- = 1.81$Å). By far the most realistic defect on spatial grounds is the vacancy.

Jump correlation and displacement factors for the possible diffusion mechanisms in the thallous chloride lattice are given below in Table (2.2)

Mechanism	Number in Fig. (2.1)	f_j	f_d	$f_j \cdot f_d$
Vacancy	1	0.655	1	0.655
Direct interstitial	2	1	1	1
Direct interstitial	3	1	1	1
Coll. interstitialcy	4	$\frac{2}{3}$	$\frac{1}{2}$	$\frac{1}{3}$
Non-coll. interstitialcy	5	0.932		0.621
Coll. interstitialcy	6	0	$\frac{1}{2}$	0
Non-coll. interstitialcy	7	1	1	1

Jump correlation and displacement factors for diffusion in the thallous chloride lattice[57].

Table (2.2)

In practice D_σ is calculated from

$$\frac{\sigma}{D_\sigma} = \frac{Ne^2}{kT} \tag{2.23}$$

and compared with $(D_c^* + D_a^*)$ which provides f^0 since

$$D_\sigma = f^0(D_c^* + D_a^*) \tag{2.24}$$

If f_c is known then $f_j \cdot f_d$ may be obtained experimentally using Eq.(2.8),

$$f^o = \frac{f_j \cdot f_d}{f_c}$$

However, the theoretical values of $f_j \cdot f_d$ for some diffusion mechanisims are extremely close – see Table (2.2) – and experimentally it is difficult to determine the diffusion coefficient to such accuracy that it is possible to assign unambiguously a certain type of defect motion using correlation considerations alone. Rather, if either Schottky or Frenkel disorder is suspected, it is often feasible to confirm the presence of one or the other by the foregoing analysis.

This will be the case with thallous chloride, where Schottky disorder has been postulated. Present conductivity measurements will be correlated with Friauf's diffusion data[57] in an attempt to define the type of diffusion mechanism involved.

2.2. SPACE-CHARGE EFFECTS

2.2.1. The Charge Carrier Model

The concentrations of anion vacancies p (positive charge carriers) and cation vacancies n (negative charge carriers) within a Schottky disordered ionic crystal in an electric field will, in general, be functions

of position x as well as time t, both because of the motion of charge carrying vacancies and because of the presence of continuous dissociation and recombination of neutral vacancy pairs.

To simplify the treatment, the concentration of any extraneous traps for vacancies will be taken as vanishingly small and all vacancies present will be assumed to have come from a concentration of N neutral pairs. Then conservation of over-all electroneutrality requires

$$\int_0^L p(x,t)dx = \int_0^L n(x,t)dx \qquad (2.25)$$

where L is the length of the crystal with electrodes at $x = 0$ and $x = L$. The initial distribution of these neutral pairs before any dissociation occurs will be assumed to be uniform throughout the length of the crystal, but after some dissociation has taken place, the concentration of neutral pairs may be a function of x and t and will be denoted by n_p.

On dissociation, a neutral pair produces a mobile negative charge carrier (cation vacancy) and a mobile positive charge carrier (anion vacancy): the number of carriers produced per second at a position x will then be proportional to the product of $n_p(x)$ and a rate constant k_1 which will depend, inter alia, on temperature. Similarly, the rate of recombination will be given $k_2 n(x)p(x)$ at any time.

With these preliminary considerations, the equations of detailed balance including the effects of diffusion and motion under the influence

of an applied electric field E may be written as[46]

$$\frac{\partial p}{\partial t} = k_1 n_p - k_2 np + D \frac{\partial^2 p}{\partial x^2} - \mu \frac{\partial(pE)}{\partial x} \qquad (2.26)$$

$$\frac{\partial n}{\partial t} = k_1 n_p - k_2 np + D' \frac{\partial^2 n}{\partial x^2} - \mu' \frac{\partial(nE)}{\partial x} \qquad (2.27)$$

$$\frac{\partial n_p}{\partial t} = - k_1 n_p + k_2 np \qquad (2.28)$$

where μ, D represent the mobility and diffusion coefficient of the anion vacancy; μ', D' of the cation vacancy. The diffusion coefficient of the neutral pair is assumed to be negligibly small.

The charge densities must also satisfy the Poisson equation,

$$\left(\frac{\partial E}{\partial x}\right)_t = \frac{4\pi e(p-n)}{K} \qquad (2.29)$$

where K is the static dielectric constant in the absence of the free charges. If the voltage between the electrodes is $V(t)$ we also require that

$$V(t) = \int_0^L E(x,t)dx \qquad (2.30)$$

As we are to investigate the case where both electrodes are blocking

for both positive and negative carriers, no conduction current arising from the motion of either type of carrier can flow across the electrodes, and the pertinent boundary conditions are:

$$\mu p E - D \frac{\partial p}{\partial x} = 0 \quad \left.\right\} \quad \text{at } x = 0, L. \tag{2.31}$$

$$\mu' n E - D' \frac{\partial n}{\partial x} = 0 \tag{2.32}$$

These conditions have been selectively relaxed by Friauf[47] and by Jacobs et al.[51] in order to explain specific experimental results, but without marked success: the reason for their remaining discrepancies apparently lies elsewhere.

Equations (2.25) to (2.32) are the fundamental equations of the problem and it now remains to solve them for n,p, and E for a simple sinusoidal forcing voltage.

$$V(t) = V_1 e^{i\omega t} \tag{2.33}$$

Since the equations are non-linear, the current through the crystal will contain all harmonics of the forcing voltage and accurate solutions for n,p, and E would show that they would all involve zero frequency (static) components together with the fundamental and all its overtones. By taking V_1 sufficiently small the ratio of higher harmonic components to

the fundamental component in n, p, and E may be made negligible and expressions for these quantities can then take the truncated, linearized form

$$n(x,t) = n_o(x) + n_1(x)e^{i\omega t} \tag{2.34}$$

We shall also assume that the static concentrations of n_o and p_o are equal. Let their mutual value be x_o. It then follows from Eqs. (2.29) and (2.30) that $E_o = 0$ and that x_o is homogeneous throughout the crystal. This assumption cannot be completely correct because it leads to expressions for $\left| n_1 \right|$ and $\left| p_1 \right|$ which may be larger than x_o near the boundaries for large applied voltages. Physically, however, it is obvious that n_o and p_o must be equal to or greater than $\left| n_1 \right|$ and $\left| p_1 \right|$, respectively, at every point in the crystal; otherwise, the over-all concentrations n and p would go negative during part of each cycle. Near the elctrodes, then, n_o and p_o will actually be neither equal nor homogeneous. Nevertheless, since the polarization capacitance and conductance are directly determined by n_1, p_1, and E_1 and only indirectly by the coupling of these quantities to n_o, p_o, and E_o we can assume that the A.C. capacitance and conductance will not be greatly effected by the neglect of the x dependence of the latter static quantities.

Since n_o and p_o are assumed equal and homogeneous the static concentration of neutral pairs n_{po} will be simply $(N-x_o)$. We then find,

on substituting expressions of the form of Eq.(2.34) into the earlier equations, that

$$0 = -k_1(N-x_0) + k_2x_0^2 \tag{2.35}$$

$$i\omega p_1 = k_1 n_{p1} - k_2(p_1 + n_1)x_0 + D\frac{d^2p_1}{dx^2} - \mu x_0\frac{dE_1}{dx} \tag{2.36}$$

$$i\omega n_1 = k_1 n_{p1} - k_2(p_1 + n_1)x_0 + D'\frac{d^2n_1}{dx^2} - \mu'x_0\frac{dE_1}{dx} \tag{2.37}$$

$$i\omega n_{p1} = k_1 n_{p1} - k_2(n_1+p_1)x_0 \tag{2.38}$$

$$\int_0^L (n_1-p_1)dx = 0 \tag{2.39}$$

$$\frac{dE_1}{dx} = \frac{4\pi e(p_1-n_1)}{K} \tag{2.40}$$

$$V_1 = \int_0^L E_1 dx \tag{2.41}$$

$$\mu x_0 E_1 - D\frac{dp_1}{dx} = 0 \tag{2.42}$$

$$\mu'x_0 E_1 - D'\frac{dn_1}{dx} = 0 \tag{2.43}$$

at $x = 0,L$

Solving Eq.(2.38) for n_{p1}, we find that

$$n_{p1} = \lambda(p_1 + n_1) \tag{2.44}$$

where

$$\lambda = \frac{1}{\left[(k_1/k_2 x_o) + i\nu_\gamma\right]} \tag{2.45}$$

ν_γ is a dimensionless frequency variable given by

$$\nu_\gamma = \frac{\omega}{k_2 x_o} \tag{2.46}$$

The dimensionless, frequency dependent quantity λ is therefore, from Eq. (2.44), the ratio of the fundamental frequency component of charge bound in the neutral pairs to the fundamental component of free charge arising from such pairs.

To solve for the x dependence of n_1 and p_1 we now substitute Eqs. (2.40) and (2.46) into Eqs. (2.36) and (2.37). After collecting terms, the results may be written as

$$\frac{d^2 p_1}{dx^2} = a_{11} p_1 + a_{12} n_1 \tag{2.47}$$

$$\frac{d^2 n_1}{dx^2} = a_{21} p_1 + a_{22} n_1 \tag{2.48}$$

where

$$a_{11} = 2(M/L)^2 \left[1 + i(1+\lambda)\nu\right]$$

$$a_{12} = 2(M/L)^2 \left[-1 + i\lambda\nu\right]$$

$$a_{21} = 2(M/L)^2\left[-1+i\lambda\nu\phi\right]$$
$$a_{22} = 2(M/L)^2\left[1+i(1+\lambda)\phi\right]$$

and $(M/L)^2 = \dfrac{2\pi e x_0 \mu}{KD} = \dfrac{2\pi e^2 x_0}{KkT}$ (2.49)

$$\phi = \frac{\mu}{\mu'} = \frac{D}{D'}$$ (2.50)

$$= \frac{K\omega}{4\pi e x_0 \mu}$$ (2.51)

The Einstein relation $\dfrac{\mu}{D} = \dfrac{\mu'}{D'} = \dfrac{e}{kT}$ has been used in Eqs. (2.49) and (2.50). ν is another dimensionless frequency variable connected with the motion of the vacancies.

The characteristic equation associated with Eqs. (2.47) and (2.48) is easily solved. After simplification, its roots $\rho^{\pm}$ are given by

$$(\rho^{\pm})^2 = 2(M/L)^2\left[1+i(1+\lambda)\frac{(1+\phi)}{2}\nu\right.$$
$$\left. \pm \left\{1-\left[\lambda\frac{(\phi+1)}{2}\nu\right]^2 - (1+2\lambda)\left[\frac{(\phi-1)}{2}\nu\right]^2 - i\lambda(1+\phi)\nu\right\}^{\frac{1}{2}}\right]$$ (2.52)

There are thus four roots, and n_1 and p_1 will be given by the sum of four terms each of the form $\exp(\rho x)$. Considerable simplification is produced however when the symmetry of the problem is taken into account, and

it is seen that n_1 and p_1 must be odd functions of x about the centre of the crystal at L/2. They may therefore be written as

$$p_1 = B^+ \sinh\left[\rho^+(x-L/2)\right] + B^- \sinh\left[\rho^-(x-L/2)\right] \tag{2.53}$$

$$n_1 = A^+ \sinh\left[\rho^+(x-L/2)\right] + A^- \sinh\left[\rho^-(x-L/2)\right] \tag{2.54}$$

where A^+, A^-, B^+, and B^- are completely defined by Eqs. (2.40)-(2.43), (2.47) and (2.48).

The current entering and leaving the crystal may now be computed and used to evaluate the complex admittance of the whole crystal considered as a lumped circuit element.

The current density $j(x)$ within the crystal will then be given by the sum of a displacement term and two convection terms arising from the motion of the vacancies.

$$j(x) = \frac{K}{4\pi}\frac{\partial E}{\partial t} + e\left[\mu x_0 E_1 - D\cdot\frac{dp_1}{dx} + \mu' x_0 E_1 + D'\cdot\frac{dn_1}{dx}\right] \tag{2.55}$$

The total current density J_1 flowing into the crystal is obtained by taking a space average of $j(x)$ over the length of the crystal.

$$J_1 = Y_1 V_1 = \frac{i\omega K V_1}{4\pi L} + \frac{e}{L}(\mu + \mu')x_0 V_1$$
$$- D\left[p_1(L)-p_1(0)\right] + D'\left[n_1(L)-n_1(0)\right] \tag{2.56}$$

The admittance/cm.^{2}, Y_1 is made up of terms arising from the normal capacitance/cm.^{2}, C_g, of the crystal in the absence of macroscopic charge motion and terms coming from the space-charge parallel capacitance/cm.^{2} and conductance/cm.^{2}, C_p and G_p respectively. We now find Y_p, the admittance/cm.^{2} due to space-charge effects by substituting Eqs. (2.53) and (2.54) into (2.56).

$$Y_p = \frac{e(\mu + \mu')x_o}{L} + \frac{e\mu' x_o \cdot Z}{L} = G_p + i\omega C_p \qquad (2.57)$$

where $Z = \dfrac{\chi_A \left(1 - \dfrac{1}{\phi\gamma^-}\right) \sinh\eta^+ - \left(1 - \dfrac{1}{\phi\gamma^-}\right) \sinh\eta^-}{\left[\begin{array}{l} \chi_A \left(1 - \dfrac{1}{\gamma^+}\right)\left(\dfrac{L\rho^+}{\sqrt{2M}}\right)^{-2}(\eta^+ \cosh\eta^+ - \sinh\eta^+) \\[2ex] -\chi_A \eta^+ \cosh\eta^+ + \eta^- \cosh\eta^- \\[2ex] - \left(1 - \dfrac{1}{\gamma^-}\right)\left(\dfrac{L\rho^-}{\sqrt{2M}}\right)^{-2}(\eta^- \cosh\eta^- - \sinh\eta^-) \end{array}\right]}$

$$2.58$$

$$\gamma^- = \frac{A^+}{B^+} : \quad \gamma^- = \frac{A^-}{B^-} : \quad \chi_A = \frac{-A^+}{A^-} : \quad \eta^{\pm} = L\rho^{\pm}/2$$

$$C_g = \frac{K}{4\pi L} \qquad (2.59)$$

Eq. (2.58) is a very complicated complex, though general, formula for G_p and C_p, but we are interested only in the case where the anion vacancies are appreciably more mobile than the cation vacancies (as predicted for thallous chloride) i.e. where $\emptyset$ is large ($\geqslant 30$). Second and higher order terms in $\frac{1}{\emptyset}$ may then be neglected on expanding Eq. (2.52) which gives

$$(\rho^+)^2 = \infty \qquad (2.60)$$

$$(\rho^-)^2 = 2(M/L)^2(1+\delta)(1+i\nu) \qquad (2.61)$$

where $\delta = \frac{\lambda}{1+\lambda}$ i.e. the ratio of the fundamental frequency component of charge bound in neutral pairs to the fundamental component of total charge, free and bound. From Eq. (2.61) therefore

$$\eta^- = M\left[\tfrac{1}{2}(1+\delta)(1+i\nu)\right]^{\frac{1}{2}} \qquad (2.62)$$

For arbitrary dissociation, when δ may vary from 0 to 1, the expressions for C_p and G_p resulting from Eq. (2.58) are

$$C_p = \frac{C_o}{\eta_o^- \coth \eta_o^- - 1} \ \text{Real}\left[\frac{\eta^- - \tanh \eta^-}{\tanh \eta^- + i\nu \eta^-}\right] \qquad (2.63)$$

$$G_p = -\nu G_\infty \text{ Imag.}\left[\frac{\eta^- - \tanh\eta^-}{\tanh\eta^- + i\nu\eta^-}\right] \tag{2.64}$$

$$C_o = (\eta_o\coth\eta_o^- - 1)C_g \tag{2.65}$$

$$G_\infty = \frac{e\mu x_o}{L}\left(\frac{\phi - 1}{\phi}\right)$$

$$= \frac{e\mu x_o}{L} \quad \text{for large } \phi \tag{2.66}$$

η_o^- is the value of η^- when $\nu = 0$. It is equal to M for small dissociation ($\delta = 1$). C_o is the zero frequency limit of C_p and G_∞ is the limiting value of G_p of very high frequencies i.e. the normal ohmic conductance/cm.^{2} of the crystal which would be obtained at all frequencies were the electrodes not blocking.

For the practical case where $\frac{C_p}{C_g} \approx 10^2$, $\nu \leqslant 10^{-3}$ and $M \geqslant 10^4$, Eq. (2.63) reduces to

$$\frac{C_p}{C_g} = \frac{\sqrt{2}}{M(1+\delta)^{\frac{1}{2}}\nu^2} \tag{2.67}$$

Using Eqs.(2.51) and (2.66) we then obtain

$$C_p^2 = \frac{G_\infty^4 kT}{(1+\delta)Ke^2\pi^3 f^4} \cdot \frac{1}{x_o} \tag{2.68}$$

$$= \frac{\sigma_\infty^4 kT}{(1+\delta)Ke^2\pi^3 f^4 L^4} \cdot \frac{1}{x_o} \tag{2.69}$$

with σ_{∞}, the specific conductivity, equal to LG_{∞} and $\omega = 2\pi f$.

2.2.2. The Enthalpy of Formation of a Schottky Defect

The equilibrium defect concentration x_o varies with temperature as $\exp -\dfrac{\Delta H_s}{2kT}$ where ΔH_s is the enthalpy of formation of a Schottky pair. This quantity is therefore obtained by plotting $\log \left(\dfrac{T G_{\infty}^4}{C_p^2} \right)$ against $1/T$ under conditions where the restricted validity of Eq. (2.68) is assured.

The three principal factors resulting in deviation from this model are listed below.

(i) Although dissociation is normally considered to be small or complete, the temperature and frequency dependence of δ is unknown.

(ii) The electrodes are not completely blocking. This may be dealt with theoretically using the concept of a blocking parameter, as did Jacobs et al., but the inevitable electrolysis may completely alter the nature of the electrode and give rise to experimental irreproducibility.

(iii) The contribution of the cation vacancies may become appreciable as the temperature is raised.

Nevertheless it should be possible to work in certain temperature and frequency ranges where these three effects, in turn, may either be neglected or assigned a numerical degree of importance.
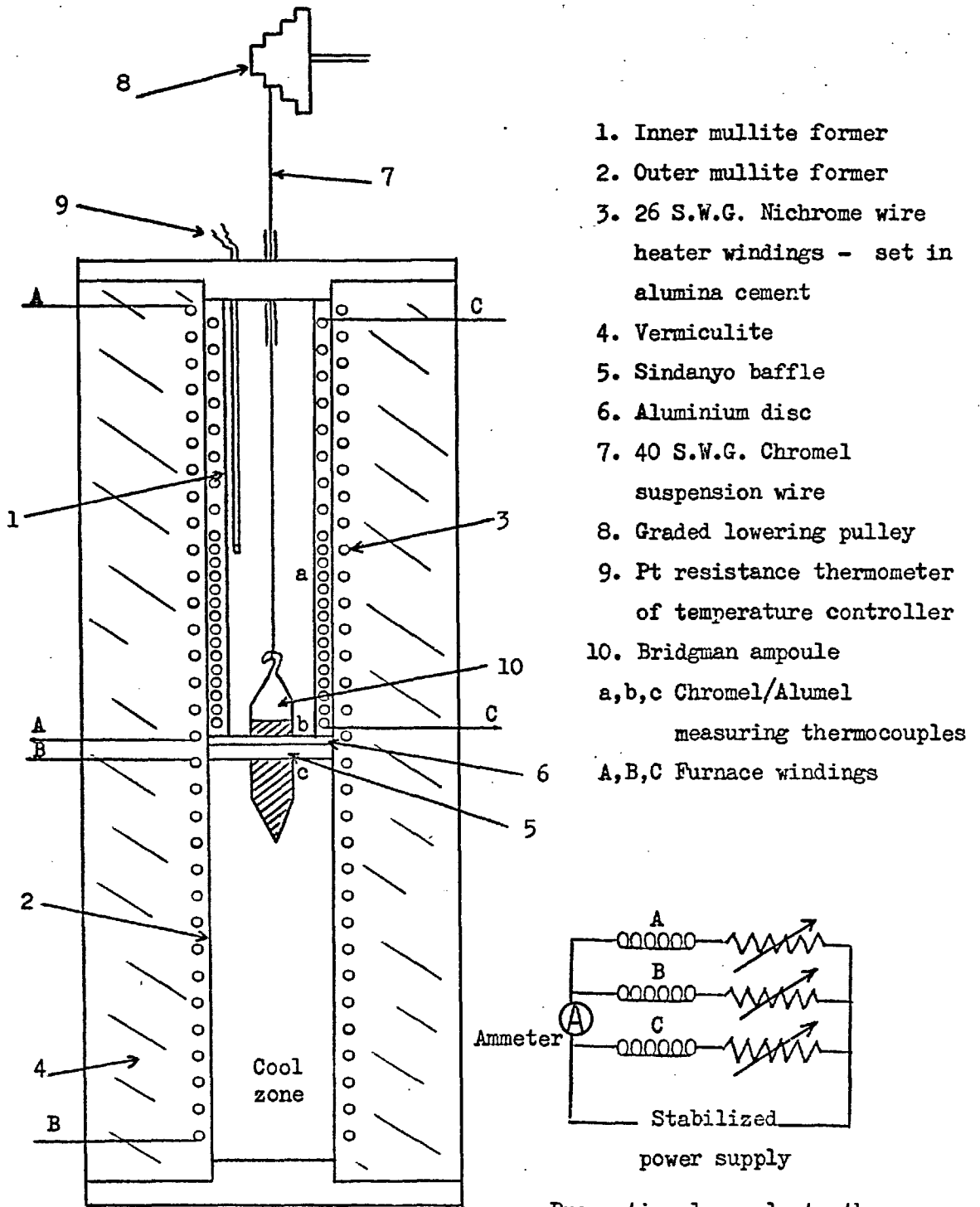
CHAPTER 3

EXPERIMENTAL PROCEDURES

3.1. CRYSTAL GROWTH

For the purpose of investigating the electrical conductivity and space-charge polarization effects in ionic systems, large single crystals of pure material are essential.   Such crystals may be grown from solution, the vapour or the melt but, in general, sizeable crystals are most easily obtained by growth from the melt.[63]   This process reduces the possibility of impurity inclusion since, other than the pure material, no substance, such as a solvent or carrier gas, is required to be present during the actual crystal growth.   In addition the passing of a solid/melt interface throughout the length of the material effects a single zone-refining pass which may reduce the impurity level in the central portion of the material by at least one order of magnitude[64].

The Bridgman[65] method which involves slowly lowering the melt, contained in a sealed ampoule, through a sharp temperature drop across the melting point of the material was found to be very suitable for the materials being studied.   The conical tip of the ampoule preferentially selects one of the seed crystallites first formed which subsequently finishes the single crystal.

A Bridgman furnace was therefore designed and constructed to operate most favourably in the temperature range, $600^{\circ}K. — 800^{\circ}K.$, which includes

1. Inner mullite former
2. Outer mullite former
3. 26 S.W.G. Nichrome wire
   heater windings – set in
   alumina cement
4. Vermiculite
5. Sindanyo baffle
6. Aluminium disc
7. 40 S.W.G. Chromel
   suspension wire
8. Graded lowering pulley
9. Pt resistance thermometer
   of temperature controller
10. Bridgman ampoule
a,b,c Chromel/Alumel
      measuring thermocouples
A,B,C Furnace windings

Proportional supply to the
heater windings.

THE BRIDGMAN FURNACE

Fig. (3.1)

the melting points of thallous chloride (703°K.), thallous bromide (733°K.), and lithium iodide (719°K.).

3.1.1. The Bridgman Furnace

The furnace is described in Fig. (3.1), but the more important features are listed below.

(i) The inner heating coil is wound differentially with a large number of turns per unit length at the baffle. This enables us to keep the upper half of the furnace at a much higher temperature than the lower half, providing a large heat input drop across the baffle.

(ii) The aluminium disc on the baffle ensures a horizontal isotherm at the upper surface of the baffle.

(iii) The baffle itself is made of $\frac{1}{4}$" 'Sindanyo' (thermal conductivity ≈ 0.0005 cals./cm.^{3}/$^{\circ}$K.). The temperature gradient of the baffle can therefore be maintained at $\sim 35^{\circ}$K./cm.

(iv) The over-all temperature of the furnace is controlled to within 0.2°K. by an A.E.I. platinium resistance thermometer controller, type RT3/R Mk.2, coupled with an A.E.I. thyristor, voltage-stabilized regulator, model RS4XVI. The proportion of current fed to the three separate furnace windings is regulated by air-cooled rheostats in series with the windings - see Fig. (3.1).

(v) Lowering of the ampoule, which must be uniformly slow, is achieved by use of a graded pulley and a suitably geared synchronous motor. This

arrangement provides lowering rates of 2, 6, 10, and 12 mms./hour.

3.2. MATERIAL PREPARATION

Prior to crystal growth, all material must be carefully purified and degassed. The procedures involved were varied from one material to another and between samples of the same material: they are outlined in this section.

3.2.1. Thallous Chloride

This poisonous, light-sensitive, material has an unusually high vapour pressure (1-2 mms. at 700°K.)[66] at temperatures approaching the melting point. The Bridgman technique, with its sealed ampoule, is therefore especially suitable for growing single crystals of thallous chloride. In addition, the high vapour pressure indicates that sublimation may be used for purification purposes. It may also be purified by recrystallization from water (3.2 gms./l. at 20°C. : 19.7 gms./l. at 100°C.)[67] or dilute hydrochloric acid.

EXPERIMENTAL

Thallous chloride of nominal purity 5N with respect to foreign cations was recrystallized twice from de-ionized water, dried over phosphorus pentoxide, and subsequently outgassed in a pyrex ampoule at 600°K. in a hard vacuum. Other samples were prepared similarly by recrystallization

from dilute hydrochloric acid, instead of water, or by direct sublimation
of the outgassed starting material. The ampoule was then sealed off under
vacuum and introduced into the upper half of the Bridgman furnace where
it was maintained at a temperature 50°K. above the melting point of the
material in order to homogenize the melt. It was apparent in trial
samples that the viscosity of the melt was quite high as small bubbles
resulting from inadequate outgassing of the starting material were unable
to rise quickly enough to the surface and became trapped in the ensuing
crystal. After 12 hours, therefore, the ampoule was lowered at 6 mms./hour
through a temperature drop across the baffle of 750°K./680°K. and into
the cooler annealing zone.

The glass–clear, colourless, monocrystalline boules so obtained were
machined on a lathe into right cylinders of height 5 – 8 mms. The origin of
every sample investigated is shown in Table (3.1).

Sample	Recrystallization	Outgassing ^{O}K	Sublimation
TC–1	H_2O	$300^{O} - 600^{O}$	–
TC–2	H_2O	$300^{O} - 600^{O}$	–
TC–3	–	600°	YES
TC–4	–	600°	YES
TC–5	HCl	$300^{O} - 600^{O}$	–
TC–6	HCl	$300^{O} - 600^{O}$	YES

The preparation of thallous chloride samples

Table (3.1)

Electrodes were applied to the plane parallel faces with either a soft graphite rod or an alcoholic colloidal graphite 'dag'. The material was handled throughout in the dark or in a subdued red light.

3.2.2. Thallous Bromide

This material is extremely similar to the chloride, both in its physical and chemical properties, but it is insufficently soluble in hot water for fractional crystallization to be an effective means of purification.

EXPERIMENTAL

5N pure thallous bromide, outgassed at $600^{\circ}K.$, was sublimed into a Bridgman ampoule and passed through the furnace using a similar procedure to that employed for the chloride. The lowering rate was 6 mms./hour and the temperature drop at the baffle was shifted to $785^{\circ}K./700^{\circ}K.$ The clear, pale yellow, monocrystals were again machined on a lathe to provide right cylindrical discs. Both TB-1 and TB-2 were prepared by this technique and were subsequently given colloidal graphite 'dag' electrode coatings.

3.2.3. Lithium Iodide

In contrast to the thallous salts, this material is extremely difficult to handle on account of its chemical nature. It is highly deliquescent, but may be obtained commercially as an approximate trihydrate with an impurity level of less than 100 p.p.m. with respect to metallic cations. Recrystallization

of this reagent grade material as a means of purification is unsatisfactory because lithium iodide is extremely soluble in water (>3 Kgms./l. at 30°C)[68] and all common polar organic solvents. Lithium iodide is also chemically unstable in aqueous environments. Thus it decomposes in moist air at room temperature, liberating free iodine, and is unstable even in dry air at temperatures much above its m.p. (719°K.). This means that its water of crystallization must be removed under vacuum at as low a temperature as feasible, otherwise the inevitable introduction of large amounts of oxide and hydroxide make subsequent purification tedious, if not impossible. The stoichiometric trihydrate, in fact, melts at about 350°K., losing water at the same temperature forming the monohydrate. The final molecule of water is not liberated, at atmospheric pressure, until the temperature is raised to 570°K[67]. Since the trihydrate is initially powdered to facilitate the loss of water, care must be taken to ensure that the material is not fused during the dehydration.

Several methods are available for crystal growth from the melt but the Kyropoulos[69] and Czochralski[70] methods, which also involve critical seeding techniques, together with the Stockbarger[71] method were all found to be unsuitable since the crystals have to be grown in open capsules which facilitates the decomposition of the melt. The Bridgman method, on the other hand, enables the growth ampoule to be sealed off under vacuum, thus limiting the loss of iodine to the small volume within the ampoule. It is essential, however, with this method that the ampoule be made of an easily
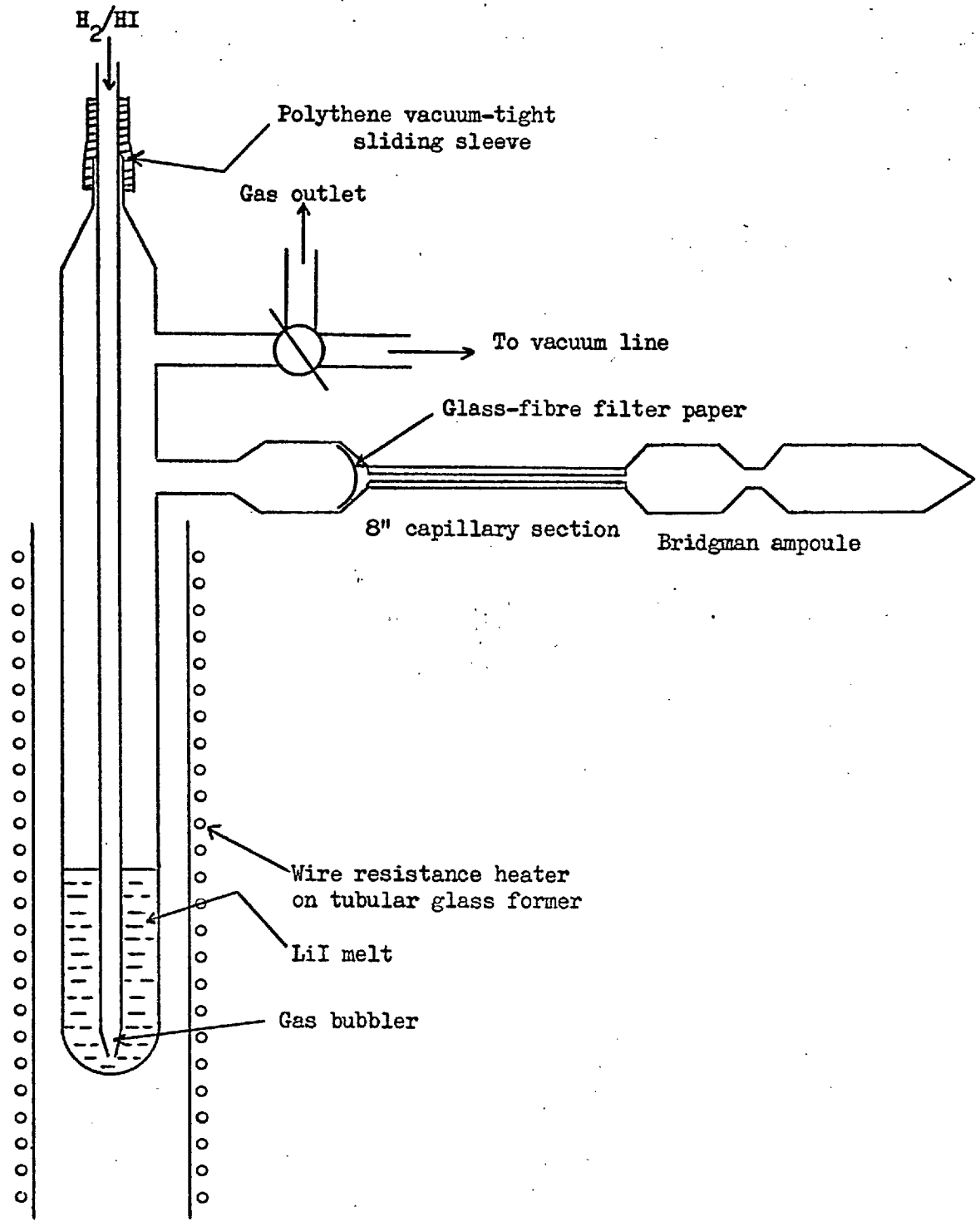
The Hydrogen/Hydrogen Iodide Purification Apparatus for Lithium
Iodide.

Fig. (3.2)

worked material since it must be provided with a conical tip for self-seeding

and also that the crystal must detach itself cleanly from the walls of any

container in which it is grown.   This is especially important with lithium

iodide since the crystal cleaves very readily in the (100) plane.

Borosilicate glass satisfies the first condition, but it is attacked by

lithium oxide.   It is therefore important that the melt is oxide-free and

that the glass ampoule is carefully outgassed – whereupon the crystal of

lithium iodide detaches itself quite readily upon cooling, without

internal cleavage.

It has often been the practice to coat the inner walls of growth

capsules with a material such as graphite to prevent sticking[63], but the

danger of such a layer cracking and flaking, causing subsequent polynucleation,

is an obvious one.   Such coatings were therefore avoided in this work.

EXPERIMENTAL

Lithium iodide trihydrate was finely powdered in a dry-box and

introduced into the purification apparatus – Fig. (3.2) – where it was

degassed at 320°K under a pressure of 10^{-5} mms. Hg for 20 hours to convert

the material into the anhydrous compound.   The temperature was then raised

slowly to 500°K. and the final traces of water removed completely over a

period of several hours.   The anhydrous lithium iodide was then heated to

50°K. above its m.p. and a dry gaseous mixture of hydrogen and hydrogen

iodide was bubbled through the melt for 2-3 hours.

The hydrogen iodide, prepared by warming a concentrated 'Analar' solution of hydriodic acid, was carried in a current of hydrogen and dried through phosphorus pentoxide. Moisture was excluded at the outlet by a second phosphorus pentoxide column and a silicone oil trap.

The purification apparatus was then turned through 90° thus enabling the capillary section to be heated and further outgassed in the tubular furnace. The purified melt was run into this section through the glass-fibre filter paper (Whatman G/A), subsequently undergoing capillary filtration and finally solidifying in the upper half of the Bridgman ampoule. In order to leave the lower section untouched prior to crystal growth a constriction was made in the ampoule to ensure solidification of the melt in the upper section. The ampoule was then evacuated and sealed.

The crystal was grown in the Bridgman furnace with a temperature differential at the baffle of $780^{\circ}K./700^{\circ}K.$ and a lowering rate of 6 mms./hour, which was found to be the most practical and effective rate for this material.

This technique furnished solid cylindrical boules, sometimes only bicrystals, which measured some 16 mms. in diameter and 30-40 mms. in length and which were capable of being cleaved to provide cuboidal single crystals with dimensions of about 5 mms. These crystals were absolutely clear and colourless.

Electrodes were applied to these crystals with a soft graphite rod since all good conductivity graphite 'dags' are dispersed in hydrophilic solvents and are therefore unsuitable.

Both the crystal-cleaving process and the electrode application were carried out under a dry nitrogen atmosphere in a glove-box.

### 3.2.4. Impurity Doped Lithium Iodide

In order to make a systematic study of impurity-controlled conduction, attempts were made to grow lithium iodide crystals containing divalent magnesium in solid solution. The simplest method of achieving this would be to add magnesium iodide to the lithium iodide before the dehydration procedure, but much of the magnesium reacting with the water present, precipitates from the crystal as the oxide. If large quantities (2-3 mole %) of magnesium iodide are used unclean crystal growth ensues, resulting in polycrystallization. Ideally therefore, anhydrous magnesium iodide needs to be added to molten, oxide-free lithium iodide, but experimentally this is extremely difficult to achieve on account of the highly deliquescent nature of both materials. Several crystals, however, were obtained by adding dehydrated magnesium iodide octohydrate to anhydrous lithium iodide and passing hydrogen iodide through the melt in the same way as for the undoped crystals. The anhydrous lithium iodide was from unused sections of previous single crystals.

The origin of every lithium iodide crystal investigated in this work is outlined in Table (3.2).

Table(3.2)

Origin of lithium iodide samples

Sample crystals	Starting material	Added to starting material	Dehydration and outgassing under 10^{-4} mms. Hg	H_2/HI passage
LI-1 (A-B)	Powdered $LiI.3H_2O$	-	Overnight at 325°K., slowly to m.p.	No
LI-2 (A-B)	Powdered $LiI.3H_2O$	-	Overnight at 325°K., slowly to m.p.	2 Hrs.
LI-3 (A-D)	Cleavings from LI-1 and LI-2	-	3 Hrs. at 325°K., slowly to m.p.	2 Hrs.
LI-DA(1-14)	Cleavings from crystals grown as LI3	0.1% MgI_2	3 Hrs. at 325°K., slowly to m.p.	3 Hrs.
LI-DB(1-3)	Cleavings from crystals grown as LI-3	1% MgI_2	3 Hrs. at 325°K., slowly to m.p.	3 Hrs.
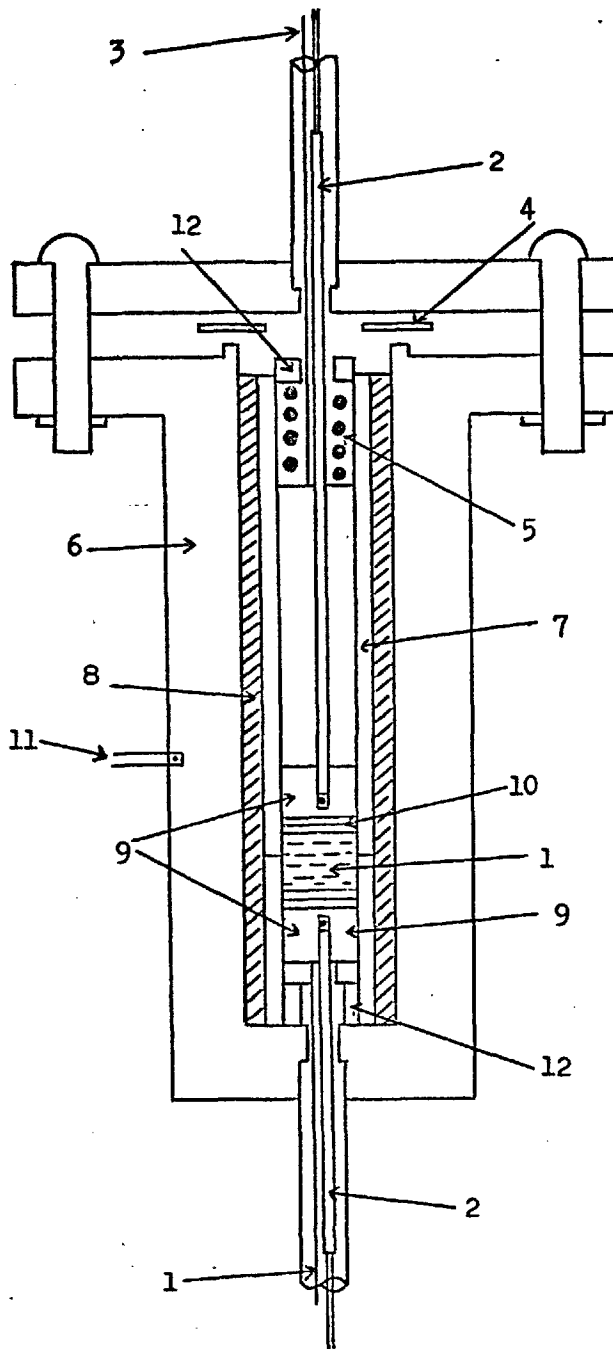
1. Single crystal samples
2. Pt/Pt-10%Rh thermocouples
   sheathed in alumina twin-
   bore tubing
3. Chromel lead wires
4. Aluminium gasket
5. Tension spring
6. Copper block body
7. Pyrex sleeve
8. Boron nitride sleeve
9. Polycrystalline graphite
   block electrodes
10. Platinum discs for lithium
    iodide
11. Temperature control
    thermocouple
12. Boron nitride insulating
    discs

The Conductance–Capacitance Cell.

Fig. (3.3)

3.3. ANALYSIS OF SAMPLES

Trace elements in the thallous halides and undoped lithium iodide were determined by emission spectroscopy. The magnesium in the doped samples was also determined by this method, but in addition a volumetric method was employed, using sodium E.D.T.A. as titrant and Eriochrome Black T as indicator, as this can detect magnesium in the presence of large quantities of alkali metal ions. Divalent and trivalent iron were estimated colorimetrically using ammonium thiocyanate.

3.4. THE SAMPLE MEASUREMENT CELL

All electrical measurements were carried out in the cell described in Fig. (3.3). Since both thallous chloride and thallous bromide have vapour pressures of several mms.Hg at the melting point, the cell was constructed with minimum void space thus reducing sublimation to neglible proportions. This was facilitated by the use of a machinable grade of densified boron nitride as the insulating sleeve. In order to eliminate stray capacitance from the measuring circuit the Pt/Pt10%Rh thermocouples were insulated from the graphite block electrodes by thin pyrex sheaths. The entire electrode/sample/sleeve system was then encased in a solid copper body which served the dual purpose of guard electrode and temperature equalizer.

The over-all temperature was controlled to within $0.1^{\circ}K$. by a Philips single point recorder, type PR2210 A/21, adapted for use as an automatic
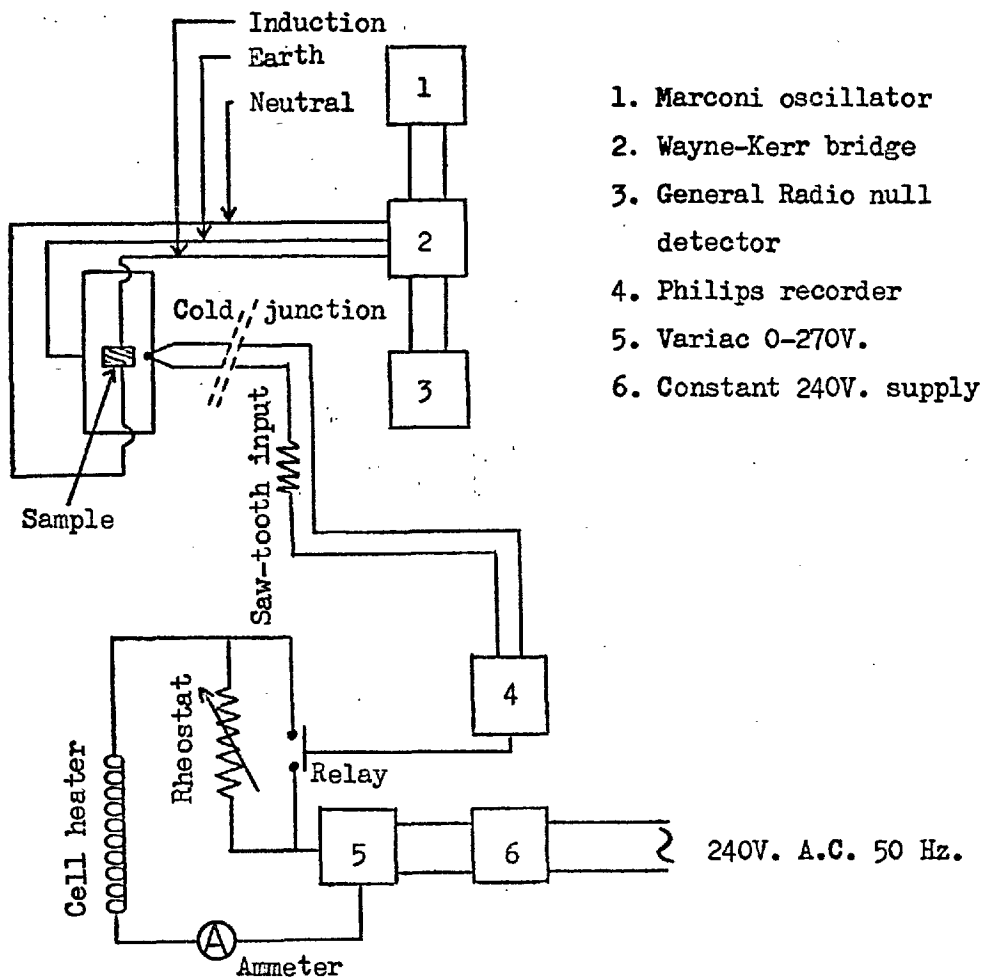
temperature controller. The input to the relay was given by a chromel/
alumel thermocouple, embedded in a glass pod (for electrical insulation)
in the copper body of the cell, in series with a transistorized saw-tooth
microvolt source, which provided proportional control in the range $\pm 5^{\circ}$K.
about the required temperature.

In operation with the thallous halides the cell was first evacuated
to 10^{-3} mms. Hg, then flushed and filled with dry argon before it was
heated. This precaution effectively inhibited sublimation even at
temperatures only 10°K. below the melting point.

However, the deliquescent nature of lithium iodide necessitated
outgassing the cell overnight at room temperature before slowly heating
the sample still under hard vacuum to 550°K. The cell was then flushed
several times, by evacuating and re-filling with dry argon, before being
finally filled to one atmosphere pressure. Subsequently throughout the
electrical investigation the cell was evacuated for one minute every hour
and re-filled with dry argon.

3.5. CONDUCTANCE AND CAPACITANCE MEASUREMENTS

The conductance and capacitance of samples were measured as a function
of frequency normally between 500 and 18000Hz., but exceptionally to
200 KHz., at temperatures ranging from just above room temperature to just
below the melting point of the sample, and also as a function of temperature
at selected frequencies.

Induction
Earth
Neutral

1. Marconi oscillator
2. Wayne-Kerr bridge
3. General Radio null
   detector
4. Philips recorder
5. Variac 0–270V.
6. Constant 240V. supply

Cold junction

Sample

Saw-tooth input

Cell heater

Rheostat

Relay

Ammeter

240V. A.C. 50 Hz.

The Electrical Circuit

Fig. (3.4)

In order for equilibrium to be attained, readings were normally taken at hourly intervals, but in lower temperature annealing studies with thallous chloride, measurements were spread over several days.

A Marconi R.C. oscillator signal generator (TF 1370) supplying 3 mV. - 30 V. injected a sinusoidal voltage into high (B601) and low (B221) frequency Wayne-Kerr conductivity bridges with a Telequipment oscilloscope (D43) as null detector. The oscilloscope was initially employed to detect the presence of any harmonics, but once it had been shown that harmonics were not produced in the sample it was replaced by a General Radio frequency-tuned amplifier and null detector (1232-A).

The Pt/Pt10%Rh thermocouple outputs were measured on a Cambridge microstep potentiometer. Throughout the temperature range of study the two thermocouples agreed to within 0.2°K. : the sample temperature was therefore taken as a mean of the two.

All leads in the measuring circuit were carefully screened to eliminate any stray capacitance, and a common earth was employed for the complete electrical circuit which is represented diagrammatically in Fig. (3.4).

CHAPTER 4

RESULTS AND DISCUSSION

4.1 THE ELECTRICAL CONDUCTIVITY OF THALLOUS CHLORIDE

The isothermal specific conductivity σ displayed a weak frequency dependence, asymptoting to a high frequency limiting value σ_∞ in accordance with the space-charge model. In the most extreme cases studied the conductivity was constant to within 0.4% of the observed limit above 15 KHz. and fell to about 0.9 σ_∞ at 500 Hz.

In addition to these measurements the conductivity was measured as a function of temperature at a number of fixed frequencies. A selection of these data for the samples listed in Table (3.1) is plotted as log $\sigma_\infty T$ against $\frac{1}{T}$ in Fig. (4.1) at 20 KHz. where the conductivity is essentially σ_∞ at all temperatures.

4.1.1. The Intrinsic Region

For freshly grown crystals the log $\sigma_\infty T$ against $\frac{1}{T}$ plot is linear from 330°K. to about 600°K., above which temperature the line curves smoothly upwards. Accordingly between 330°K. and 600°K. the intrinsic conductivity may be represented by

$$\sigma_\infty T = \sigma_0 \exp \frac{-\Delta H_1}{kT} \tag{4.1}$$

with $\Delta H_1 = 0.750 \pm 0.005$ eV. in excellent agreement with Friauf's value[53]
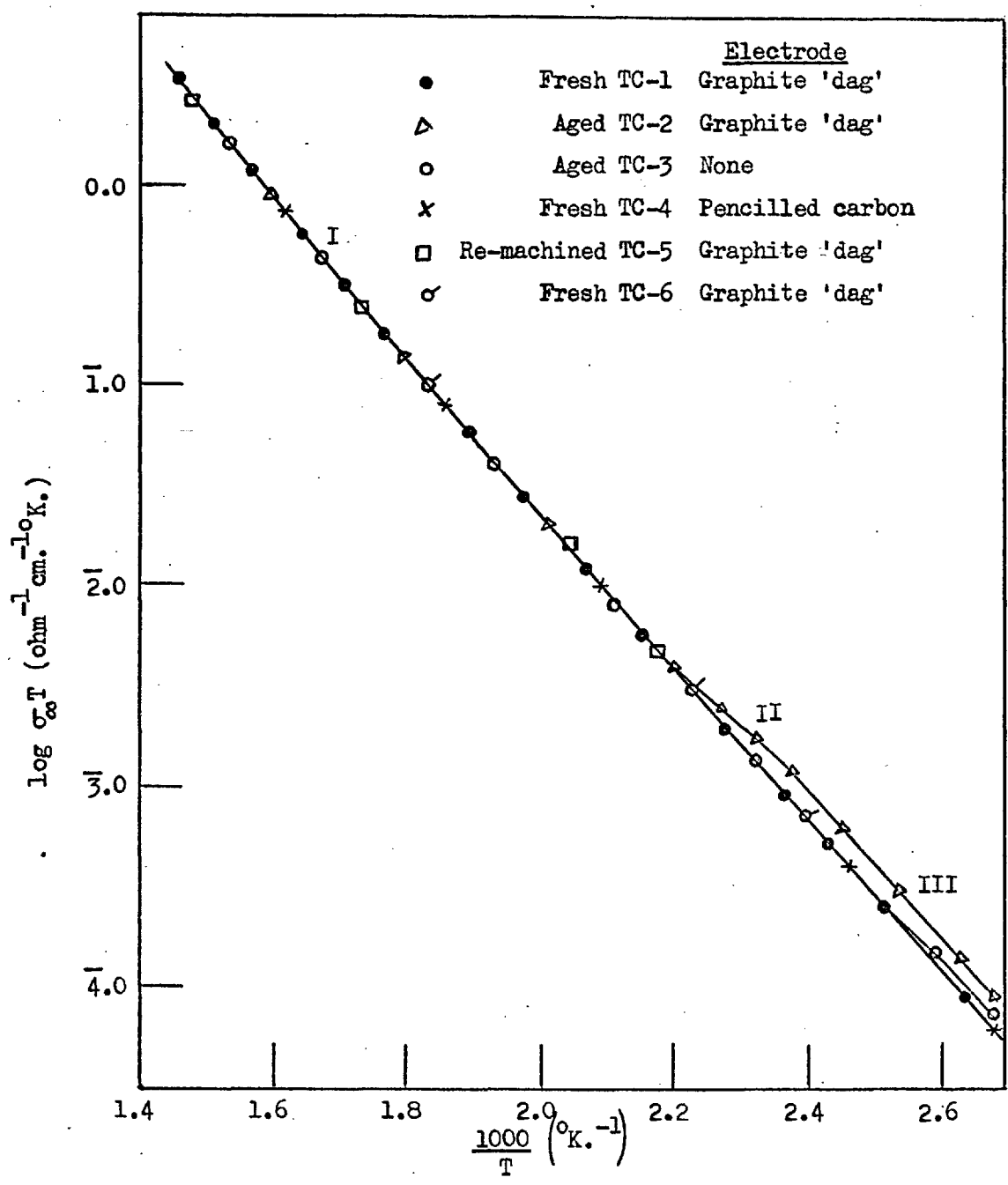
The conductivity of thallous chloride at 20 KHz. Superimposed data points are omitted for clarity. All samples give the same results in region I.

Fig. (4.1)

of 0.76 eV. In addition, the absolute value of the conductivity σ (575°K.), 4.06 x 10^{-4}ohm^{-1}cm.$^{-1}$, lies close to Friauf's value of 3.8 x 10^{-4}ohm^{-1}cm.$^{-1}$ - Table (1.1) - emphasizing the reproducibility that may be obtained with pure single crystals.

The linearity of the plot in this region indicates the presence of only one mobile charge carrier. Were this not so and two mobile carriers contributed to the conduction, the activation enthalpy $\left(\Delta H_f + \Delta H_m \right)$ for one carrier would necessarily equal that of the other.

All samples, TC-1 to TC-6, provide conductivity curves which are superimposable within experimental error throughout region I. Such reproducibility is uncommon in this field but was in part made possible in the present work by the use of large single crystals whose dimensions could be accurately measured with a micrometer. Discrepancies of up to 100% amongst different workers investigating the same material have, in general, been ascribed both to this geometric factor and to the varying electrode coatings employed, impurity content not being of prime importance in region I. In order to assess such electrode effects, the conductivities of some samples were first measured without any conducting coating, and then re-measured with graphite 'dag' electrodes. These graphite coatings were then r e m o v e d by machining about 1 mm. off each parallel face of the sample disc. Further electrodes were then applied by pencilling with a soft carbon rod and the conductivity re-determined. In all cases the specific conductivity agreed to within 2% - see Fig. (4.1). Active
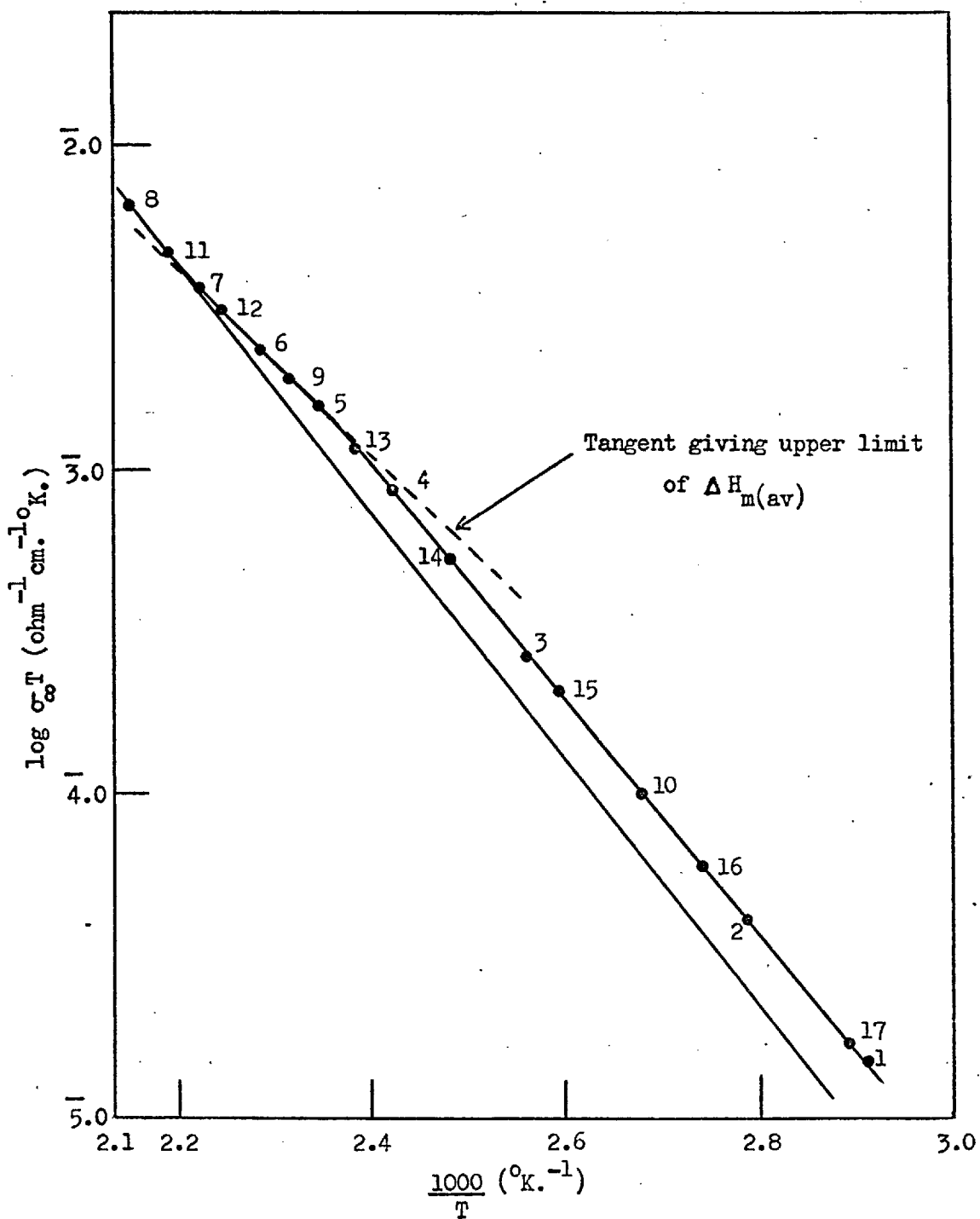
TC-2. Low temperature annealing run. The experimental points were
recorded in the numbered order, points 1 and 17 being separated by 4 days.

Fig. (4.2)

metallic coatings, such as silver and gold, were avoided in order to
maintain the blocking electrode conditions vital for capacitance studies.

4.1.2. The Extrinsic and Association Regions

On ageing, through time and temperature cycling procedures, the samples
appeared to develop characteristic regions II and III in the conductivity
plots - the so-called extrinsic and association regions respectively. These
regions were completely reproducible during heating and cooling cycles
lasting for several days, but became more pronounced over a period of months
when stored in the dark at room temperature in a dessicator. In Fig. (4.2)
the time interval between measurements was varied from 2 - 48 hours in
order to detect any time-dependent annealing effects - there were none.
Normally, after a change of temperature it was only necessary to wait for
one hour before taking readings, this time interval being quite adequate
for the attainment of equilibrium as evidenced by the absence of transients.

Region II was in each case too short for a direct determination of the
enthalpy of mobility of the charge-carrying species, but tangents drawn to
the central portion of region II gave an upper limit of 0.45 eV. for ΔH_m.

Region III, however, is long and straight and is characterized by an
enthalpy of activation $(\Delta H_a + \Delta H_m) = 0.64 \pm 0.02$ eV. Since Friauf's
diffusion data indicate that the conduction is almost exclusively anionic
at region III temperatures $\dfrac{D^*_{Cl}}{D^*_{Tl}} = 652$ at $380^oK.$, it is probable that
on ageing the samples have acquired a polyvalent anionic impurity which,

being only slightly soluble in the host, tends to form complexes with vacant anion sites. We suppose this impurity to be the oxide ion. Spectrochemical analyses of the samples indicated a cationic impurity of less than 5 p.p.m. but detection of the small amount of oxide required to be present was not practicable. If we take $\Delta H_{m(av)}$, calculated later, as 0.09 eV. we obtain a value of 0.55 eV. for the binding enthalpy of an oxide ion – vacant anion site complex which is typical for a large ion[52].

Deliberate doping with oxide[7,33,72] in other crystal systems has not proved particularly successful because of the difficulty in estimating O^{2-} apart from OH^-. In addition to this, any reluctance on the part of the oxide ion to pass into substitutional solid solution, which is evident in potassium chloride[7], would immediately reduce the effectiveness of this approach. This may well be the case for thallous chloride as Christy[58] has shown that the sulphide ion S^{2-}, which resembles the oxide ion both physically and chemically, is only sparingly soluble in the host thallous chloride lattice. Christy[73] also claimed that polyvalent cations were equally insoluble in this lattice and although Hauffe and Griessbach-Vierk[56] found that the conductivity of lead-doped thallous chloride decreased with increasing impurity concentration, they reported no region II and their results, obtained as they were on pressed material, indicate that only a fraction of this amount was, in fact, incorporated substitutionally. Hoodless[21] has also experienced difficulty in dissolving polyvalent cations in cesium chloride where the transport number of the cation is approximately
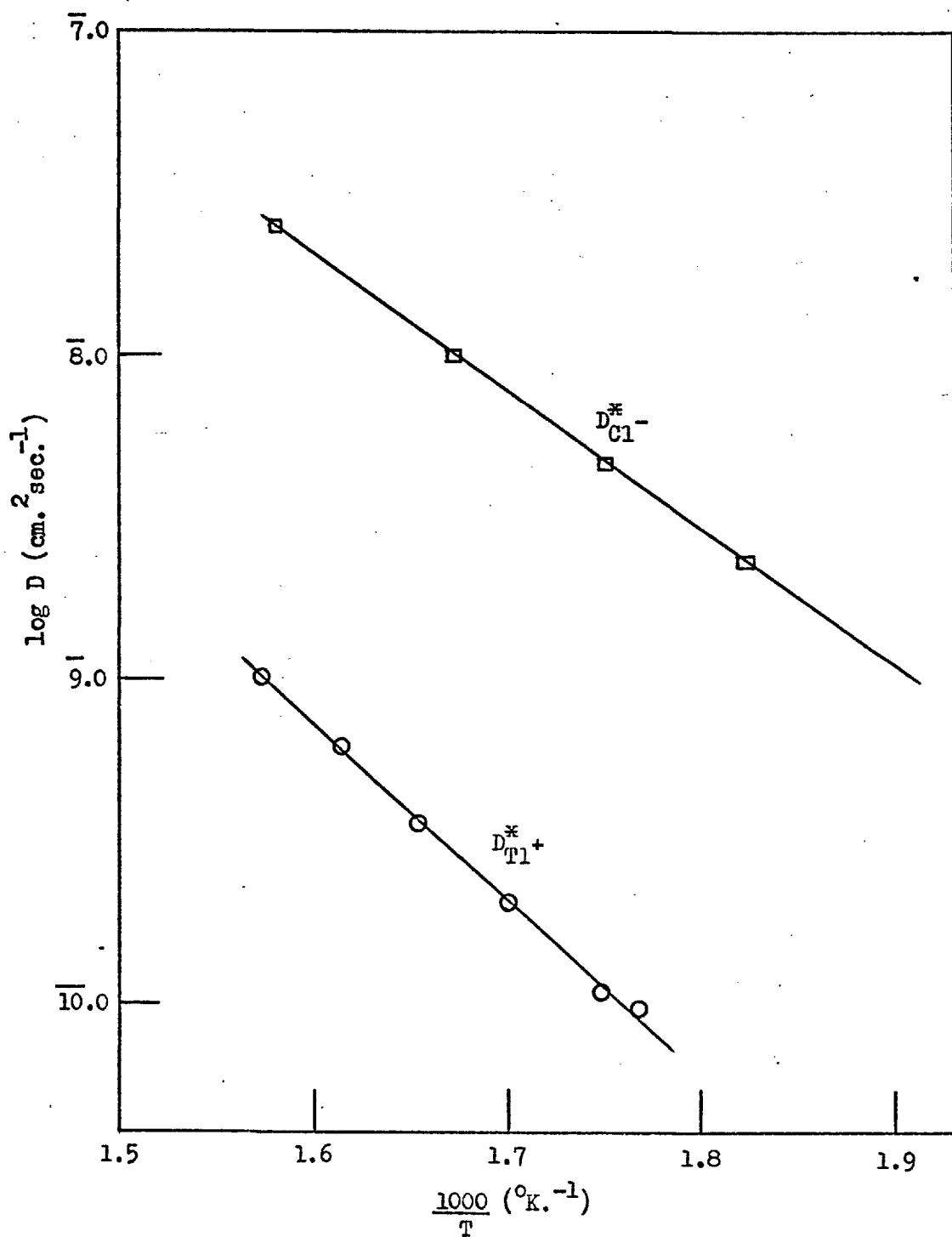
Diffusion coefficients for TlCl from reference 57.

Fig. (4.3)

0.4, obtaining only a short irreproducible region II. This restricted solubility of most impurity ions in the cesium chloride structure rules out accurate analysis of the extrinsic region but provides an intrinsic region that is long and reproducible.

Hauffe's and Friauf's data, together with our vacancy-oxide association can therefore be explained if anion vacancies are the predominant charge carriers in thallous chloride. The presence of such carriers is confirmed in the next section by diffusion correlation arguments.

4.2. SELF-DIFFUSION IN THALLOUS CHLORIDE

Friauf[57] has measured the temperature dependence of the self-diffusion coefficients of the anion and cation in thallous chloride using radioactive ^{36}Cl and ^{207}Tl. His results are illustrated in Fig. (4.3). The anion and cation are associated respectively with activation enthalpies ΔH_D of 0.76 eV. and 1.07 eV. respectively, whereas ϕ, the ratio of anion mobility to cation mobility, is given by $0.1124 \exp\left(\frac{3380}{T}\right)$ which means that the thallium ion carries about 10% of the total conduction current near the melting point. This strongly suggests Schottky disorder since the presence of interstitial ions on both sub-lattices, or even one sub-lattice, is extremely unlikely as pointed out in section 2.1.3., on account of the large size of both ions.

Frenkel disorder is more favourable in structures, such as the silver halides, where the co-ordination number of the cation is larger and the
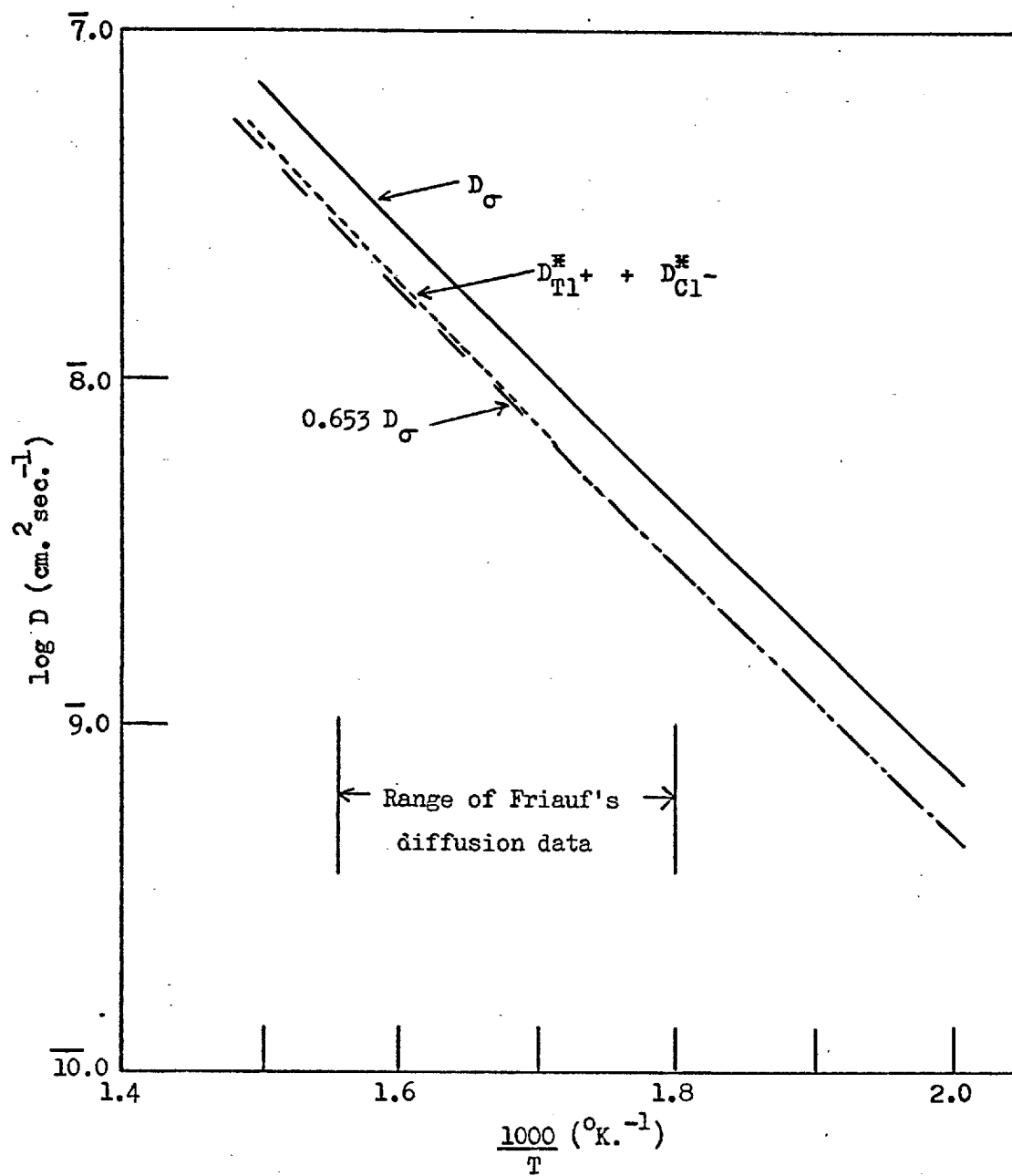
Correlation between ionic conductivity and diffusion in the simple cubic thallous chloride lattice.

Fig. (4.4)

greater radius ratio of the two ions is capable of providing room for one type of ion in an interstitial site on the conjugate sub-lattice. Thus cesium chloride[21], cesium bromide[74] and cesium iodide[74], which possess the simple cubic structure, all exhibit Schottky disorder with the transport number of the cation about 0.4 in each case.

The greater mobility of the anion may seem surprising in view of the relative sizes of the ions. (The appropriate Goldscmidt radii, in Angstrom units, are[57] Cs^+ = 1.65, Tl^+ = 1.49, Cl^- = 1.81, Br^- = 1.96, and I^- = 2.20). In fact, the coulombic terms at the saddle point involved in a jump into a vacancy are the same to a first approximation, no matter which ion is jumping, as these are determined for both anion and cation in the cesium chloride lattice, by the interactions of the jumping ion, positioned at a face-centre on the conjugate sub-lattice, with the nearest neighbour ions of opposite charge which are situated one each at the four corners of the same face. Such a configuration involves considerable distortion of the lattice and the more important factor, therefore, is probably the relaxation and polarization of the surrounding ions and the polarizability of the jumping ion itself. We shall return to this problem when discussing the conductivity of thallous bromide.

4.2.1. The Calculation of $D\sigma$

The sum $\left(D^*_{Tl^+} + D^*_{Cl^-} \right)$ of the cation and anion tracer diffusion coefficients is compared in Fig. (4.4) with the theoretical value D_σ of

this sum calculated from the present conductivity results using Eq. (2.23).

$$\frac{\sigma}{D_\sigma} = \frac{Ne^2}{kT}$$

The upward sweep of the conductivity plot above $600^\circ K$ is then seen to be a direct consequence of the increasing cationic transference number.

Vacancy motion on a simple cubic lattice is characterized by a jump correlation factor of 0.653 and a displacement factor equal to 1 ; thus in the ideal case for Schottky disorder the values of $\left(D^{\mathbf{x}}_{Tl^+} + D^{\mathbf{x}}_{Cl^-} \right)$ should coincide with the values of $0.653 \, D_\sigma$ as conduction in thallous chloride is known to be purely ionic[59] giving $f_c = 1$ as well. As seen in Fig. (4.4) the agreement is remarkably good, and may be taken as confirmation of the vacancy mechanism, but as the temperature is raised the correlation factor increases towards 0.73 at $680^\circ K$. This may in fact be a consequence of the need to extrapolate the diffusion data, but a realistic explanation of this observation is the formation of neutral vacancy pairs which can contribute to diffusion but not to the conductivity. On the basis of this explanation the product of the concentration times the mobility of these vacancy pairs evidently increases with temperature, but the terms can not be separated with our present information. This is an obvious pitfall, therefore, in separating the intrinsic curve into anionic and cationic components alone, as Dawson and Barr[75] have done, in order to determine the ion transference numbers.
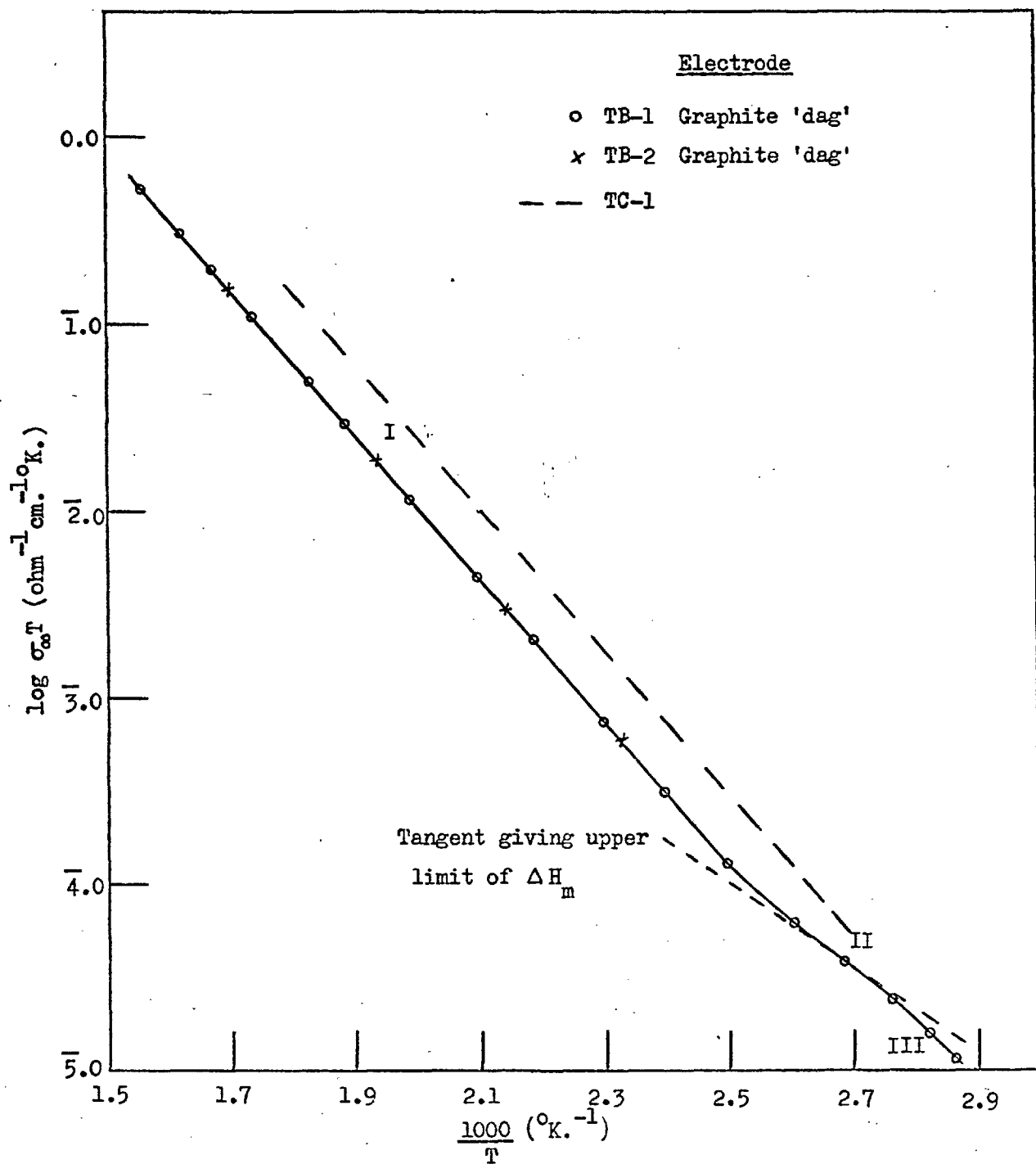
The ionic conductivity of thallous bromide at 20 KHz.

Fig. (4.5)

Ionic conduction in thallous chloride is thus due to the presence of Schottky defects with the vacant anion site the predominant charge carrier at all temperatures. In this material therefore

$$\Delta H_1 = \Delta H_{f(av)} + \Delta H_{m(av)} = 0.755 \pm 0.005 \text{ eV.} \qquad (4.2)$$

4.3. THE ELECTRICAL CONDUCTIVITY OF THALLOUS BROMIDE

The conductivity of thallous bromide is shown in Fig. (4.5) to be lower than that of thallous chloride at all temperatures, although the shape of the log σT against $\frac{1}{T}$ plot is very similar. Both samples, TB-1 and TB-2, gave superimposable results in the long intrinsic region and provided values of the conductivity which were reproducible within experimental error as with thallous chloride. Region I appears to be linear over a wide temperature range in support of Hermann's conclusion that the bromine ion is the dominant charge carrier. In fact this linearity appears to extend to a higher temperature than with the chloride indicating a higher value of $\emptyset = \left(\dfrac{\mu_{anion}}{\mu_{cation}} \right)$ at all temperatures. This is completely analogous to the situation in the cesium halides where the transport number of the anion at any particular temperature increases as one passes from the chloride $\rightarrow$ bromide $\rightarrow$ iodide. In addition, $\sigma(500^{\circ}\text{K.}) = 2.0 \times 10^{-5} \text{ohm}^{-1}\text{cm.}^{-1}$, and the region is characterized by an activation enthalpy $\Delta H_1 = 0.75$ eV. This latter value agrees extremely

well with Phipps and Partridge's[55] value of 0.75 eV., but the value of σ is twice that obtained by Phipps and three times that by Hermann[60], both of whom used pressed material.   As with thallous chloride our results emphasize the greater reproducibility and higher more accurate, values of the conductivity which may be obtained with single crystals.

The activation enthalpy ΔH_1 is identical to that of the chloride, indicating a similar conduction mechanism.   By analogy with the cesium halides, therefore it would appear likely that Schottky disorder exists in thallous bromide with the bromine ion vacancy as the dominant charge carrier.

Region II is again too short for direct analysis although it provides an upper limit of 0.40 eV. for ΔH_m.   Region III is associated with an enthalpy of 0.66 eV. which is again very close to that for the chloride and not unexpected in view of the fact that it probably represents the binding energy of an oxide ion-anion vacancy complex in a similar environment.

In the absence of self-diffusion data for thallous bromide it is difficult to carry the argument for Schottky disorder any further, but a direct comparison of the conductivity of the bromide with that of the chloride helps to emphasize the important factors involved in vacancy motion and clarifies the expected close relationship between the two materials.

4.3.1.   The Conductivity Relation

The sum of the enthalpies of formation and mobility of the chlorine

ion vacancy in thallous chloride, calculated from the present conductivity results, is equal to 0.755 eV. which agrees very closely with the value of 0.76 eV. calculated from Friauf's diffusion data in Fig. (4.3). Intrinsic conduction on thallous bromide is also associated with an activation enthalpy of 0.75 eV. which means that,

$$\left[\Delta H_{f(av)} + \Delta H_{m(av)}\right] TlCl \approx \left[\Delta H_{f(av)} + \Delta H_{m(av)}\right] TlBr \qquad (4.3)$$

if we assume that the vacant anion site is the predominant charge carrier in thallous bromide.

Boswarva[22] has calculated the energy of formation of Schottky defects in the cesium halides, all of which except the fluoride possess the simple cubic structure of the thallous halides.   He considered in detail the effect of various elastic and polarization terms on the final value ΔH_s of the Schottky defect formation energy, but a typical set of values is given in Table (4.1)

Crystal	ΔH_s eV.
CsF	1.920
CsCl	1.337
CsBr	1.267
CsI	1.334

Calculated energies of formation of a Schottky defect in the cesium halides.[22]

Table (4.1)

The values were calculated using the Born ionic model with a Born-Mayer repulsive potential, but included Brauer elastic terms and deformation dipoles. The important aspect of this table is that ΔH_s is very similar for the chloride, bromide, and iodide, but is noticeably different for the fluoride where a different crystalline structure is known to exist. This, as Boswarva pointed out, is not brought about by a coincidental balancing of the terms that make up ΔH_s for the chloride, bromide and iodide, but rather by a marked similarity between these three substances for each individual term that together determine ΔH_s. The thallous ion is comparable in size to the cesium ion and a similar trend is to be expected in the thallous halides.

If $\Delta H_s(TlCl) \approx \Delta H_s(TlBr)$, and $\Delta H_{f(cv)} \approx \Delta H_{f(av)}$, as indicated by Boswarva, then

$$\Delta H_{f(av)}^{TlCl} \approx \Delta H_{f(av)}^{TlBr}$$

It now remains to explain why $\Delta H_{m(av)}^{TlCl} \approx \Delta H_{m(av)}^{TlBr}$.

It has already been mentioned that for a vacancy mechanism the polarizability of an ion is important in determining its mobility. The polarization energy contributes a positive term to the jump activation energy, for the ion in the ground state is appreciably polarized by the electric field of the neighbouring vacancy, whereas there is no polarization

in the activated state since the field is zero. Hence ions of small polarizability are favoured by this term. Since the polarizabilities are in the order $Tl^+ > Br^- > Cl^-$ [76], the jump preference is in the reverse order, which would explain the incongruous size/mobility relation. It is evident, however, that this is only a partial, tentative explanation and detailed calculations are needed to make accurate predictions.

The displacement of thallium ions at the saddle-point would tend to favour the smaller chlorine ion in preference to the bromine ion, but on the other hand there would be a larger relaxation cum polarization energy compensation for the newly formed vacant anion site in the case of the latter.

However, the energy of activation for an ion jumping into a vacancy is determined by the energy change in the surrounding lattice as a whole when the ion moves from its initial site into the saddle-point. The calculations of Boswarva[22] on the cesium halides indicate that this energy is much the same whether a chlorine ion or a bromine ion is jumping. Close agreement is therefore to be expected for the anion diffusion activation energies of the two thallous halides, but the identity of the two values is probably coincidental.

The absolute value of the conductivity, nevertheless, is lower for the bromide in the intrinsic range and must be a direct consequence of a lower pre-exponental mobility factor.

4.3.2. The Ion Mass Effect

The ratio $\dfrac{\sigma(TlCl)}{\sigma(TlBr)}$ is about 2.37 instead of 1.51 as calculated from classical rate theory[23], assuming the jump distance to be approximately the same for both materials, where the jump probability ω is inversely proportional to the square root of the jumping mass M. According to Eq. (1.9)

$$\omega = \nu \exp\left[\frac{-\Delta G_m}{kT}\right]$$

where ν is of the order of the mean vibrational frequency of an ion about its equilibrium site given by the simple harmonic expression $\dfrac{1}{2\pi}\sqrt{\dfrac{\lambda}{M}}$. However, this rigorous dependence on $M^{-\frac{1}{2}}$ is seldom obeyed even for two isotopes and for the interstitial diffusion of hydrogen and deuterium in tantalum[77] the conductivity ratio is found to be 80 instead of $\sqrt{2}$ although the jump activation energy is the same. Nevertheless, the mass effect goes some way towards explaining the reduced conductivity in the bromide as compared with the chloride.

4.4. SPACE-CHARGE POLARIZATION IN THALLOUS CHLORIDE

The space-charge model of Chapter 2 was developed for the situation where the anion vacancies are, at least, 30 times as mobile as the cation vacancies which is the case in thallous chloride up to 600°K. Accordingly,

Eqs. (2.63) and (2.64) are applicable to this substance at temperatures below 600°K and we have

$$C_p = C_g \text{ Real } \left[\frac{\eta^- - \tanh \eta^-}{\tanh \eta^- + i \gamma \eta^-} \right] \qquad (2.63)$$

$$\text{and } G_p = -\gamma G_\infty \text{ Imag.} \left[\frac{\eta^- - \tanh \eta^-}{\tanh \eta^- + i \gamma \eta^-} \right] \qquad (2.64)$$

However, these equations themselves are complicated and they can only be simplified, as stated in Chapter 2, for the case where $\gamma \leqslant 10^{-3}$ and $M \geqslant 10^4$. In addition, C_p/C_g is required to be $< 10^4$ in Eq. (2.63) and $G_p/G_\infty < 10^{-1}$ in Eq. (2.64) for all practical cases where these two ratios can be measured accurately i.e. where $C_p/C_g > 2$ and $G_p/G_\infty < 0.9$. The conditions for γ and M are satisfied in thallous chloride at all temperatures above 450°K with the frequency of the applied A.C. field less than 10 KHz. However, the studies were limited to frequencies above 500 Hz. in order to avoid the spurious, low frequency, electrolytic effects described in the next section and the observed value of G_p/G_∞ never fell below 0.9, even in the most extreme cases studied. The frequency dependence of the conductivity was thus too weak for independent analysis on the space-charge model, according to Eq. (2.64), although the limited data are consistent with this model.

C_p/C_g , on the other hand, varied from 2 - 10^4 over the specified temperature (450°K. - 600°K.) and frequency (500 Hz - 5 KHz) ranges where the conditions for $\emptyset$, and M are satisfied. The space-charge capacitance
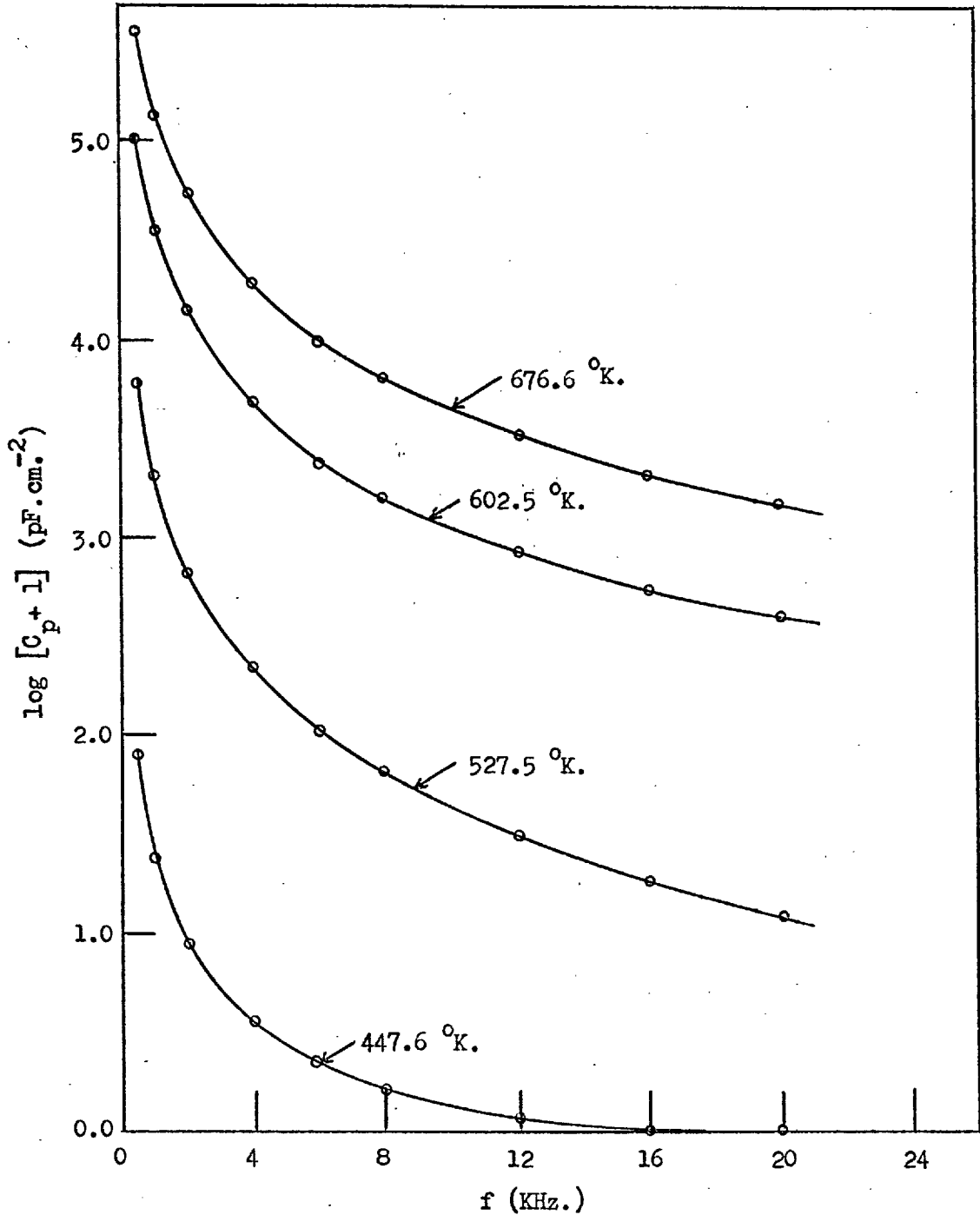
TC-1. Log $(C_p + 1)$ against f showing the approach to zero of C_p at low temperatures and high frequencies. Data points at other temperatures and frequencies are omitted for clarity.

Fig. (4.6)

is therefore suitable for analysis on our model using Eq. (2.63).in its reduced form of Chapter 2, i.e. Eq. (2.69) below.

$$c_p^2 = \frac{\sigma_\infty^4 \, kT}{(1+\delta)Ke^2 \pi^3 f^4 L^4} \cdot \frac{1}{x_o} \qquad (2.69)$$

The space-charge capacitance C_p per unit area is plotted in Fig. (4.6) as a function of frequency at a number of temperatures. At higher temperatures C_p approaches the static field value C_o as the frequency is reduced below 1 KHz. On the other hand, as the frequency is raised and the temperature lowered the measured capacitance $(C_p + C_g)$ asymptotes to a value C_g wholly consistent with the geometry and static dielectric constant $(K = 31.9)$[78,79] of the crystal. This close agreement between the theoretical and experimental values of C_g is encouraging in that it shows all spurious, stray capacitance to be absent. Accordingly in all calculations the observed capacitance is corrected for C_g determined in this way, giving the true space-charge capacitance C_p.

4.4.1. Electrode Effects on Capacitance

During thermal cycling at low frequencies C_p dropped slowly whereas σ remained unchanged. Jacobs[49] et al. detected similar behaviour in potassium chloride and noted that the passage of D.C. through the crystal for several seconds could lower the measured value of the capacitance by a factor of two. The persistent application of low frequency (below 1 KHz.)
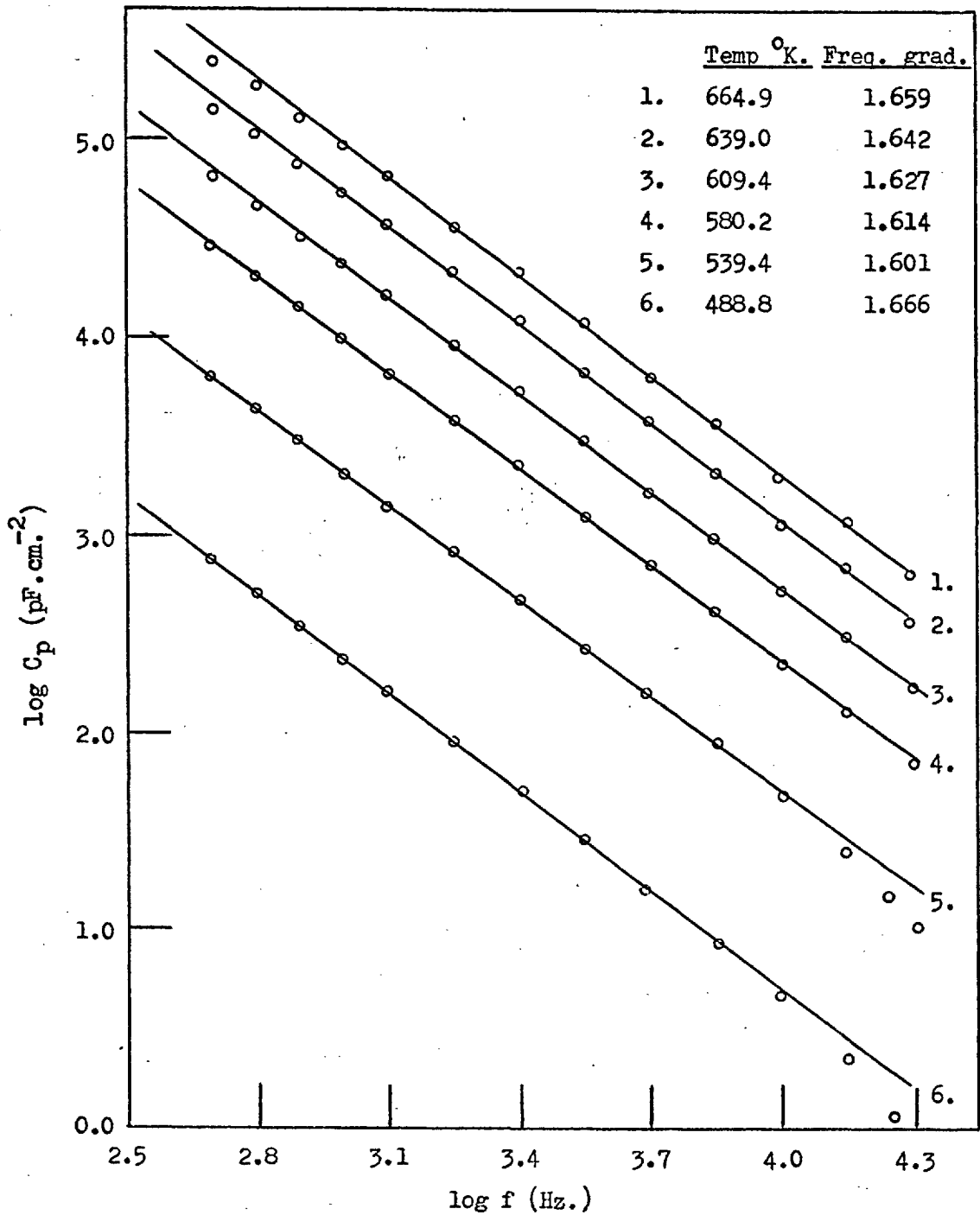
voltage must therefore be avoided. Even so C_p was found to decrease by about 3% during a heating/cooling cycle and was at least halved by D.C. This was presumed to be an electrode effect - possibly electrolysis - since by machining 1 mm. off each plane surface the original value of C_p, prior to the passage of D.C. and low-frequency currents, could be regained to within 5%, taking into account the reduced length of the crystal. Samples were therefore cycled once only before re-machining - all readings, except where stated, being taken during heating.

The nature of the electrode surface was found to be extremely important since crystals with these surfaces roughened by carborundum paper gave irreproducible data for C_p, σ being unaltered within experimental error. All crystals were therefore machined accurately parallel with plane polished surfaces. The capacitance data for samples with and without colloidal graphite electrodes then agreed to within 5%.

Measurements of C_p were also taken with the sample under vacuum instead of one atmosphere pressure of argon in order to determine any vitiating effects due to surface moisture. Such moisture, by virtue of its conduction, would only slightly increase σ but would reduce C_p substantially. No such effects were however observed, C_p being unchanged by evacuation, and argon was used throughout.
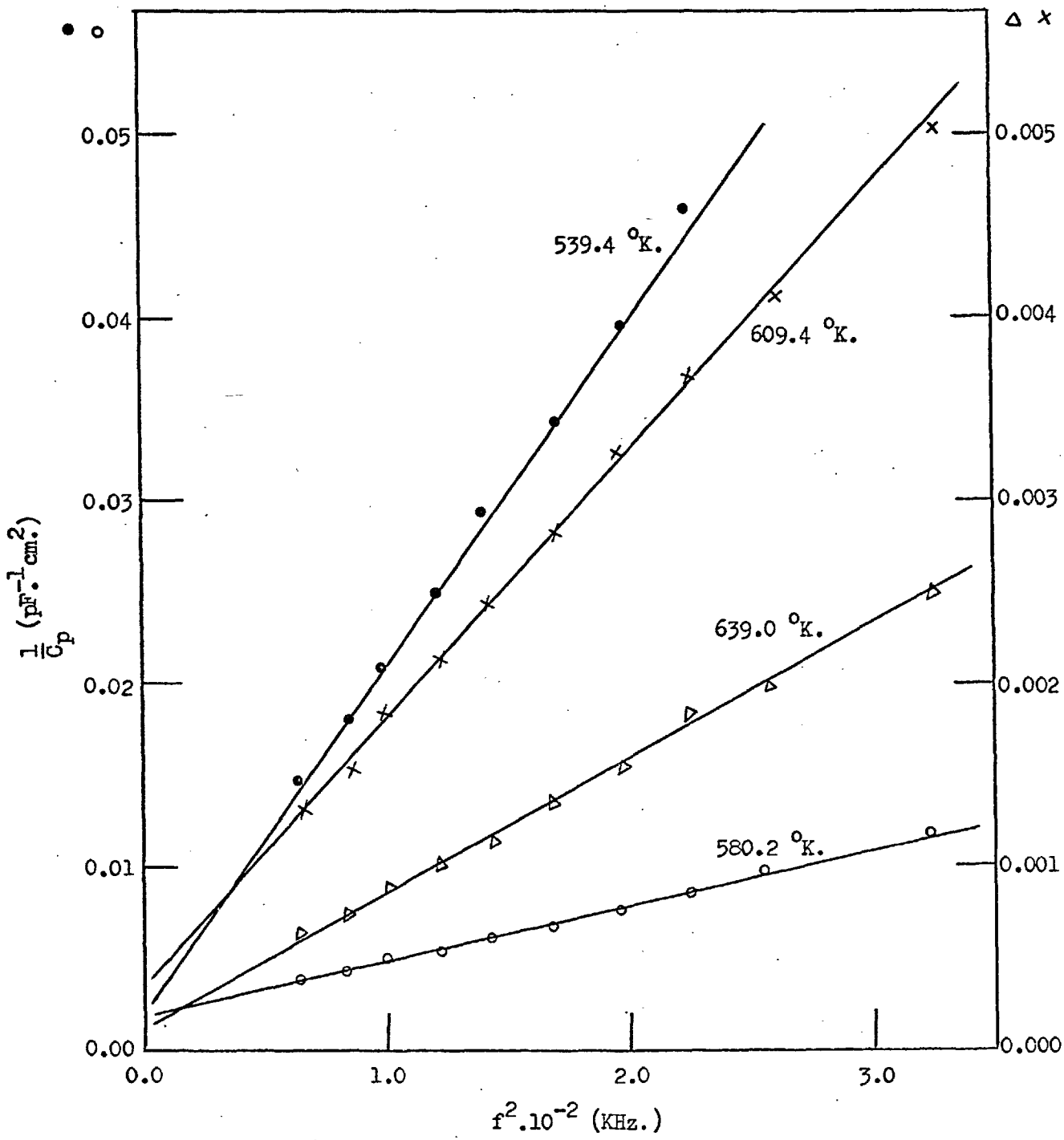
Providing the foregoing precautions are rigorously observed therefore the measured value of capacitance is considered to be in error by no more than 10%.

	Temp °K.	Freq. grad.
1.	664.9	1.659
2.	639.0	1.642
3.	609.4	1.627
4.	580.2	1.614
5.	539.4	1.601
6.	488.8	1.666

TC-2. Typical 'frequency gradient' plots.

Fig. (4.7)

100

The f^2 dependence of C_p^{-1} at higher frequencies.

Fig. (4.8)

4.4.2. The Frequency Gradient

The logarithm of C_p is plotted in Fig. (4.7) against the logarithm of f, the frequency (Hz.) of the applied A.C. field. These plots are apparently linear over wide temperature and frequency ranges, but C_p does of course approach C_o and zero for the two extreme cases already mentioned. The central regions of these logarithmic plots have slopes, or 'frequency gradients', in the range 1.6 - 1.75 for all crystals whereas Eq. (2.69) predicts a value of 2. Nevertheless plots $\frac{1}{C_p}$ against f^2 in the range 8-16 Hz. are accurately linear, all passing through or near to the origin as shown in Fig. (4.8). As Jacobs[50] pointed out, this is a better test of the f^2 dependence than the logarithmic display of Fig. (4.7) where, in fact, the plots show definite curvature and the inclusion of experimental points at the lowest frequencies, which as mentioned in the last section are liable to be low and more in error than those obtained at higher frequencies, would account for a reduction in the 'frequency gradient'.

Approximate values of x_o, the chlorine ion vacancy concentration, may therefore be calculated from the slopes of the linear plots in Fig. (4.8) using Eq. (2.69)

$$C_p^2 = \frac{\sigma_\infty^4 kT}{(1+\delta)Ke^2\pi^3 f^4 L^4} \cdot \frac{1}{x_o} \qquad (2.69)$$

at a number of different temperatures in the range $450^\circ K.-600^\circ K$, where the
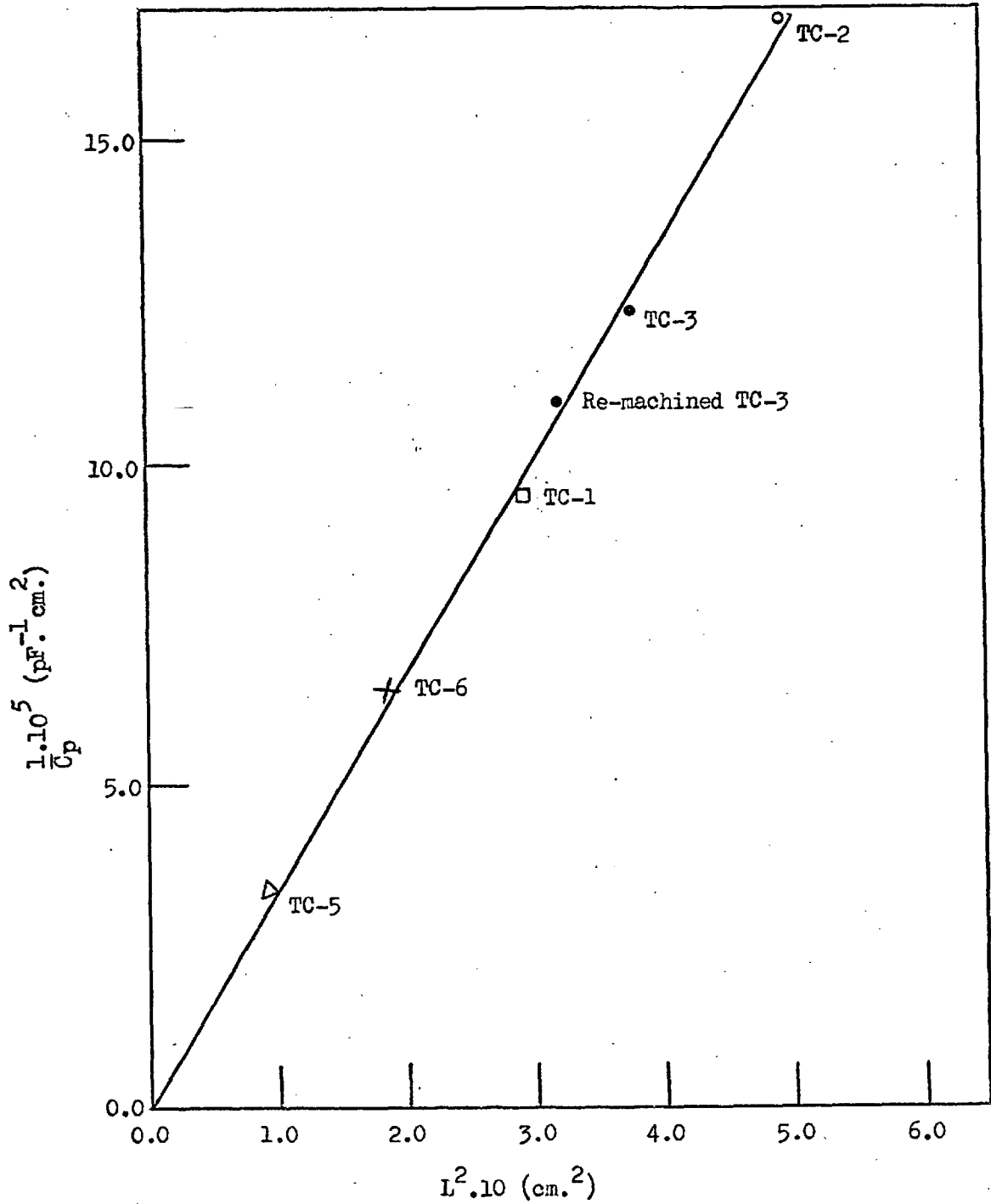
Temp. = 565.7 $^\circ$K.; f = 1 KHz.; the dependence of $\frac{1}{C_p}$ upon L^2.

Fig. (4.9)

validity of this equation is assured.

The temperature dependence of x_o, plotted as log x_o against $\frac{1}{T}$, then provides a preliminary estimate of $\Delta H_{f(av)}$, the enthalpy of formation of the chlorine ion vacancy. This quantity however will be derived by a more rigorous graphical technique in section 4.4.5.

4.4.3 The Length Dependence

Normal geometric capacitance is inversely proportional to the thickness of the dielectric. Eq. (2.69), on the other hand, predicts that the space charge capacitance C_p should be inversely proportional to the square of the length L of the crystal. This prediction is tested in Fig. (4.9) where $\frac{1}{C_p}$ is plotted against L^2. The resulting trace is linear and passes accurately through the origin in excellent agreement with the theory.

4.4.4. The Voltage Dependence

One of the conditions for the linearization of the differential equations governing the charge carrier concentrations in the space-charge model is that the applied voltage V_1 should be small, and in any case $< kT/e$. In view of the fact that several assertions of this model are vindicated through the implications of Eq. (2.69) it is interesting to examine the stringency of this condition.

The neglect of harmonic terms is only justified, therefore, if V_1 < 0.07 volts (at $600°K.$) : at higher applied voltages theory predicts a

V_1^2 dependence for C_p. Experimentally, however, the oscilloscope reveals the absence of any harmonics and C_p is independent of voltage in the range 30 mV. - 30 V. This is difficult to understand unless the linearization condition is unnecessarily severe. The assumption that the linearized equations are quite sufficient in accurately representing the situation in any circumstances is then supported by the absence of harmonics.

4.4.5. The Determination of x_o

Within the approximations of the space-charge model it is not possible to compute x_o precisely as δ is unknown and the exact nature of the frequency dependence is uncertain. This has already been discussed in section 4.4.2. where it was shown that a graphical technique could be employed to calculate preliminary values of x_o and $\Delta H_{f(av)}$ using Eq. (2.68) or (2.69).

$$C_p^2 = \frac{G_\infty^4 kT}{(1+\delta)Ke^2\pi^3 f^4} \cdot \frac{1}{x_o} \tag{2.68}$$

The 'frequency gradient', however, is independent of temperature within the limits of experimental accuracy and the numerical value of $(1+\delta)$ lies only between 1 and 2, which means that by plotting $\log\left(\frac{TG_\infty^4}{C_p^2}\right)$ against $\frac{1}{T}$ for a series of fixed frequencies we eliminate any effects on $\Delta H_{f(av)}$ due to the uncertainty in the frequency dependence.
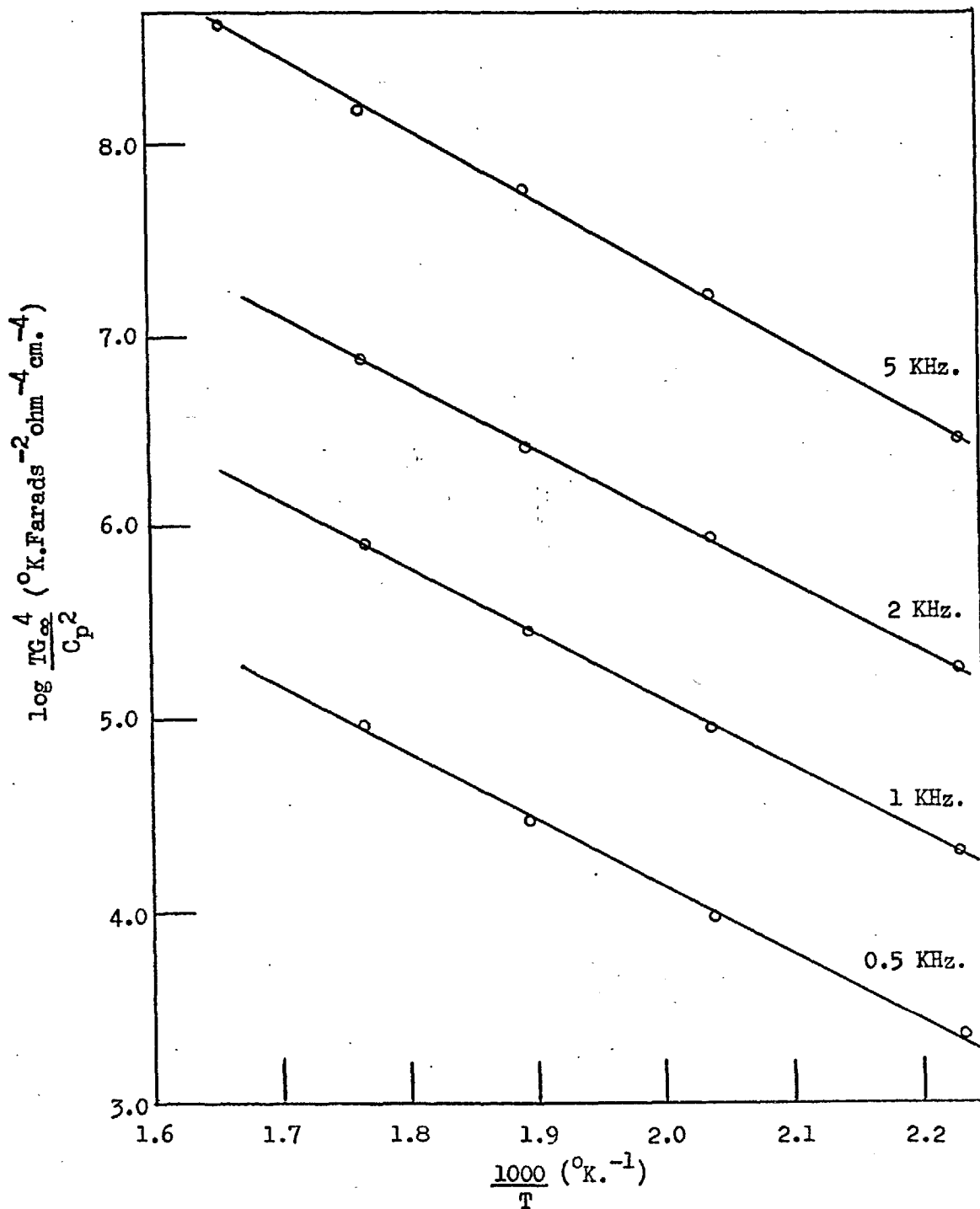
The test of Eq. (2.68). Apart from a proportionality factor these plots are, in essence, plots of x_o against $1/T$.

Fig. (4.10)

Linear plots are obtained in Fig. (4.10) between 475°K. and 600°K. in the frequency range 500 Hz. – 5 KHz. where Eq. (2.68) is valid. The slopes of these plots are identical as they should be if Eq. (2.68) is sound, giving a value of 0.68 ± 0.015 eV. for the enthalpy of formation of a chlorine ion vacancy, in good agreement with the value of 0.65 ± 0.05 eV. obtained by Christy and Dobbs[58] from thermoelectric measurements.

If we assume $\Delta H_s = 2 \Delta H_{f(av)}$, we obtain a value of 1.36 ± 0.03 eV. for the enthalpy of formation of a Schottky defect in thallous chloride.

The 0.5, 1 and 2 KHz lines in Fig. (4.10) are equally spaced as predicted but again require a frequency dependence for C_p of $f^{1.75}$ before coincidence is obtained. By assuming adherence to this dependence we can obtain values of x_o which may be written as

$$x_o = \exp \left(\frac{+\Delta S_s}{2k} \right) \exp \left(\frac{- 1.36 \text{ eV}}{2kT} \right)$$

where ΔS_s, the entropy of formation of a Schottky defect, lies in the range 7.5 – 8.5 k compared with the value of 10.3 k obtained by Christy and Dobbs. On this basis the chlorine ion vacancy concentration, or Schottky defect concentration, is approximately 0.08 atomic % at the melting point.

Using Friauf's value[57] for ϕ, the ratio of anion mobility to cation mobility, of $0.1124 \exp \left(\frac{3380}{T} \right)$ and the present conductivity σ and x_o data, we calculate the characteristic parameters for the thallous chloride system as follows:

	ΔH_1 eV.	ΔH_s eV.	$\Delta H_{m(av)}$ eV.	$\Delta H_{m(cv)}$ eV.	$\Delta S_s/k$
Present work	0.755 ± 0.005	1.36 ± 0.03	0.09	0.40	8 ± 0.5
Friauf[53]	0.76	–	(0.12)	(0.43)	–
Christy and Dobbs[58]	–	1.3 ± 0.1	0.2	0.5	10.3

Defect parameters for the thallous chloride system

Table (4.1)

The data in parentheses were calculated directly from the slopes of Friauf's log D against $\frac{1}{T}$ plots using $\Delta H_{m(i)} = \Delta H_{D(i)} - \dfrac{\Delta H_s}{2}$ where $\Delta H_{D(i)}$ is the activation enthalpy for diffusion of species i. Neglect of the temperature dependence of the correlation factor makes these values too high.

The Schottky defect concentration in thallous chloride is now known to within 20%. In all other ionic systems it is only rarely known to an accuracy greater than one order of magnitude.

4.5. SPACE-CHARGE POLARIZATION IN THALLOUS BROMIDE

In the absence of self-diffusion results for thallous bromide a completely self-consistent analysis of capacitance data in the manner detailed for thallous chloride in the preceding sections is not possible. It is nevertheless worthwhile to measure C_p as a preliminary for further investigation and to compare the results obtained with those for thallous chloride.

C_p is again reproducible providing the precautions observed for the chloride are still heeded.   However, C_p was measured for only two samples — one determination for each — resulting in the data for the bromide being less reliable.

The space-charge capacitance is plotted in Fig. (4.11) as log C_p against f, the frequency of the applied A.C. field, at a number of fixed temperatures, C_p again approaching the static field value C_o in one extreme case (low f, high T) and zero in the other.   The measured value of the capacitance again approaches the geometric value C_g in the lower limit where K, the static dielectric constant, of the bromide at 30.3[80] is very close to the value of 31.9 for the chloride.   Since K is determined mainly by electronic and lattice polarization it would imply that the polarization terms involved in computing vacancy formation energies are similar for the two substances, as predicted by analogy with Boswarva's calculations on the cesium halides.
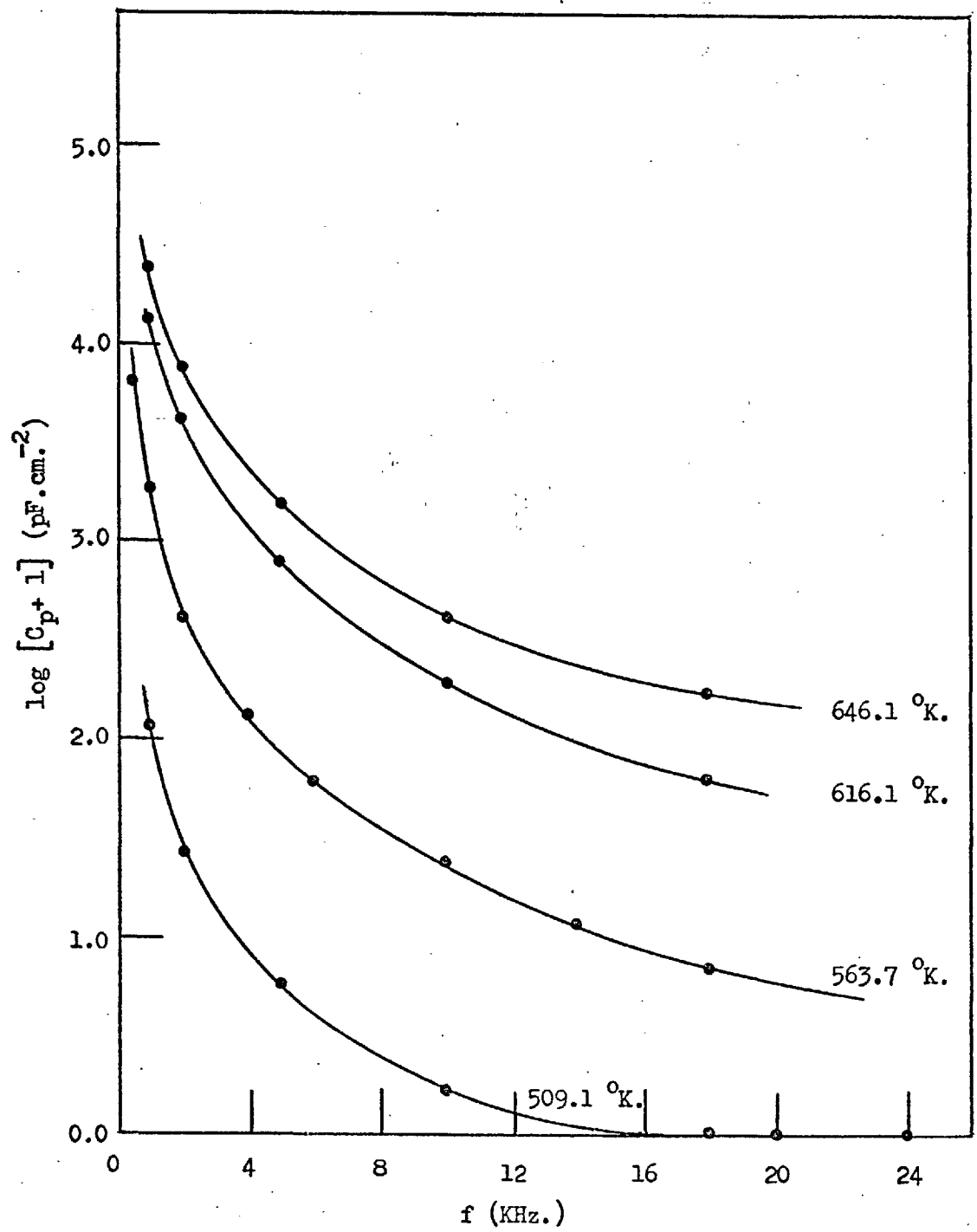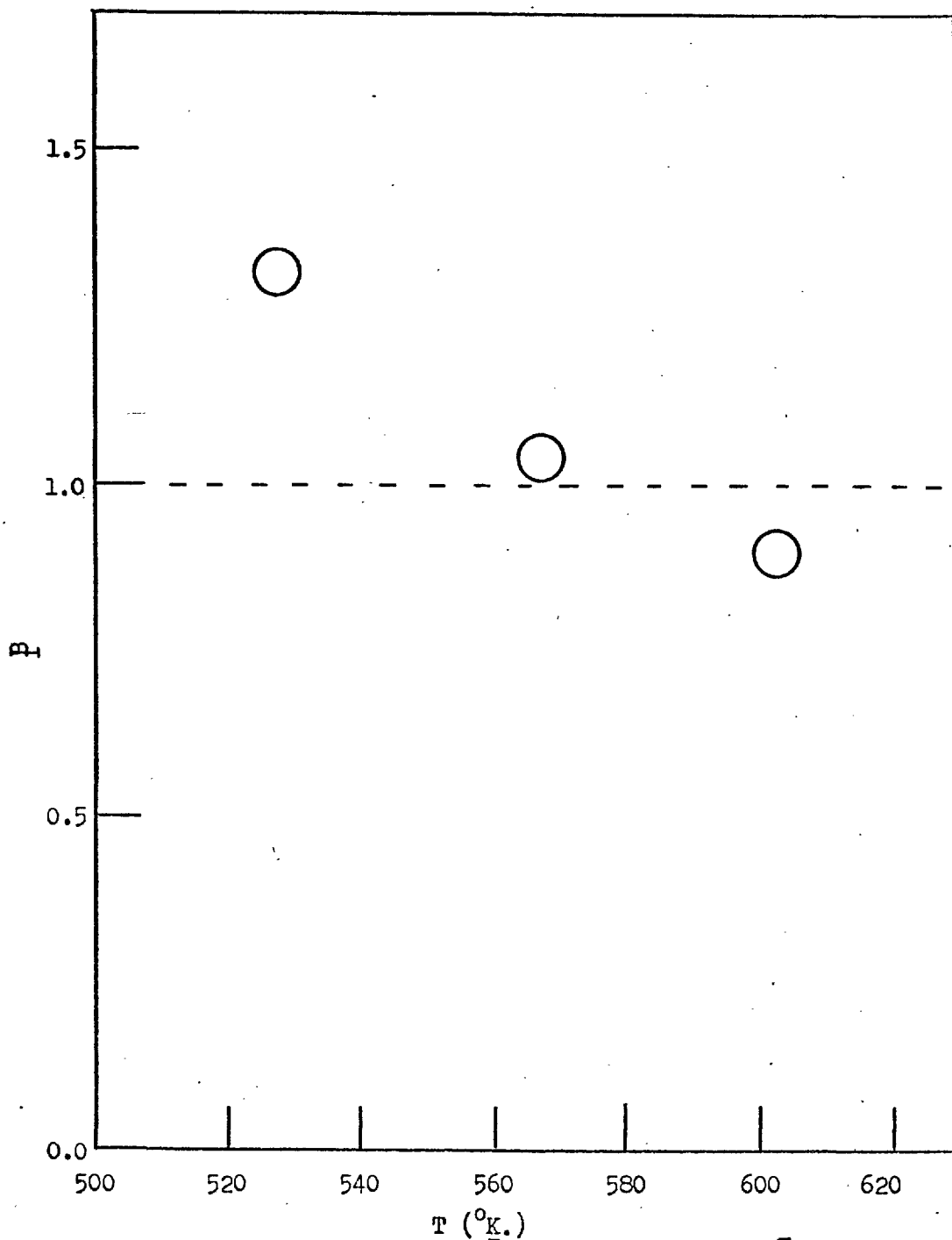
TB-1. Log $(C_p + 1)$ against f showing the approach to zero of C_p at low temperatures and high frequencies.

Fig. (4.11)
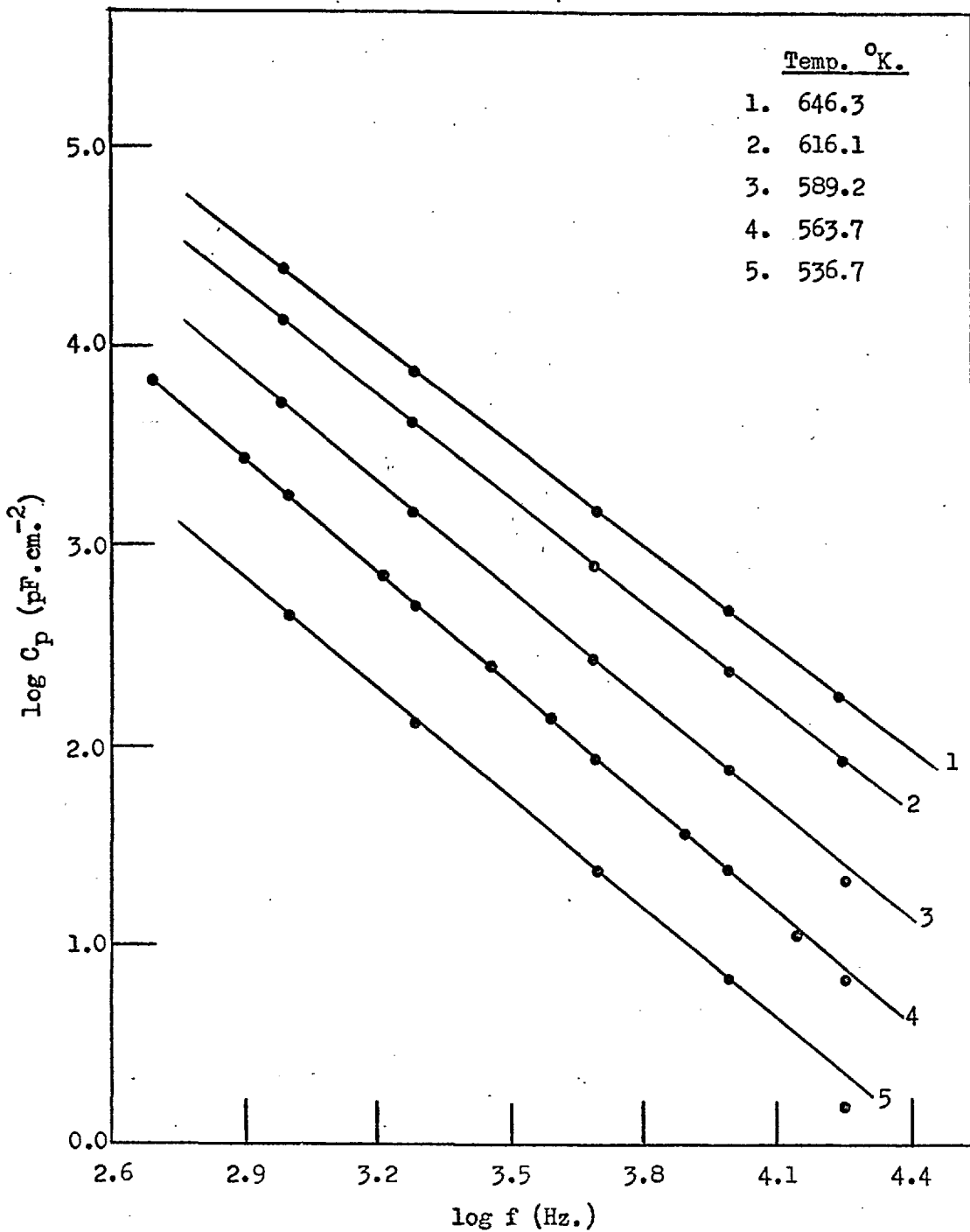
TB-1. The 'frequency gradient' plot.

Fig. (4.12)

A plot of β against T, where $\beta = \left[\dfrac{C_p}{G_\infty^2}(TlCl) \cdot \dfrac{G_\infty^2}{C_p}(TlBr) \right]$, indicating

the similarity between thallous chloride and thallous bromide. f = 1 KHz.

Fig. (4.13)

Log C_p is plotted against log f in Fig. (4.12) providing a value of the frequency gradient in the range 1.7- 1.8 .

All else being equal Eq. (2.61)

$$C_p^{\ 2} = \frac{G_\infty^{\ 4} kT}{(1 + \delta) Ke^2 \pi^3 f^4} \cdot \frac{1}{x_o}$$

predicts that the space charge capacitance/unit area should be proportional to the square of the conductance/unit area. To test this prediction we have, in Fig. (4.13), plotted the term $\left(\dfrac{C_p(TlCl)}{G_\infty^2} \cdot \dfrac{G_\infty^2(TlBr)}{C_p} \right)$ against T at 1 KHz. in the temperature range $525^\circ K - 600^\circ K$ where the 'frequency gradients' are approximately linear for both materials. The value of this lies close to 1 throughout. Since the static dielectric constants of thallous chloride and thallous bromide are approximately equal this would imply that the Schottky defect concentration x_o at any one temperature must be very similar for the two crystals.

4.6. THE ELECTRICAL CONDUCTIVITY OF PURE LITHIUM IODIDE

Following Haven[61], we shall assume the existence of Schottky disorder

in lithium iodide with the positive ion vacancy as the dominant charge

carrier and examine our experimental results in the light of this postulate.

The practical difficulties in preparing and handling lithium iodide have

already been mentioned. In addition, the extreme hygroscopy of the material

can lead to spurious results because samples inevitably absorb a certain amount

of moisture on introduction into the cell and possibly during measurements.

Such surface moisture can increase the conductivity by several orders of

magnitude at temperatures around 350°K. where the monohydrate is known to

melt, but the effects are too irreproducible to be studied systematically.

The cell and sample were therefore kept under a hard vacuum at room temperature

for at least 24 hours before being slowly heated as described in section 3.4.

It would appear advantageous to keep the cell evacuated throughout, but this

had the effect of increasing the conductivity quite steadily at higher

temperatures ($\sim 10\%$ per hour at 673.5°K.)- an effect which was immediately

suppressed by the introduction of an argon atmosphere. This upward drift of

the conductivity is probably a direct result of the gradual decomposition

the sample which is accelerated by evacuation through the removal of iodine.

The incorporation of oxide into the host would then increase the concentration

of anion vacancies which may contribute significantly to the conduction at

elevated temperatures. This is known to be the case in one of the other
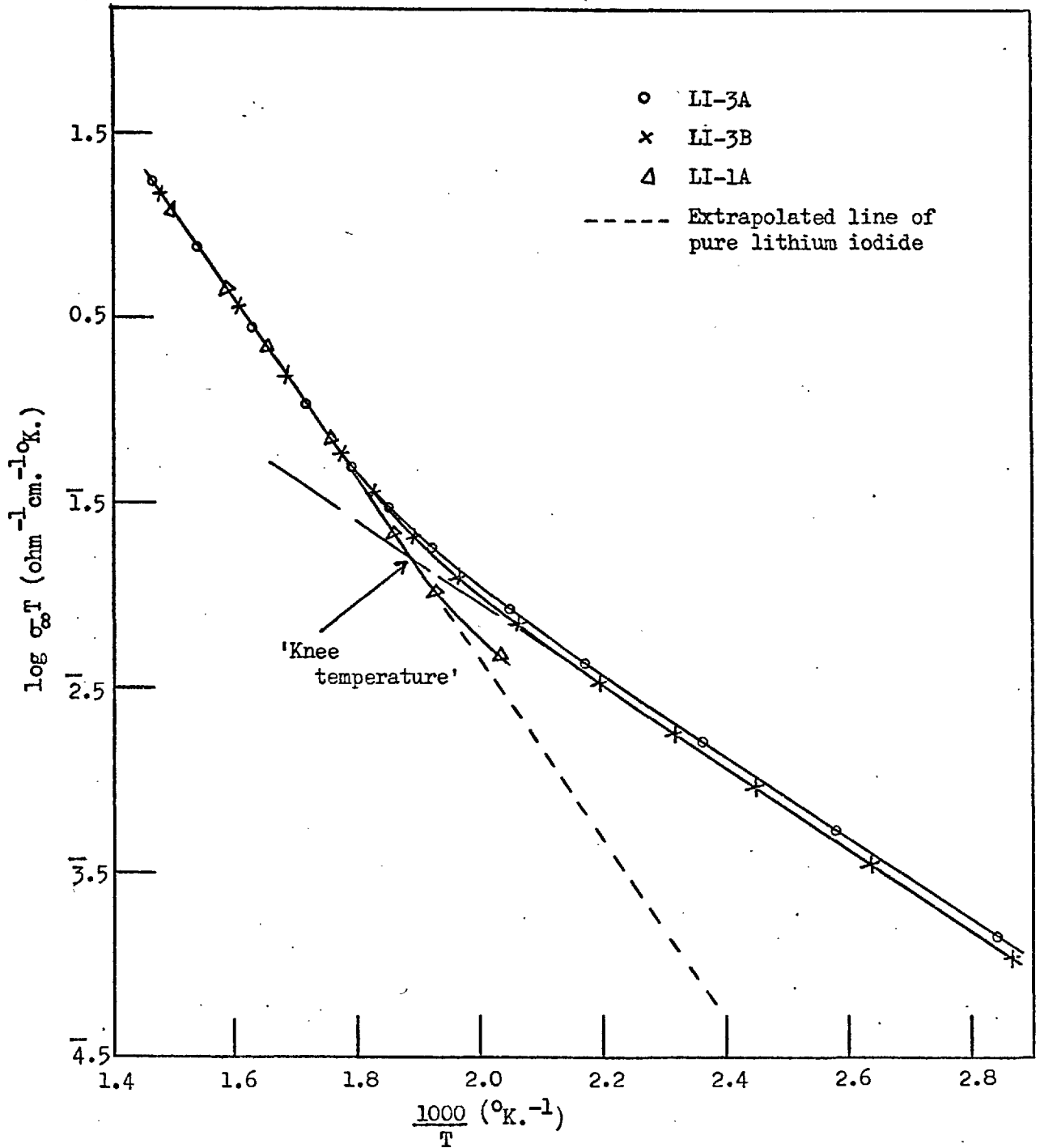
The conductivity of undoped lithium iodide. Superimposed data points
are omitted for clarity.

Fig. (4.14)

lithium halides, namely the fluoride[10], where the anion carries some 30% of the charge at temperatures approaching the melting point.

The experimental procedure, already described in section 3.4., took account of these invalidating effects and enabled the conductivity to be reproduced to within 2% on thermal cycling, always keeping the temperature of the sample below 675°K. to avoid any oxidation.

For this work softened platinum foils were inserted between the sample and the graphite blocks in the cell. The impression on the foil left by the sample after measurement then enabled the effective electrode surface area to be determined. This determination, together with weight measurement and direct micrometer readings, provided an acceptable value of the geometric factor which is so important in obtaining absolute values of the specific conducting σ.

4.6.1. The Intrinsic Region I

The conductivity of undoped lithium iodide is plotted as $\log \sigma_{\infty} T$ against $\frac{1}{T}$ in Fig. (4.14) for a number of typical samples. All curves are superimposable in the intrinsic region which is quite straight with a slope of 0.96 ± 0.1 eV. over a range of 120°K. to within 50°K. of the melting point, indicating the presence of only one mobile charge carrier. This is assumed to be the lithium ion vacancy and we therefore write

$$\Delta H_1 = \Delta H_{f(cv)} + \Delta H_{m}(cv) = 0.96 \text{ eV.}$$

The extended intrinsic range for sample LI-1A is unusual. This sample was prepared from material which had not been treated with hydrogen/ hydrogen iodide and consequently contained a higher concentration of oxide. The presence of oxide reduces the electrical effect of divalent cationic impurities by forming impurity-oxide ion pairs. It is not necessary, however, to postulate the existence of such complex pairs as the enhanced anion vacancy concentration produced by the oxide automatically reduces the cation vacancy, or charge carrier, concentration by virtue of the 'solubility product' equilibrium described in Eq. (1.6):

$$x_{(av)} \cdot x_{(cv)} = K^{-1}$$

in both events the extrinsic region is reduced in importance.

Spectrochemical and colorimetric analyses of these samples indicate that divalent magnesium and divalent iron account for about 90% of the total polyvalent cation impurity content. In LI-3A magnesium is present at a level of ~ 30 p.p.m. and iron at ~ 40 p.p.m.

4.6.2. The Extrinsic Region II

These divalent impurities give rise to a long, straight extrinsic region characterized by an enthalpy of 0.43 eV. which on our assumed model is attributed to the motion of a lithium ion vacancy: that is

$$\Delta H_2 = \Delta H_{m(cv)} = 0.43 \text{ eV.}$$

We therefore calculate ΔH_s, the Schottky defect formation enthalpy, as $2\Delta H_{f(cv)} = 1.06$ eV.

If we assume the magnesium and iron in LI-3B to be dissolved substitutionally in the lithium iodide lattice, then x_o, the atom fraction of cation vacancies, is equal to 7×10^{-5} throughout the linear range of region II. Furthermore, at the 'knee' – see Fig. (4.14) – where the extrapolated linear portion of region I intersects with that of region II, the intrinsic atom fraction of cation vacancies is also equal to 7×10^{-5}. This intersection occurs at a 'knee temperature' of 1000/1.9 whence we may calculate ΔS_s, the entropy of Schottky defect formation, from

$$x_o = 7 \times 10^{-5} = \exp\left(\frac{\Delta S_s}{2k}\right) \quad \exp\left(-\frac{\Delta H_s}{2kT}\right) \qquad (4.4)$$

$$= \exp\left(\frac{\Delta S_s}{2k}\right) \quad \exp - \left(\frac{0.53 \times 1.9}{1000k}\right)$$

Re-plotting Haven's results as log σT against $\frac{1}{T}$, we calculate as follows:

	ΔH_1 eV.	$\Delta H_{m(cv)}$ eV.	ΔH_s eV.	$\Delta S_s/k$	$x_o(T_m)$ at.%
Haven[61]	~1.08	~0.42	~1.34		~1.17
Present work	0.96	0.43	1.06	4.5	~0.18

Defect parameters for lithium iodide

Table (4.3)

Haven, however, took all his measurements with a current of nitrogen passing over his sample which would facilitate decomposition of the sample at elevated temperatures in a manner similar to that described for evacuation in this work. In addition, any oxygen present in the nitrogen gas would accelerate the oxidation of his samples. The upward drift of the conductivity would then explain the pronounced curvature in Haven's log σT against $\frac{1}{T}$ plots and his high value of ΔH_1. Secondly, he extended his measurements no lower than $420^\circ K.$ and thus could only estimate ΔH_2. Indeed Haven emphasizes the unreliability of his results with lithium iodide.

For the two alkali halides where the data are sufficiently accurate to determine ΔS_s, the entropy of Schottky defect formation, we have $\Delta S_s = 6.2k$ (NaCl)[6] and $5.4k$ (KCl)[7]. A value of $4.5k$ for lithium iodide is therefore within the framework of existing measurements. No accurate values of $x_o(T_m)$ greater than 0.2at.% have been reported[52] for Schottky disorder in alkali halides and our value of 0.18% for lithium iodide complies with this observation. For many crystals the defect concentration at the melting point lies between 0.02 and 0.2at.% - a range of only one order of magnitude. ΔS_s for these ionic crystals, where known, lies in the range $4.5 - 8.5k$ which means that even in the two extreme cases x_o, in Eq. (4.4), is only altered by half an order of magnitude by the entropy term. The implications, therefore, are that the exponential enthalpic term in this equation is approximately constant for many crystals at their respective melting points. We shall examine this postulate in the following Table (4.4).

Crystal	Disorder	Structure	T_m m.p. $^\circ K$	$\Delta H_{s(f)}$ eV	Ref.	$1000 \Delta H_s / 2 T_m$
TlCl	Schottky	B.C.C.	703	1.34	This work	0.96
CsBr	Schottky	B.C.C.	909	2.0	74	1.10
CsI	Schottky	B.C.C.	894	1.9	74	1.06
LiF	Schottky	F.C.C.	1115	2.34	10	1.05
LiI	Schottky	F.C.C.	719	1.06	This work	0.73
NaCl	Schottky	F.C.C.	1074	2.30	6	1.07
KCl	Schottky	F.C.C.	1049	2.26	7	1.08
AgCl	C.Frenkel	F.C.C.	728	1.44	8	0.99
AgBr	C.Frenkel	F.C.C.	703	1.06	9	0.75
CaF_2	A.Frenkel	Fluorite	1633	2.80	81	0.86

Defect formation enthalpies and melting points for some ionic crystals

Table (4.4)

The value of $1000 \Delta H_s / 2 T_m$ is seen to be about 1.0 for well-studied crystals, regardless of the crystal structure and the type of disorder present. This indicates a close correlation between the enthalpy of defect formation in the crystal and the melting point, which is not totally unexpected in view of the common forces involved in determining these two parameters. If sufficient

features are held in common between these crystals a law of corresponding

states may apply and a pure crystal would melt when the intrinsic

concentration of vacancies reached a certain critical value.   This

interpretation involves some far-reaching assumptions but it provides for

a useful estimate of the enthalpy of defect formation from a knowledge of

the fusion temperature alone.

4.6.3. Magnesium Doped Lithium Iodide

Haven[61] attempted to dope lithium iodide with a high concentration of

magnesium but evidently failed to dissolve the magnesium substitutionally

in the host because the extrinsic conductivity was less than doubled by an

increase in the dopant level from 0.07 - 0.40 atomic %.   In region II

this conductivity should be given by

$$\sigma T = \frac{c_0}{N} \cdot \sigma_0' \; \exp\left(-\frac{\Delta H_{m(cv)}}{kT}\right) \qquad (4.5)$$

where c_0 is the concentration of magnesium ions, assuming no other impurities

to be present.   If the magnesium is not incorporated substitutionally the

above relation will not be true and a detailed analysis is not possible.

We believe that magnesium iodide is only slightly soluble in lithium iodide

inasmuch as sample LI-DB3 contained only $\sim$120 atom p.p.m. magnesium in

spite of being grown from a melt containing 1 mole % of magnesium iodide.

The boule obtained from the Bridgman furnace in this case was milky in
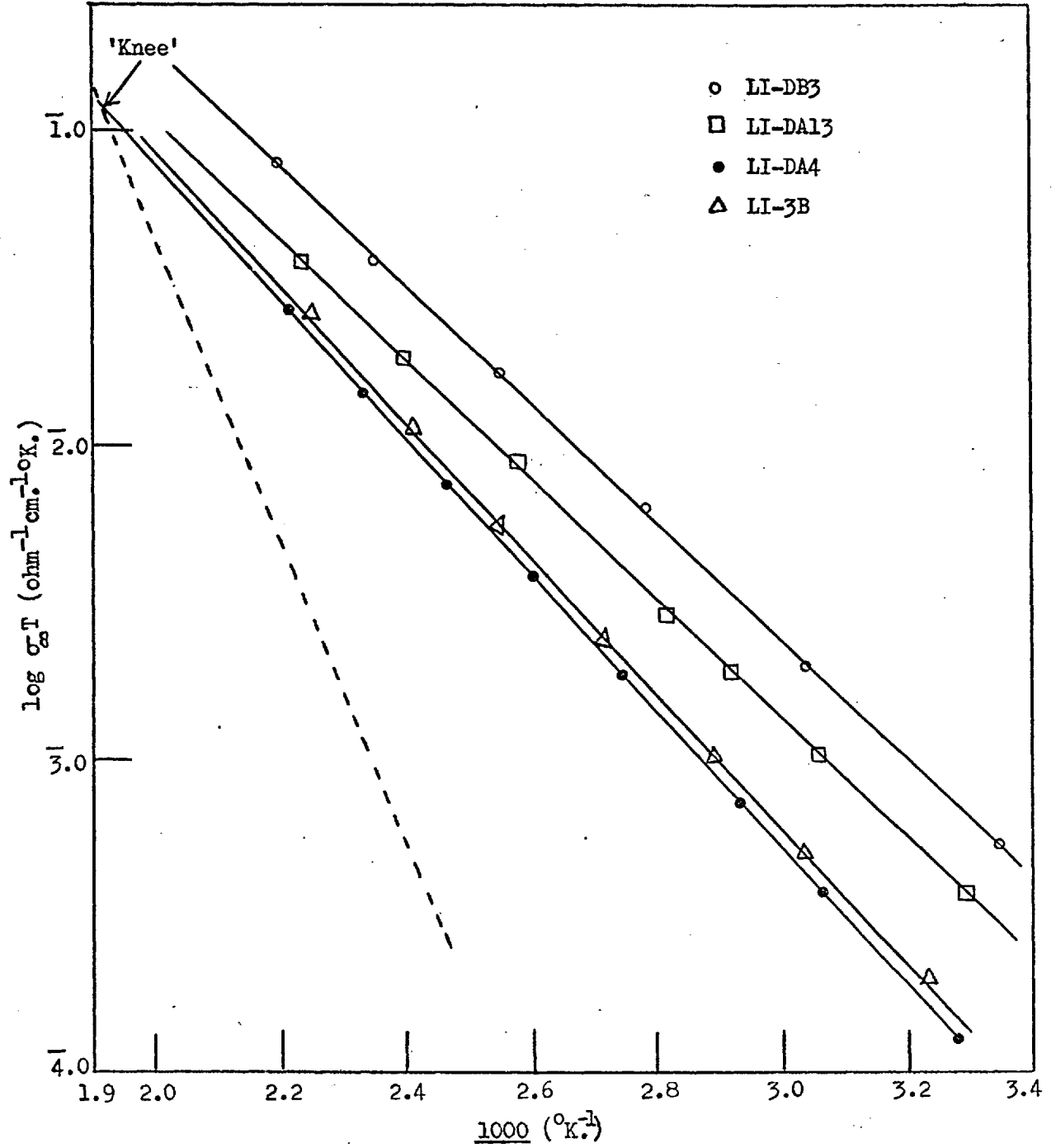
The extrinsic region for magnesium doped lithium iodide. The 'knee' point is shown as the intersect of the extrapolations of the intrinsic and extrinsic conductivity plots.

Fig. (4.15)

appearance at both ends, LI-DB3 being cut from a clear section in the middle. It is well known that the Bridgman growth technique, with its effective single zone pass, is capable of sweeping impurities to the ends but it requires a low solubility of magnesium iodide in lithium iodide for the impurity level to be reduced as severely as in LI-DB3 with one zone pass. Admittedly, small amounts of oxide were seen to precipitate magnesium from the melt in LI-DB, but this accounted for only a fraction of the total magnesium present. No such precipitation was observed with LI-DA which yielded a clear boule, opaque only at its upper end. In order to take advantage of the uneven distribution of magnesium in as-grown crystals, samples were cleaved throughout the length and breadth of LI-DA which contained a total of 0.1 mol % magnesium. However, the magnesium content of all these samples ranged only from 30-60 a.p.p.m.

The conductivity of magnesium doped lithium iodide is plotted in Fig. (4.15) in the form of log $\sigma_\infty T$ against $\frac{1}{T}$ for several typical samples. The intrinsic conductivity of all these samples agrees well with the conductivity of undoped samples in this region. This high degree of reproducibility generally confirms that the present experimental techniques can yield meaningful results even with so intransigent a material as lithium iodide.

On thermal cycling region II was also completely reproducible for each sample although the slope of this accurately linear region appears to decrease with increasing dopant concentration - Table (4.5).

Sample	Mg^{++} a.p.p.m.	Fe^{++} a.p.p.m.	Knee temp. T_k $^{\circ}$K 1000/T_k	ΔH_2 eV.
LI-3B	30	40	1.9	0.43
LI-DA4	30	(40)	1.91	0.43
LI-DA13	60	(40)	1.87	0.38
LI-DB3	120	(40)	1.8	0.37

Parameters for impurity-controlled conduction in lithium

iodide (concentrations to nearest 10 a.p.p.m.)

$$\sigma = \frac{c_0}{N} \cdot \frac{\sigma_0'}{T} \exp\left(\frac{-\Delta H_2}{kT}\right)$$

Table (4.5)

This is in direct contrast to Stoebe's observation in magnesium doped lithium fluoride where ΔH_2 increased with dopant level. Stoebe, however, pointed out that region II became progressively shorter for increasing impurity concentration and the inclusion of experimental points in the transition region above or below region II tends to increase the apparent slope of this region. This is not the case with lithium iodide where region II is accurately linear over some 150°-200°K. This decrease in motional enthalpy with increasing concentration of extrinsic vacancies therefore appears to be systematic although the data is too restricted to be conclusive as the mean is 0.4 ± 0.03 eV. which is a very small error for this parameter.
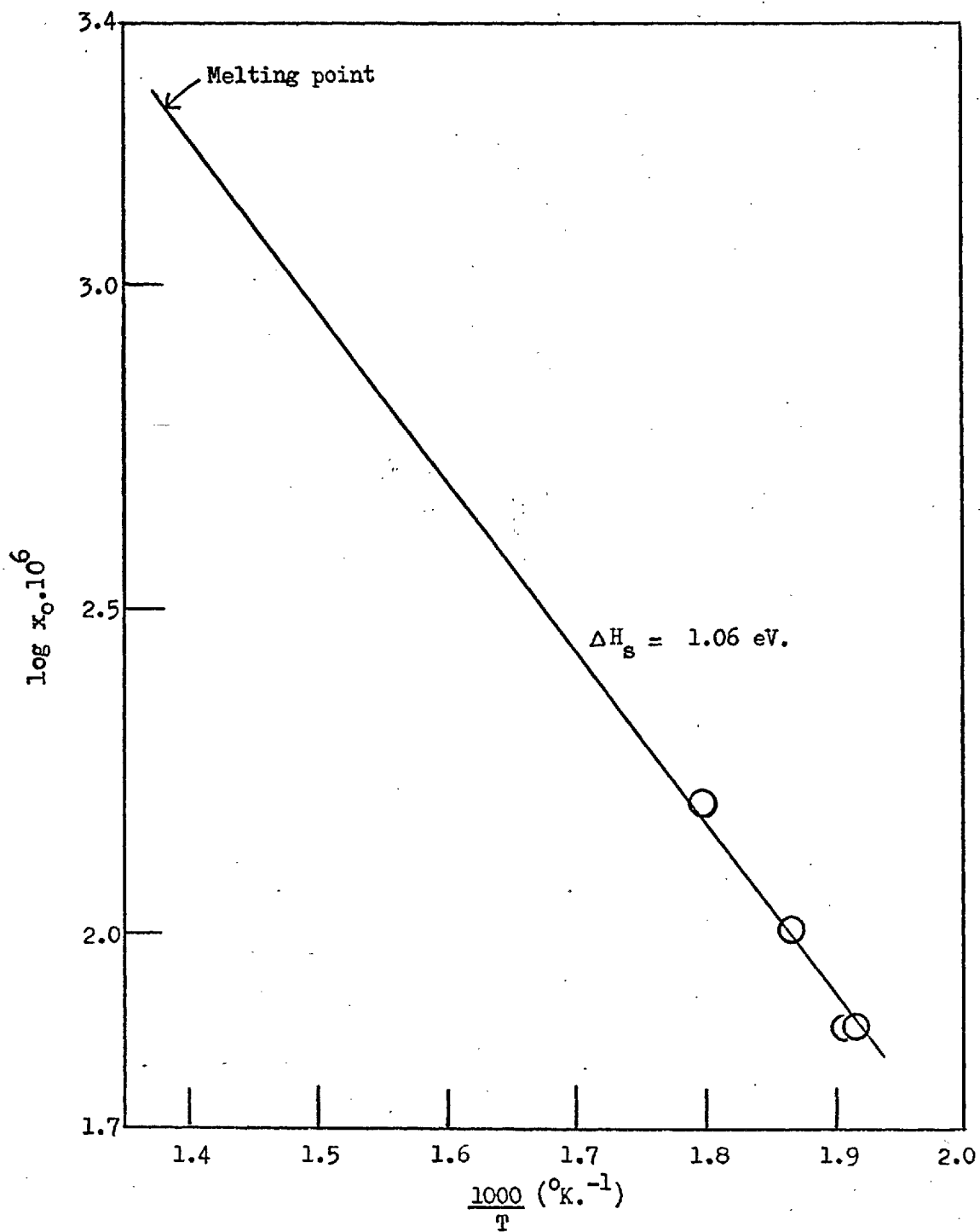
The concentration of lithium ion vacancies as a function of temperature

Fig. (4.16)

A rigorous correlation between the conductivity and c_0, the concentration of magnesium ions, in the manner of Eq. (4.5) is therefore impossible. If, however, we assume a constant background impurity of $\sim$40 a.p.p.m. of divalent iron we see in Fig. (4.15) that the impurity-controlled conduction is roughly proportional to the total divalent cation content. In support we calculate x_0, the intrinsic lithium ion vacancy concentration at the 'knee temperature', using the data given in Table (4.5), and plot it against $\frac{1}{T}$ in Fig. (4.16) where we already have a pre-determined line from our estimate of $x_0(T_m)$ and ΔH_s in lithium iodide. The experimental points lie close to this line indicating that we are studying the motion of lithium ion vacancies deliberately introduced by divalent cationic impurities.

4.7. SPACE-CHARGE POLARIZATION IN LITHIUM IODIDE

If we assume Eq. (2.69)

$$C_p^2 = \frac{\sigma_\infty^4 kT}{(1+\delta)Ke^2\pi^3f^4L^4} \cdot \frac{1}{x_0}$$

$$= \frac{e^2\mu^4 kT}{(1+\delta)k\pi^3f^4L^4} \cdot x_0^3$$

to hold for lithium iodide, with cation vacancies (mobility μ) appreciably more mobile than anion vacancies, then the square of the space-charge polarization capacitance C_p is proportional to the cube of x_0, the

concentration of lithium ion vacancies. It is possible to control x_o
by the addition of aliovalent impurities, but the limited solubility of
magnesium in lithium iodide restricts x_o to such a value that C_p is not
measurable in the extrinsic range and only becomes appreciable (>100 pF.
at 1 KHz.) for temperatures around the 'knee' and upwards.

C_p, however, is extremely sensitive to evacuation of the sample holder
although in a different manner from the conductivity. Whereas the conductivity
rises slowly on evacuating, C_p rises sharply over a few seconds of evacuation
often by as much as 50% and then increases very slowly. This phenomenon
was too irreproducible for systematic investigation but the prompt
re-introduction of dry argon usually restored the original value of C_p to
within 10% after several minutes. The conductivity was unchanged over such
a short period.

The influence of evacuation on C_p is probably a surface effect, whereby
the presence of chemically absorbed moisture on the surface of the lithium
iodide gives rise to a preferred conduction path on the surface of the sample
which would effectively short-circuit some of the space-charge and relax
the blocking electrode boundary condition. The concomitant increase in
conduction would be extremely small in comparison with the over-all
conductivity by virtue of the minute conduction cross-section and poor
electrode contact of the lateral surfaces of the sample (parallel to the
electric field). If this were the case the correct space-charge
capacitance would be that which is obtained with the sample continuously
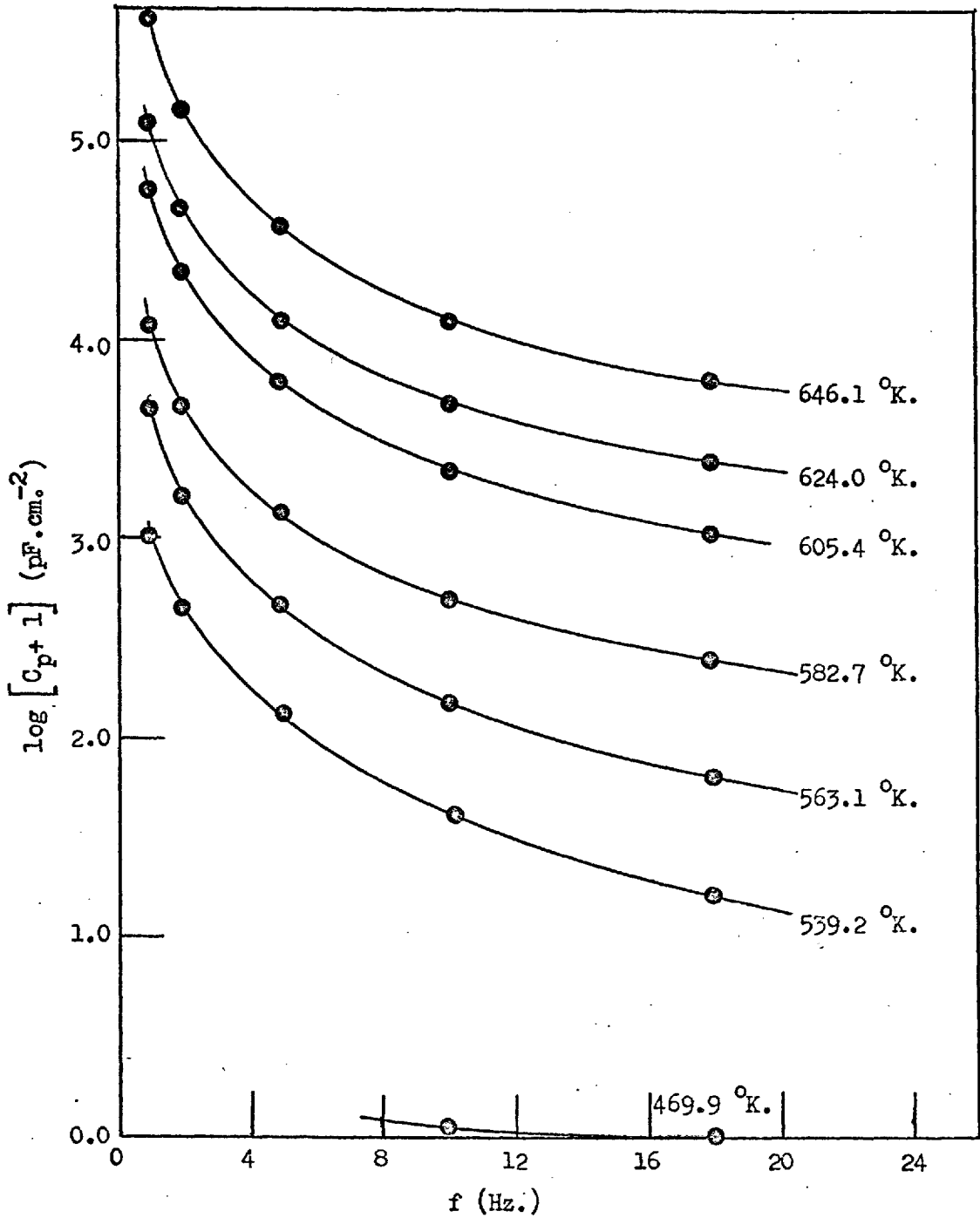
LI-3B. Log $(C_p + 1)$ against f showing the zero approach of the space-charge polarization.
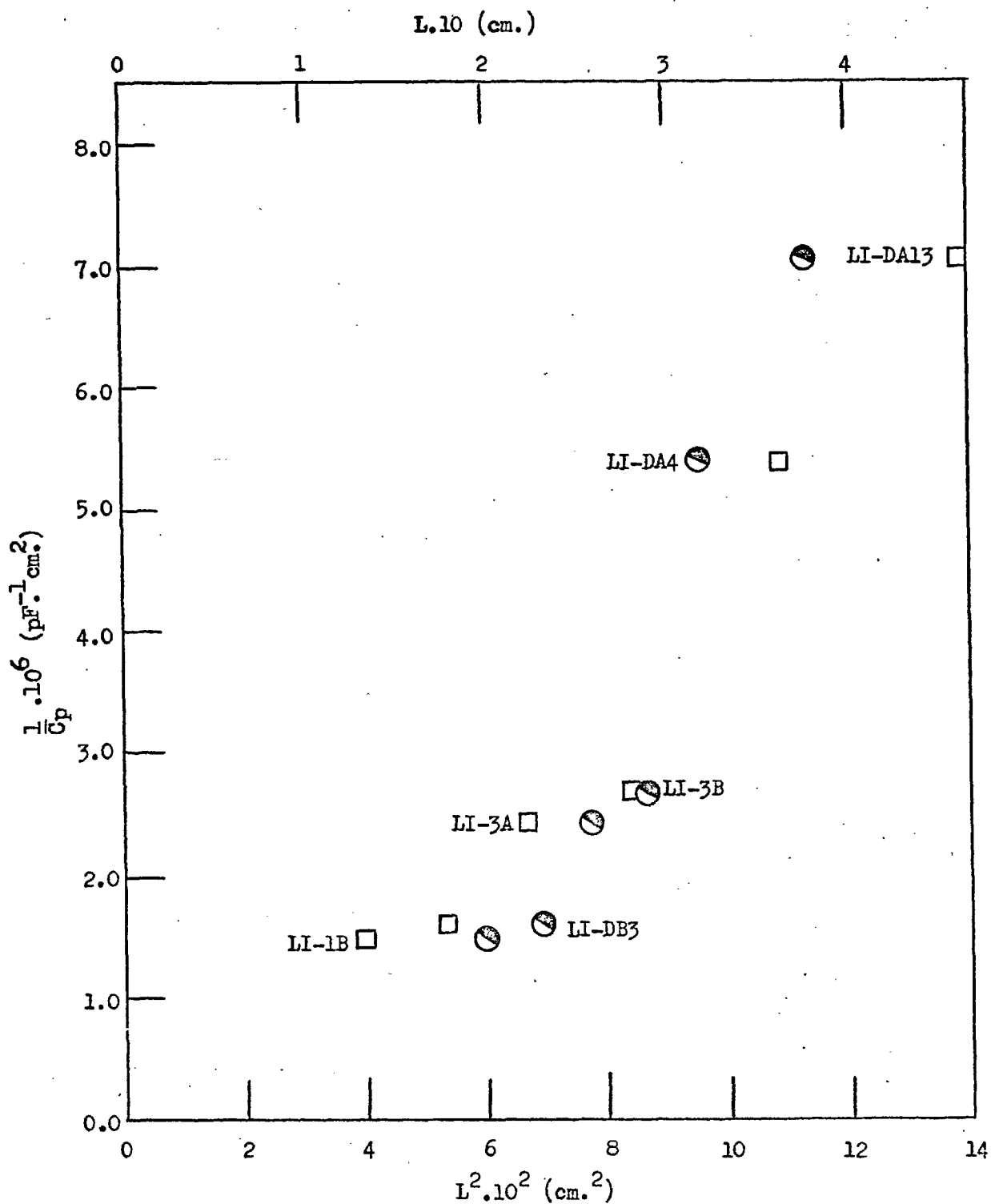
Fig. (4.17)
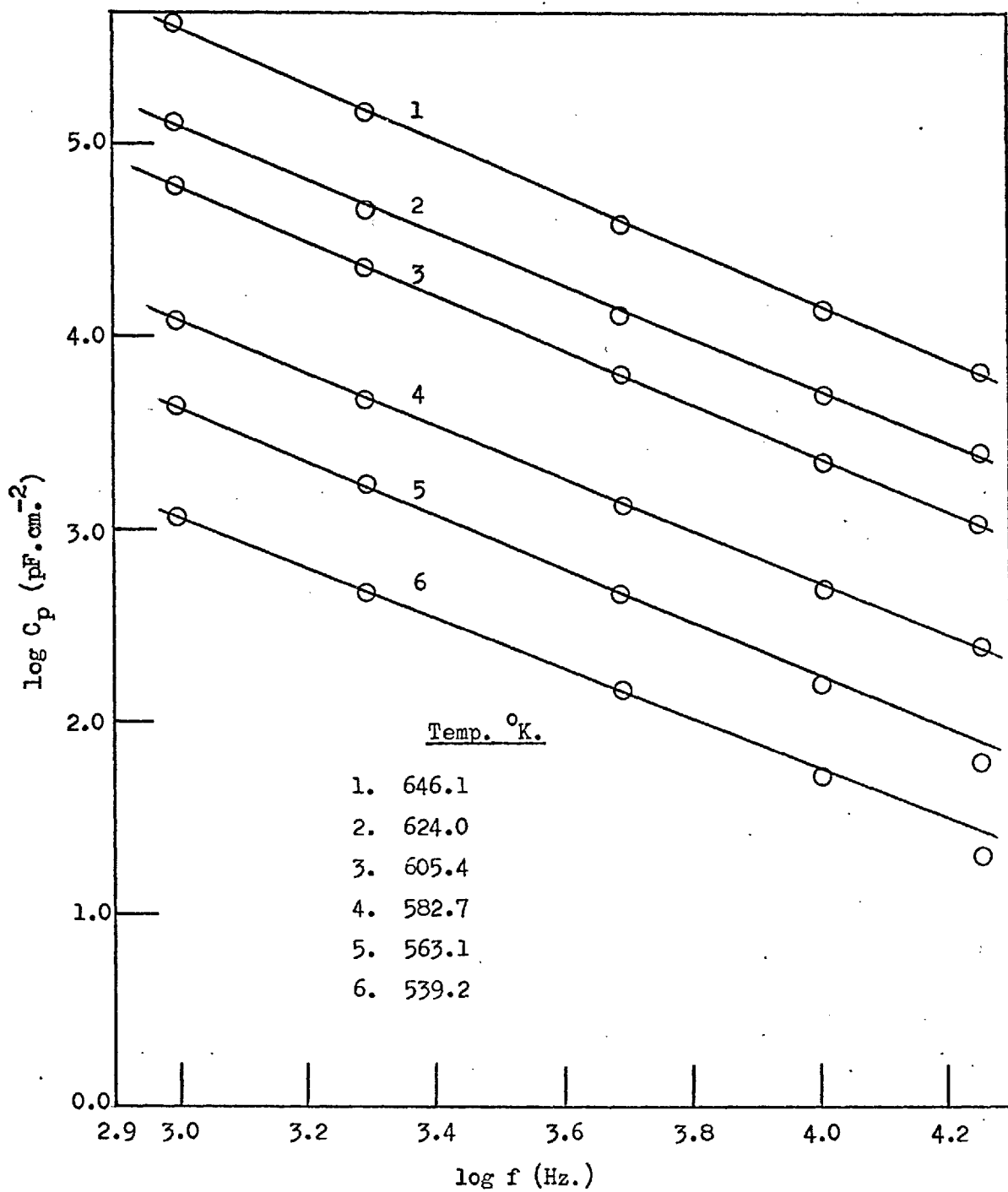
The 'frequency gradient' plot for LI-3B.

Fig. (4.18)

under vacuum. Evacuation, however, has an undesirable effect on the long term conduction as described in section 4.6. , probably introducing a secondary effect on the capacitance, and can therefore not be employed as an effective dehydrant. Accordingly, it was necessary to use the less efficient technique of maintaining a dry atmosphere by periodic flushing with dried argon. Our values of C_p, therefore, are possibly in error by a factor of 2 in some cases. One can, nevertheless, determine the isothermal frequency dependence of C_p obtaining useful insight into space-charge effects in this material.

The polarization of sample LI-3B is plotted in Fig. (4.17) as log C_p against f for a number of temperatures. As with the thallous halides C_p asymptotes to zero at high frequenies and low temperatures with the measured capacitance $(C_p + C_g)$ providing a value of C_g consistent with the geometry and static dielectric constant $(11.1)^{80}$ of the crystal. The low frequency, high temperature approach to C_o is not so obvious with lithium iodide because of the restricted temperature range of study.

Log C_p is further plotted against log f in Fig. (4.18) providing values of the 'frequency gradient' between 1.35 and 1.50 in LI-3B. Data for a number of other crystals are given in Table (4.6) where it is seen that the 'frequency gradient' varies widely - increasing with temperature for some samples and decreasing for others.

The dependence of C_p upon L in lithium iodide.

Fig. (4.19)

Sample	Conditions	Temp. °K.	Frequency gradient
LI-3A	All readings	535 — 640	1.59 — 1.43
LI-3B	taken on	539 — 646	1.33 — 1.50
LI-DA4	cooling with	557 — 641	1.17 — 1.28
LI-DA13	an argon	593 — 643	1.59 — 1.53
LI-DB3	atmosphere	572 — 643	1.53 — 1.30

The 'frequency gradient' for lithium iodide.

Table (4.6)

Both Friauf[47] and Jacobs[49] detected similar inconsistencies in their results when they altered the electrode conditions by lengthy annealing or changing the electrode material, in each case varying the blocking characteristics of the electrode. The figures in Table (4.6) therefore appear symptomatic of the leaking capacitance model described in section 4.7.

The reciprocal values of C_p are plotted against L, the length of the sample, and L^2 in Fig. (4.19). Although the space-charge polarization decreases, as expected, with increasing length of the sample and both curves must pass through the origin, the absolute values of C_p are insufficiently accurate for us to differentiate between the two types of power dependence.

Finally if we assume complete dissociation of neutral vacancy pairs and strict dependence on the equation

$$c_p^2 = \frac{\sigma_\infty^4 kT}{(1+\delta)Kf^4 e^2 \pi^3 L^4} \cdot \frac{1}{x_o}$$

using the values given in Table (4.7)

L	T	f	x_o	σ_∞	c_p(theor.)	c_p(expt.)
2.90mms.	624°K.	1KHz.	9.45x10^{18} per. cc.	6.09x10^{-3} ohm^{-1}cm^{-1}	1.18x10^6 pF/sq.cm.	1.22x10^5 pF/sq.cm.

Values for the theoretical calculation of C_p

Table (4.7)

we find that C_p (theoretical) is approximately one order of magnitude higher than the experimental value. This is encouraging as our values of C_p were often half those obtained under vacuum which, as we have already indicated, may be the more accurate.

4.8. THE DISORDER IN LITHIUM IODIDE

We have obtained a consistent analysis of our results on lithium iodide

by assuming the presence of Schottky disorder with $\mu_{(cv)} > \mu_{(av)}$, but we may obtain equal self-consistency if we assume that Frenkel disorder exists on the cation sub-lattice with the vacant cation site again the predominant charge carrier. The addition of magnesium enhances the conductivity indicating mobile cation vacancies or anion interstitials, but the presence of mobile iodine interstitials is unlikely on account of the large size of the ion. On the other hand, it might be argued that cationic Frenkel disorder exists with the interstitial ion more mobile than the vacancy and that we have artificially increased the conduction due to vacancies over that due to interstitials by divalent cationic doping. However, in situations like these, as with silver chloride[8], the log σT against $\frac{1}{T}$ plot is more complex than that obtained in Fig. (4.14) and distinct non-linearity is apparent throughout the plot where we have two conducting species. We suggest therefore that conduction in lithium iodide is due to mobile cation vacancies but we are unable to say whether the complementary defects are anion vacancies or cation interstitials.

In order to differentiate between these two types of disorder we may determine the thermal expansion of lithium iodide which, as Simmons pointed out, will contain a contribution from the additional vacant sites created in the case of Schottky disorder. In addition, the measurement of the self-diffusion coefficient of the iodine ion will enable us to determine whether or not the vacant anion site contributes significantly to the conduction.

REFERENCES

1. F. Seitz, "Imperfections in Nearly Perfect Crystals", (J. Wiley, New York, 1952).

2. C. Wagner and W. Schottky, Z. physik. Chem. (B), (1930), 11, 163.

3. J. Frenkel, Z. Physik, (1926), 35, 652.

4. A.B. Lidiard, Handbuch der Physik, (Berlin, Springer Verlag, 1956), 20, 246.

5. W. Jost, J. Chem. Phys., (1933), 1, 466; Trans. Far. Soc., (1938), 34, 860.

6. D.L. Kirk and P.L. Pratt, Proc. Brit. Ceram. Soc., (1967), 9, 215.

7. J.H. Beaumont and P.W.M. Jacobs, J. Phys. Chem. Solids, (1966), 45, 1496.

8. H. Abbink and D.S. Martin, J. Phys. Chem. Solids, (1966), 27, 205.

9. A.S. Miller and R.J. Maurer, J. Phys. Chem. Solids, (1958), 4, 196.

10. E. Barsis, E. Lilley, and A. Taylor, Proc. Brit. Ceram. Soc., (1967), 9, 203.

11. R.O. Simmons and R.W. Balluffi, Phys. Rev., (1960), 117, 52.

12. R.O. Simmons and R.W. Balluffi, Phys. Rev., (1962), 125, 862.

13. R.D. Fouchaux and R.O. Simmons, Phys. Rev., (1964), 136A, 1664.

14. A.W. Lawson, Phys. Rev., (1950), 78, 185.

15. N.F. Mott and M.J. Littleton, Trans. Far. Soc., (1938), 34, 485.

16. J.G. Mullen, Phys. Rev., (1966), 143, 658.

17. P. Brauer, Z. Naturf., (1952), 7A, 372.

18. J.R. Hardy and A.B. Lidiard, Phil. Mag., (1967), 15, 825.

19. K.J. Rao and C.N.R. Rao, Solid State Comm., (1968), 6, 45.

20. Z. Morlin, Acta phys. aung., (1966), 21, 137.

21. P.J. Harvey and I.M. Hoodless, Phil. Mag., (1967), 16, 543.

22. I.M. Boswarva, Metallurgy Dept., Imperial College, London, Private
    Communication.

23. C. Wert, Phys. Rev., (1950), 79, 601.

24. G.H. Vineyard, J. Phys. Chem. Solids, (1957), 3, 121.

25. S.A. Rice, Phys. Rev., (1958), 112, 804.

26. W. Franklin, J. Phys. Chem. Solids, (1967), 28, 829.

27. M. Omini, Nuovo Cim., (1968), 54, 116.

28. P.G. Shewmon, "Diffusion in Solids," (McGraw-Hill, New York, 1963).

29. J. Teltow, Ann. Phys. Lpz., (1949), 5, 63, 71.

30. R.G. Fuller and M.H. Reilly, Phys. Rev. Letts., (1967), 19, 113.

31. K. Tharmalingam and A.B. Lidiard, Phil. Mag.,(1961), 6, 1157.

32. A.W. Lawson, J. Appl. Phys., (1962), 33, 466; but see also J. Teltow,
    reference 29.

33. P.L. Pratt and B.A.W. Redfern, Proc. Brit. Ceram. Soc., (1964), 1, 175.

34. G.M. Hood and J.A. Morrison, J. Appl. Phys., (1967), 38, 4796.

35. H. Crooks, D. Mapother,and R. Maurer, J. Chem. Phys., (1950), 18, 1231.

36. A.R. Allnatt and P.W.M. Jacobs, Trans. Far. Soc., (1962), 58, 116.

37. S.C. Jain and S.L. Dahake, Indian J. Pure Appl. Phys., (1964), 2, 71.

38. T.G. Stoebe and P.L. Pratt, Proc. Brit. Ceram. Soc., (1967), 9, 181.

39. N. Brown and I.M. Hoodless, J. Phys. Chem. Solids, (1967), 28, 2297.

40. R.W. Dreyfus and A.S. Norwick, Phys. Rev., (1962), 126, 1367.

41. R.Chang, Proc. Brit. Ceram. Soc., (1967), 9, 193.

42. P.H. Sutter and A.S. Nowick, J. Appl. Phys., (1963), 34, 734.

43. J.S. Dryden and R.J. Meakins, Disc. Far. Soc., (1957), 23, 29.

44. G. Jaffé, Ann. Physik, (1933), 16, 217, 249.

45. H. Chang and G. Jaffé, J. Chem. Phys., (1952), 20, 1071.

46. J.R. Macdonald, Phys. Rev., (1953), 92, 4.

47. R.J. Friauf, J. Chem. Phys., (1954), 22, 1329.

48. D.O. Raleigh, "Progress in Solid State Chemistry Vol. 3", (Pergamon, Oxford, 1967), p. 115.

49. A.R. Allnatt and P.W.M. Jacobs, J. Phys. Chem. Solids, (1961), 19, 281.

50. P.W.M. Jacobs and J.N. Maycock, J. Chem. Phys., (1963), 39, 757.

51. J.H. Beaumont and P.W.M. Jacobs, J. Phys. Chem. Solids, (1967), 28, 657.

52. P.Süptitz and J. Teltow, Phys. Stat. Sol., (1967), 23, 9.

53. R.J. Friauf, J. Phys. Chem. Solids, (1961), 18, 203.

54. W. Lehfeldt, Z. Physik, (1933), 85, 717.

55. T.E. Phipps and E.G. Partridge, J. Amer. Chem. Soc., (1929), 51, 1331.

56. K. Hauffe and A.L. Griessbach- Vierk, Z. Elektrochem., (1953), 57, 248.

57. R.J. Friauf, J. Appl. Phys., (1962), 33, 494.

58. R.W. Christy and H.S. Dobbs, J. Chem. Phys., (1967), 46, 722.

59. C. Tubandt, Handbuch der Expt. Physik, (1932), 12, 383.

60. P. Hermann, Z. phys. Chem., (1964), 227, 338.

61. Y. Haven, Rec. Trav. Chim., (1950), 69, 1471.

62. K. Compaan and Y. Haven, Trans. Far. Soc., (1956), 52, 786.

63. J.J. Gilman, "The Art and Science of Growing Crystals", (J. Wiley, New York, 1963).

64. W.G. Pfann, "Zone Melting", (J. Wiley, New York, 1958).

65. P.W. Bridgman, Proc. Am. Acad. Arts Sci., (1925), 60, 305; (1929), 63; 351.

66. Gmelins Handbuch der Anorganischen Chemie, 8th Ed., 38, 261, (Verlag Chemie, GmbH, Berlin, 1953).

67. "Handbook of Chemistry and Physics", (The Chemical Rubber Company, Cleveland, Ohio, 1967).

68. G.F. Hüttig and F. Pohle, Z. anorg. allgem. Chem., (1924), 138, 14.

69. S. Kyropoulos, Z. anorg. Chem., (1926), 154, 308.

70. J. Czochralski, Z. phys. Chem., (1917), 92, 219; Z. anorg. Chem., (1925), 144, 131.

71. D.C. Stockbarger, Rev. Sci. Inst., (1936), 7, 133.

72. J. Penley, J. App. Phys., (1967), 38, 1978.

73. R.W. Christy, Dept. of Physics and Astronomy, Dartmouth College, Hanover, New Hampshire, U.S.A., Private Communication.

74. D.W. Lynch, Phys. Rev., (1960), 118, 468.

75. D.K. Dawson and L.W. Barr, Phys. Rev. Letters, (1967), 19, 844.

76. J.R. Tessman, A.H. Kahn, and W. Shockley, Phys. Rev., (1953), 92, 890.

77. G. Cannelli and L. Verdini, Ricerca Sci., (1966), 36, 246.

78. K.V. Rao and A. Smakula, J. Appl. Phys., (1965), 36, 3953.

79. A. Eucken and A. Büchner, Z. physik. Chem. (B), (1934), 27, 321.

80. "American Institute of Physics Handbook", (McGraw-Hill, New York, 1963).

81. R.W. Ure, J. Phys. Chem., (1957), 26, 1363.